UNIVERSITY OF CALIFORNIA,
IRVINE

Strategies to Increase the Synthesis of Biorenewable Chemicals Derived from Second-Generation Feedstocks

DISSERTATION

submitted in partial satisfaction of the requirements
for the degree of

DOCTOR OF PHILOSOPHY

in Chemical and Biochemical Engineering

by

Pamela Botero Besada-Lombana

Dissertation Committee:
Professor Nancy A. Da Silva, Chair
Professor Szu-Wen Wang
Professor Suzanne B. Sandmeyer

2018

To my family,

present, past and future.

To my teachers.

'*Research is formalized curiosity; it is poking and prying with a purpose*'

- Zora Neale Hurston

'*No tenemos otro mundo al que podernos mudar.'*

- Gabriel García Márquez

TABLE OF CONTENTS

LIST OF FIGURES

LIST OF TABLES

ACKNOWLEDGMENTS

I am deeply thankful to my advisor, Professor Nancy Da Silva. I can't thank her enough for her guidance and support throughout this five-year journey. I appreciate the independence she has provided for exploring different ideas, and the enthusiasm she has projected despite the many roadblocks that inevitably come with research. Her thoughtful insight and knowledge have been invaluable and I have learned a lot from her. I would also like to express my gratitude to the committee members, Professor Szu-Wen Wang and Professor Suzanne Sandmeyer. Their insights have led to significant improvements to this research.

I would like to thank Prof. Wilfred Chen (University of Delaware) for plasmids pAT and pBGL, Prof. Jered Haun (UC Irvine) for providing the genes encoding 4-4-20 scFv and mRFP and Dr. Xing at the TEM facility for her guidance.

I have been very fortunate to work along with great people! Thanks to all past and present members of the Da Silva group; your comments and discussions have been very important for my work. Special mention to my mentors Dr. Fernandez-Moya, Dr. Que, Dr.Choi and, Dr. Leber, thanks for taking the time to teach me. Thanks to Tami, Anh, Hannah, and Danielle for making the lab a more amenable and fun place to work. I would also like to acknowledge the Wang lab group, particularly, Medea Neek and Tae II Kim for their help running SDS-PAGEs, Western Blots and, most importantly, the plate reader. To all of you, thanks for all our (very necessary) trips to Starbucks, they definitely helped to relief stress and increase productivity, one coffee at a time!

I would also like to acknowledge the support of Jacob Fenster and Michael Wiedeman. They have been fundamental for the development of part of this research. I would also like to thank my friends for giving me a proper balance in life. My cohort is full of amazing people and we have shared great moments. Thanks also to my Spanish-Californian family, for our dinners and endless

conversations, and to my friends in Barcelona, as every Christmas reunion feels like as if I have never left! I would also like to thank Salvador, for his empowerment along my undergraduate years.

Finally, I would also like to acknowledge a very important part of my life, my family. I'd like to thank my grandfather, Dr. Arturo Besada-Lombana, he has been an inspiring figure for all of us and an intellectual stimulus in my early years. Thank you, Mimia for being such a great female role model, who proved to me that balance between work and life was possible, I will forever miss you. Llilla, thanks for teaching me altruism, forgiveness and compassion. I would also like to thank my loving mom, for her efforts and encouragement to help me achieve whatever goal I set my mind to. Thanks to Ivan, for sharing his life with her and bringing a smile in tough times. Thanks to Nina for being a role model despite the distance, I have always looked up to you. Jorge Andres, thanks for grounding me when I needed it, our conversations have always been refreshing. Thanks to Javier for his kindness and to Santi, a free spirit that has been unconditional to me. Thanks to my aunt, Dr. Sandra Besada-Lombana, for inspiring me to pursue a career in science. Finally, I would also like to thank my in-law-family, Nuria and Carles, for their care and support over the last five years. And last, but never least, a special thanks to my loving husband Carles for his encouragement, he has been my rock, my support during this journey. His curiosity and positivity are contagious! Can't wait for what the future holds for us!

This research was supported by the National Science Foundation (Grant No. CBET-1263799 and No. EEC-0813570 through the Engineering Research Center CBiRC: Center for Biorenewable Chemicals).

CURRICULUM VITAE

Pamela Botero Besada-Lombana

Education

2013-2018	Ph.D. in Chemical and Biochemical Engineering, University of California, Irvine
2013-2015	M.S. in Chemical and Biochemical Engineering, University of California, Irvine
2010- 2013	M.S. Bioengineering, IQS School of Engineering, Barcelona, Spain
2005-2010	B.Sc. Organic Chemistry, IQS School of Engineering, Barcelona, Spain

Professional experience

2016	Teaching Assistant, Chemical Processing and Material Balances, University of California, Irvine
2015	Teaching Assistant, Chemical Processing and Material Balances, University of California, Irvine
2014	Teaching Assistant, Chemical Processing and Material Balances, University of California, Irvine
2013	Researcher, Sagetis Biotech SL, Barcelona, Spain
2010-2011	Researcher, Grupo de Ingeniería de Materiales (GEMAT) and Almirall, LLC, Barcelona, Spain
2010	Undergraduate Researcher, Chemical Formulations Research Group, IQS School of Engineering, Barcelona, Spain
2009	Undergraduate Researcher, Biological Chemistry and Biotechnology Group, IQS School of Engineering, Barcelona, Spain

Selected Publications and Presentations

1. **Pamela B. Besada-Lombana**, Tami Lee McTaggart, Nancy A. Da Silva. (2018), Molecular tools for pathway engineering in Saccharomyces cerevisiae. *Current Opinion in Biotechnology.* 53:39–49.

2. **Pamela B. Besada-Lombana,** Ruben Fernandez-Moya, Jacob Fenster, Nancy A. Da Silva (2017), Engineering *Saccharomyces cerevisiae* fatty acid composition for increased tolerance to octanoic acid. *Biotechnology and Bioengineering*. 114:1531–1538.

3. **Pamela B. Besada-Lombana**, Nancy A. Da Silva. (2017), Strategies for increasing *Saccharomyces cerevisiae* tolerance to medium-chain fatty acids. *Abstracts of papers of the American Chemical Society* 253.

4. **Pamela B. Besada-Lombana**, Nancy A. Da Silva. (2016), Substrate-dependent surface display of a cellulosome by *Saccharomyces cerevisiae*. *Abstracts of papers of the American Chemical Society* 251.

ABSTRACT OF THE DISSERTATION

Strategies to Increase the Synthesis of Biorenewable Chemicals Derived from Second-Generation Feedstocks

By

Pamela Botero Besada-Lombana

Doctor of Philosophy in Chemical and Biochemical Engineering

University of California, Irvine, 2018

Professor Nancy A. Da Silva, Chair

In response to the exhaustion of carbon feedstock from fossilized sources, dependence on foreign energy supplies, and the threat of climate change, there is an increasing incentive for the production of biofuels and bio-based chemicals. Second-generation biorefineries provide a sustainable approach by relying on lignocellulosic biomass obtained from renewable resources. To increase economic viability and lower the cost of biomass processing there is a promising approach called Consolidated Bioprocessing (CBP). CBP may be accomplished by hydrolysis of lignocellulose's main components—hemicellulose and cellulose—by displaying a xylanosome and a cellulosome on the surface of the microorganism responsible for synthesis of the desired chemical (e.g. ethanol, medium chain fatty acids, etc.). In the first part of this study, we describe strategies to increase the efficiency of CBP lignocellulosic biomass hydrolysis. First, we developed an expression system and a set of strains that showed enhancements in protein secretion of 5.8-fold to 11.5-fold. Next, we designed and characterized an extracellular glucose sensor that enables selective display of cellulose-degrading enzymes in the presence of the cellulosic fraction of lignocellulose. This is possible by leveraging cellulose-dependent signal amplification. The engineered version of the sensor showed up to 81% higher levels of expression, and a 55%-91%

amplification of the signal was observed in the presence of cellobiose. Once saccharification is complete, CBP microorganisms will ideally synthesize chemicals that can functionally substitute those currently generated by the petrochemical industry. Fatty acids with chain lengths between 8 and 12 carbons have a wide variety of industrial applications, including as biofuels and precursors to commodity and fine chemicals. Our laboratory has successfully engineered *Saccharomyces cerevisiae* to produce hexanoic acid, octanoic acid (C8) and decanoic acid (C10). However, higher levels of production are hindered by the toxic effects of the fatty acids on the cells at increased concentrations. To overcome this limitation, we successfully explored two different strategies in the last part of this study: i) changing the membrane composition to alleviate the effects of C8, and ii) identifying and overexpressing efflux pumps that export C10. This allowed growth improvements of up to 10-fold (C8) and 11-fold (C10).

INTRODUCTION

Motivation

The current model for global economic growth and technological development has allowed millions of people to escape from poverty, has raised the living standards and erased boundaries between countries and business. However, this model is necessarily linked to increased energy and resources consumption (Lopes, 2015), which has resulted in a considerable augmentation of crude oil demand during the last two decades (Anon, 2014; Wood et al., 2004). This rising demand is leading to exhaustion of carbon feedstocks from fossilized sources (Carlson, 2011). Additionally, dependence on foreign energy sources has become one of the main concerns regarding energy security in many countries (Demski et al., 2014). For this reason, the U.S. Department of Energy along with the U.S. Department of Agriculture (USDA) decided to increase the role of biomass as an energy resource, aiming to replace 30% of the current U.S. petroleum consumption with bio-based products by 2030 (Perlack et al., 2005). Furthermore, there is an increased necessity to reduce carbon dioxide emissions to mitigate climate change (Wuebbles et al., 2017). All these issues reflect the necessity for shifting from an oil-based economy to a bio-based economy, also referred to as a bioeconomy (Guo and Song, 2018; Hassan et al., 2018; Lopes, 2015). U.S. efforts toward this goal over the last decade have led to the expansion of the bioeconomy at an annual rate of more than 10%, with direct revenues of over $415 billion U.S. dollars in 2015 (Guo and Song, 2018).

In the context of a bioeconomy, the development of biorefineries is necessary. Although there are many definitions of what a biorefinery is, it is generally accepted that it refers to the "use of renewable raw materials to produce energy together with a wide range of everyday commodities

in an economic sustainable manner" (Gomes et al., 2014). By integrating production of high volume low value products, such as biofuels, with high value low volume chemicals, such as biologics, enzymes, and biomaterials, the cost of growing biomass can be compensated, ensuring economic viability and high return of investment (Bozell and Petersen, 2010). The most common example for this model is the combination of a biorefinery and a wood pulp/paper plant, where chemicals, fuel and power are being generated at the same time that wood, pulp and paper products are manufactured (Hassan et al., 2018).

Feedstock for first-generation biorefineries consists mainly of sugar, cornstarch and vegetable oils (Hadar, 2013; Lopes, 2015). However, their use has almost reached its full capacity (Faraco, 2013), and their environmental benefit is greatly limited (Robertson et al., 2017). In addition, the dilemma of diverting farmland from food production to synthesis of fuels and chemicals emphasizes the need for development of an alternative affordable process that does not threaten food supplies and biodiversity (Fan et al., 2012; Robertson et al., 2017). An alternative emerges with second generation biorefineries, which use lignocellulosic biomass as raw material (Lopes, 2015; Lynd et al., 2017). These raw materials can be sustainably obtained from agricultural wastes such as corn stoves, rice straw, wheat straw or agave bagasse, perennial grasses, short-rotation trees, and industrial or municipal solid waste, having a low environmental impact (Faraco, 2013; Gomes et al., 2014; Lynd et al., 2017; Robertson et al., 2017; Xiu and Shahbazi, 2015). However, the main barrier to a more widespread use of lignocellulosic biomass results from the high cost and difficulty of obtaining fermentable sugars by hydrolysis (Lynd et al., 2017). One strategy with great potential to overcome these limitations is known as Consolidated Bioprocessing (CBP) and relies on the combination of the saccharification step – hydrolysis of hemicellulose and cellulose into soluble fermentable sugars – and biorenewable chemical synthesis (Lynd et al., 2017). This is accomplished by engineering the microorganism in charge of the chemical synthesis

to also produce and secrete cellulolytic enzymes, eliminating the need for dedicated and separate enzyme production (Weifu Lee, 2013). In prior research, our strategy was based on efficient biomass hydrolysis via display of a synthetic cellulosome or xylanosome (Goyal et al., 2011; Srikrishnan et al., 2013), depending on the substrate available.

Another major challenge faced by biorefineries is the large number of possible targets, requiring the necessity to identify a group of chemicals that can functionally substitute for those currently used by the petrochemical industry (Bozell and Petersen, 2010; Nikolau et al., 2008). Fatty acids with chains between 8 and 12 carbons have a wide variety of industrial applications, including as biofuels (as replacements of gasoline or jet fuel) and precursors to commodities (e.g., as precursors for α-olefins and monomers for elastomers of auto parts) and fine chemicals (such as herbicides, flavors, and fragrances) (Sarria et al., 2017). To ensure sufficient supplies to meet the demand for fabrication of these industrial products, there is an emerging interest in production of medium-chain free fatty acids (MCFA). However biological production of MCFA, such as decanoic and octanoic acids, is hindered by their toxic effects in microbial cells (Jarboe et al., 2013). Our laboratory has successfully engineered *Saccharomyces cerevisiae* to produce hexanoic acid, octanoic acid and decanoic acid (Leber and Da Silva, 2013). We aimed to mitigate octanoic acid and decanoic acid toxic effects by engineering the cell fatty acid composition and overexpressing efflux pumps.

Objectives

The overall goal of this research was to design strategies that address bottlenecks that second-generation biorefineries currently face at different stages of production. In this work, we evaluated approaches directed to increase synthesis of biorenewable MCFA from lignocellulosic biomass feedstocks, by focusing on two different aspects of the process: i) efficient lignocellulose hydrolysis via CBP and ii) alleviation of octanoic and decanoic acid toxicity. Our objectives were:

1. **Improve secretion of cellulose-degrading enzymes by engineering of the secretory pathway (Chapter 1).**

   By multiplex engineering of the secretory pathway, we have successfully improved extracellular levels of an endoglucanase and a β-glucosidase. Efficient entry into the secretory pathway was accomplished by promoting co-translational translocation via secretion peptide engineering and the novel use of a 3'untranslated region. We further optimized the pathway by engineering the endoplasmic reticulum, incrementing its dimensions, limiting retro-translocation, and providing more exit points for anterograde transit to the Golgi. We then evaluated our strains for the secretion of an alternative protein, a single-chain antibody fragment.

2. **Development of an extracellular glucose sensor for substrate-dependent display of cellulases (Chapter 2).**

   We have developed an extracellular glucose sensor that would enable the display of cellulosome enzymes only in the presence of the cellulosic fraction of lignocellulose by leveraging cellulose-dependent signal amplification. Our initial design was based on the *HXT1* promoter. After characterization of its responsiveness to glucose, we engineered the *HXT1*p by changing its core to that of the strong *THD3*p. We proceeded to demonstrate glucose-mediated display of an enzyme by anchoring a β-glucosidase –

responsible for the last step of cellulose hydrolysis into glucose – to the surface of *S. cerevisiae*. The system was optimized by re-directing fatty acid pools from lipid droplet synthesis toward formation of membrane precursors.

3. **Engineering fatty acid composition for increased octanoic acid tolerance (Chapter 3).**

   Octanoic acid toxicity is primarily due to disruption of the integrity of the cell membrane in yeast, and exogenous supplementation of oleic acid had previously been shown to help alleviate this. We evaluated how the increased proportion of oleic acid due to expression of the enzyme $Acc1^{S1157A}$ mitigates the toxic effects of octanoic acid. We determined the viability of the cells at increasing concentrations of C8, and studied the effects of the increased synthesis of oleic acid on membrane integrity upon exposure to lethal C8 concentrations.

4. **Increasing tolerance to decanoic acid by overexpression of membrane transporters (Chapter 4).**

   We aimed to limit the toxic effects of decanoic acid via overexpression of efflux pumps. We first selected a series of candidate transporters. To determine their potential role in C10 transport, we screened strains with these transporter genes deleted for increased susceptibility to decanoic acid. Selected candidates were overexpressed either in a centromeric or a 2μ-based plasmid. This helped elucidate the optimal expression level that balances efficient decanoic acid export with potential adverse effects associated with membrane transporter overproduction.

The relationship between the four objectives and the yeast engineering required is illustrated in Figure A.

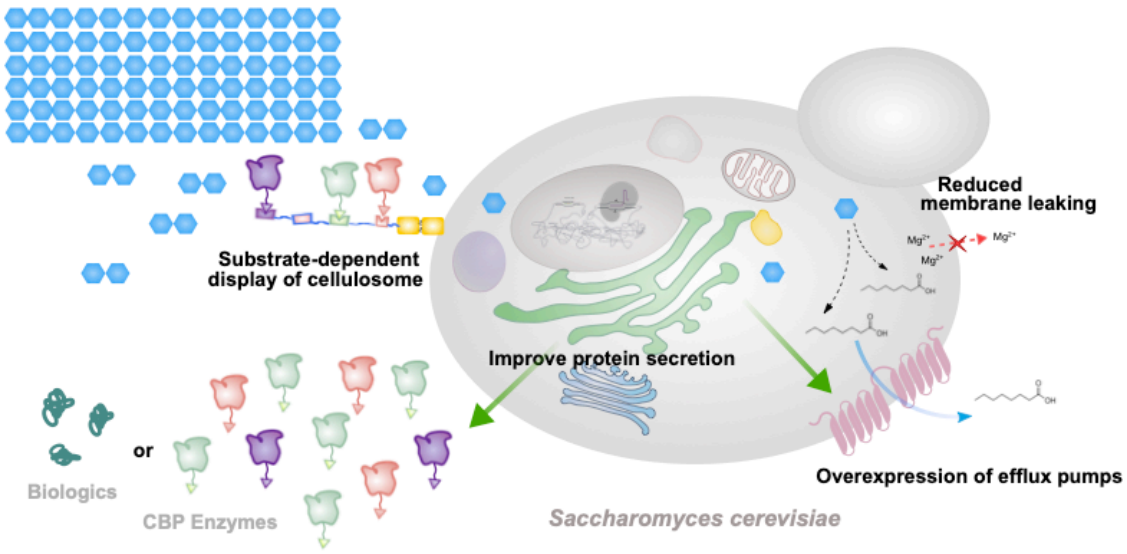

Figure A. Representation of the four objectives.

References

International Energy Outlook. 2014. . *U.S. Energy Inf. Adm.* http://www.eia.gov/forecasts/ieo/.

Bozell JJ, Petersen GR. 2010. Technology development for the production of biobased products from biorefinery carbohydrates—the US Department of Energy's "Top 10" revisited. *Green Chem.* **12**:539.

Carlson WB. 2011. The Modeling of World Oil Production Using Sigmoidal Functions—Update 2010. *Energy Sources, Part B Econ. Planning, Policy* **6**:178–186.

Demski C, Poortinga W, Pidgeon N. 2014. Exploring public perceptions of energy security risks in the UK. *Energy Policy* **66**:369–378. http://dx.doi.org/10.1016/j.enpol.2013.10.079.

Fan L-H, Zhang Z-J, Yu X-Y, Xue Y-X, Tan T-W. 2012. Self-surface assembly of cellulosomes with two miniscaffoldins on Saccharomyces cerevisiae for cellulosic ethanol production. *Proc. Natl. Acad. Sci.* **109**:13260–13265.

Faraco V ed. 2013. Lignocellulose Conversion. Berlin: Springer-Verlag 21-39 p. http://link.springer.com/10.1007/978-3-642-37861-4.

Gomes FJB, Santos F a, Colodette JL, Demuner IF, Batalha L a R. 2014. Literature Review on Biorefinery Processes Integrated to the Pulp Industry. *Nat. Resour.* **5**:419–432.

Goyal G, Tsai S-L, Madan B, DaSilva N a, Chen W. 2011. Simultaneous cell growth and ethanol production from cellulose by an engineered yeast consortium displaying a functional mini-cellulosome. *Microb. Cell Fact.* **10**:89. http://www.microbialcellfactories.com/content/10/1/89.

Guo M, Song W. 2018. The Growing U.S. Bioeconomy: Drivers, Development and Constraints. *N. Biotechnol.* https://linkinghub.elsevier.com/retrieve/pii/S1871678418301821.

Hadar Y. 2013. Sources for Lignocellulosic Raw Materials for the Production of Ethanol. In: Faraco, V, editor. *Lignocellul. Conversion. Enzym. Microb. Tools Bioethanol Prod.* Berlin:

Springer-Verlag, pp. 21–38.

Hassan SS, Williams GA, Jaiswal AK. 2018. Lignocellulosic Biorefineries in Europe: Current State and Prospects. *Trends Biotechnol.* **xx**:1–4. https://doi.org/10.1016/j.tibtech.2018.07.002.

Jarboe LR, Royce L a, Liu P. 2013. Understanding biocatalyst inhibition by carboxylic acids. *Front. Microbiol.* **4**:272.

Leber C, Da Silva NA. 2013. Engineering of Saccharomyces cerevisiae for the synthesis of short chain fatty acids. *Biotechnol. Bioeng.* **111**:347–358. http://www.ncbi.nlm.nih.gov/pubmed/23928901.

Lopes MSG. 2015. Engineering biological systems toward a sustainable bioeconomy. *J. Ind. Microbiol. Biotechnol.* **42**:813–38.

Lynd LR, Liang X, Biddy MJ, Allee A, Cai H, Foust T, Himmel ME, Laser MS, Wang M, Wyman CE. 2017. Cellulosic ethanol: status and innovation. *Curr. Opin. Biotechnol.* **45**:202–211. https://linkinghub.elsevier.com/retrieve/pii/S0958166917300058.

Nikolau BJ, Perera MADN, Brachova L, Shanks B. 2008. Platform biochemicals for a biorenewable chemical industry. *Plant J.* **54**:536–545.

Perlack RD, Wright LL, Turhollow AF, Graham RL, Strokes BJ, Erbach DC. 2005. Biomass as feedstock for a bioenergy and bioproducts industry: The technical feasibility of a billion-ton annual supply. Oak Ridge, Tenessee.

Robertson GP, Hamilton SK, Barham BL, Dale BE, Izaurralde RC, Jackson RD, Landis DA, Swinton SM, Thelen KD, Tiedje JM. 2017. Cellulosic biofuel contributions to a sustainable energy future: Choices and outcomes. *Science (80-.).* **356**:eaal2324. http://www.sciencemag.org/lookup/doi/10.1126/science.aal2324.

Sarria S, Kruyer NS, Peralta-Yahya P. 2017. Microbial synthesis of medium-chain chemicals from renewables. *Nat. Biotechnol.* **35**:1158–1166.

Srikrishnan S, Chen W, Da Silva NA. 2013. Functional assembly and characterization of

a modular xylanosome for hemicellulose hydrolysis in yeast. *Biotechnol. Bioeng.* **110**:275–285.

Weifu Lee J ed. 2013. Advanced biofuels and bioproducts. New York: Springer Science+ Bussiness Media.

Wood JH, Long GR, Morehouse DF. 2004. Long-Term Worl Oil Supply Scenarios. *U.S. Energy Inf. Adm.* http://www.eia.gov/pub/oil_gas/petroleum/feature_articles/2004/worldoilsupply/oilsupply04.html.

Wuebbles DJ, Fahey DW, Hibbard KA, Deangelo B, Doherty S, Hayhoe K, Horton R, Kossin JP, Taylor PC, Waple AM, Weaver CP. 2017. Climate Science Special Report. *Exec. Summ. Clim. Sci. Spec. Rep. Fourth Natl. Clim. Assess.* Vol. I 26 p.

Xiu S, Shahbazi A. 2015. Development of Green Biorefinery for Biomass Utilization: A Review. *Trends Renew. Energy* **1**:4–15. http://futureenergysp.com/index.php/tre/article/view/8.

Chapter 1

Multi-level Engineering of *Saccharomyces cerevisiae* for Increased Protein Secretion

1.1 Abstract

The yeast *Saccharomyces cerevisiae* is a platform host for production of heterologous proteins with a wide array of applications, ranging from cellulose saccharification enzymes to biopharmaceuticals. Efficient protein secretion may be critical for economic viability; however previous efforts have shown limited improvements that are usually protein-specific. By multiplex engineering of the secretory pathway, we have successfully improved extracellular levels of three different proteins from variety of origins: a bacterial endoglucanase (CelAt), a fungal β-glucosidase (BglDf) and a hybridoma single-chain antibody fragment (4-4-20 scFv). Efficient co-translational translocation into the endoplasmic reticulum (ER) was achieved via secretion peptide engineering and the novel use of a 3'-untranslated region, improving extracellular levels from 2.2-fold to 5.1-fold. We further optimized the pathway using a variety of new strategies including: i) increasing secretory pathway capacity by expanding the ER, ii) limiting ER-associated degradation, and iii) addition of ER exit recognition. A strain with this triple intervention showed improvement for all three proteins and was the best combination for secretion of BglDf. CelAt benefited the most by limiting ER degradation, and 4-4-20-scFv by expanding the ER. Via pathway engineering, we have developed a set of strains that improve the secretion of different heterologous proteins by 5.8-fold to 11-fold.

1.2 Introduction

The yeast *Saccharomyces cerevisiae* is a host for expression of a variety of recombinant proteins. Applications can be found at different stages of the manufacturing processes: from the production of xylanases and cellulases for lignocellulose saccharification (Davison et al., 2016; Srikrishnan et al., 2013; Tsai et al., 2009) to the fabrication of biologics (de Ruijter et al., 2016; Schmidt, 2004; Sheng et al., 2017) —an increasingly significant segment of the pharmaceutical market (Nagel, 2018). Some reasons behind the widespread use of this microorganism are its resistance to ethanol, low pH, and high osmotic pressure; its ease of cultivation in high-density cultures (Hou et al., 2012a); and the broad range of molecular tools available for genetic manipulation and pathway engineering (Besada-Lombana et al., 2018). Furthermore, contrary to bacterial hosts, *S. cerevisiae* is generally recognized as safe (GRAS) by the U.S. Food and Drug Adminstration, and capable of performing post-translational modifications — such as glycosylation and subunit assembly. These are important steps involved in the proper folding and biological activity of proteins derived from higher eukaryotes (Idiris et al., 2010; Schmidt, 2004).

Enzymatic saccharification and production of biologics often requires secretion of proteins into the extracellular milieu to access their substrate and/or facilitate downstream processing (Idiris et al., 2010; Schmidt, 2004). The secretion of proteins involves a series of complex, coordinated steps that transport the polypeptide chain through the secretory pathway. The journey starts with translocation from the cytoplasm into the lumen of the endoplasmic reticulum (ER). This process can take place either post-translationally (Ast and Schuldiner, 2013) or co-translationally (Nyathi et al., 2013). Post-translational translocation happens once the full polypeptide chain has been synthesized and it has several disadvantages. It can be slowed-down due to partially folded domains or cytosolic aggregation (Fitzgerald and Glick, 2014) and it requires the aid of cytosolic chaperones (Bukau and Horwich, 1998) as well as the driving force from Kar2 — which acts as a

molecular ratchet (Matlack et al., 1999). Instead, co-translational translocation occurs while mRNA is being translated on the cytosolic side of the ER membrane and it is the major mode of ER insertion. According to the canonical mechanism, co-translational translocation starts with the emergence of a hydrophobic secretion signal from the ribosomal tunnel, which is identified by the Signal Recognition Particle (SRP) and forms the ribosome-nascent chain (RNC)-SRP complex. This results in elongation arrest (Mandon et al., 2013; Ng et al., 1996; Nyathi et al., 2013; Pechmann et al., 2014; Rapoport et al., 2017). RNC-SRP is then targeted to the ER lipid bilayer via an ER membrane heterodimer called SRP receptor (SR). A stable SR-SRP-RNC interaction requires SR to be in the GTP-bound state. The hydrolysis of GTP leads to dissociation of the complex from the signal sequence and subsequent binding of RNC to the translocation tunnel (Mandon et al., 2013; Nyathi et al., 2013). Secretion signal probing by SRP is the most widely accepted model for co-translational translocation; however, it fails to capture other mechanisms, such as the pre-recruitment of SRP preceding emergence of the leader sequence from the ribosomal tunnel (Chartron et al., 2016; Costa et al., 2018).

Once proteins are in the ER lumen, they undergo several modifications before proceeding to the Golgi apparatus (Barlowe and Miller, 2013; Feyder et al., 2015). These modifications include signal cleavage, glycosylation, isomerization of disulfide bonds, and native folding. These processes are tightly regulated by a quality control system (QC) that ensures protein fidelity and proper maturation. When protein production exceeds the ER capacity or misfolded proteins are accumulated, the ER membrane sensor Ire1 forms a self-dimer that results in activation of its RNAse domain, leading to unconventional splicing of Hac1 mRNA (Hwang and Qi, 2018; Tyo et al., 2012). The spliced form of Hac1 activates 381 genes, including those encoding for molecular chaperones, enzymes for lipid biosynthesis, protein transport compartments, and ER-associated degradation machinery (ERAD) (Travers et al., 2000b; Young and Robinson, 2014). Ire1 also

detects membrane aberrancies caused by altered lipid composition (e.g.; increased saturation, inositol depletion, increased sterol levels etc.), highlighting the importance of ER morphology on protein QC. In fact, it has been recently suggested that UPR components play a role in detection and control of ER protein-to-lipid ratio (Covino et al., 2018). When proteins have lingered for too long inside the ER, Htm1 removes a terminal mannose and triggers their targeting to the ERAD machinery in order to proceed with their clearance. The resulting oligosaccharide is now recognized by the lectin Yos9 which is bound to Hdr3. Hdr3 is also known to recognize non-glycosylated substrates. Once aberrant proteins are selected by Yos9/Hdr3, Der1 inserts them into the ER membrane, positioning them in close proximity to Hdr1 for polyubiquitylation and targeting to the proteasome (Barlowe and Miller, 2013; Mehnert et al., 2014; Wu and Rapoport, 2018). These QC regulatory mechanisms constitute a bottleneck for heterologous protein expression, since these proteins may be identified as aberrant and their overexpression may surpass ER overall capacity (Hwang and Qi, 2018; Wang et al., 2001).

Successfully folded proteins exit the ER via COPII transport vesicles. Assembly of the vesicle coat starts with activation of Sar1 by Sec12, followed by induction of membrane curvature and recruitment of Sec23-Sec24 to form what is known as a pre-budding complex (Bonifacino and Glick, 2004; Dancourt and Barlowe, 2010; Melero et al., 2018). Interestingly, membrane curvature can be induced in absence of Sec12 via overexpression of the phospholipase B Plb3 (Melero et al., 2018), demonstrating once again the important role of lipids in the secretion process. Sec24 is in charge of cargo recognition either via direct interaction or through adaptor proteins that link luminal cargo to COPII coat (e.g.; p24, ERGIC-53 and Erv family protein) (Dancourt and Barlowe, 2010). Finally, the pre-budding complex recruits the Sec13-Sec31 subcomplex, which deforms the ER membrane and results in the bud of COPII vesicles (Bonifacino and Glick, 2004; Dancourt and Barlowe, 2010; Melero et al., 2018). Further transport though the secretory pathway

involves trafficking through the Golgi Complex and the formation of secretory granules (Bonifacino and Glick, 2004). These granules fuse with the plasma membrane and at that point, the protein is ready to be released into the extracellular milieu.

Due to the relevance of protein secretion for industrial processes, a myriad of strategies aiming to improve it have been considered, focusing on different aspects such as expression system, secretion signal, and secretory pathway optimization. The complexity of engineering secretion became evident with an early study on expression systems, where selection of a stronger promoter in a multi-copy plasmid did not simply result in higher secretion levels (Ernst, 1986). A similar conclusion was also reached in a more recent report, where *TEF1* and *TPI1* promoters were compared for secretion of α-amylase and insulin (Liu et al., 2012). Similarly, changing from a low-copy plasmid to a 2μ high-copy plasmid did not increase secretion levels of bovine pancreatic trypsin inhibitor, but instead resulted in accumulation of the misfolded protein in the interior of the cell (Parekh et al., 1995). Is therefore important to select the appropriate level of expression for efficient protein secretion.

Another key choice is the secretion peptide, as it determines the ER targeting pathway, influences interaction with the translocon, and has impact on post-cleavage events (Hegde and Bernstein, 2006). The most commonly used in yeast is the leader peptide of the *S. cerevisiae* mating factor-α, composed of the 19 residue amino terminal pre-sequence that is cleaved by the signal protease upon ER translocation and a pro-segment that has several glycosylation sites, an ER export signal, and Kex2 endoprotease recognition sequence (Kurjan and Herskowitz, 1982; Young and Robinson, 2014). The pre-pro-MFα1 leader was used for the first time to direct the secretion of the human epidermal growth factor (Brake et al., 1984) and since then has been used in numerous studies (e.g., Chigira et al., 2008; Huang et al., 2017; Robinson et al., 1994). Efforts to improve pre-pro-MFα1-mediated secretion have included directed evolution (Rakestraw et al.,

2009) and substitution of the pre- sequence to promote co-translational translocation (Fitzgerald and Glick, 2014). Other secretion signals such as those from genes such as *PHO1, SUC2*, *KILM1,* the synthetic peptide Yap3-TA57, or the native secretion signal of the heterologous protein have also been reported in the literature (Davison et al., 2016; Hashimoto et al., 1998; Hou et al., 2012a; Liu et al., 2012),

Finally, other efforts have focused on engineering strains at different steps of the pathway. Starting with translocation, overexpression of SRP subunits Srp54 or Srp14, resulted in improvements of 16%-56% and 18%-44%, respectively depending on the protein tested. Further engineering of folding machinery resulted in increases between 60% and 103% (Tang et al., 2015). Several other studies have also relied on overexpression of ER resident chaperones such as Kar2 and/or disulfide bond isomerases Pdi1 and Ero1 to improve secretion, with different degrees of success, ranging from 0.6 to 10-fold increases, depending on the protein being expressed (Butz et al., 2003; Robinson et al., 1994). Studies have also sought to determine the effect of overexpression and knock-out of the UPR-associated transcription factor *HAC1*. Deletion decreased secretion of various proteins by 40-75% (Tyo et al., 2012; Valkonen et al., 2003), while overexpression of the spliced form gave mixed results, ranging from no improvement to a 2.4-fold increase (Payne et al., 2008; Valkonen et al., 2003). Further steps of glycosylation (Wang et al., 2013) and vesicle trafficking (Hou et al., 2012b) have also been engineered. Other approaches have led to widely varying improvements depending on the protein being expressed. For instance, when *RGR1* is knocked-out, there is a ~17-fold improvement in extracellular levels of mouse α-amylase, but only a ~30% increase for *S. cerevisiae* invertase (Sakai et al., 1988). This variability also demonstrates the complexity of promoting efficient protein secretion and is illustrated in a recent transcriptional genome-scale level analysis of high-secreting mutants (Huang et al., 2017). It was found that beyond genes from the secretory pathway itself, efficient secretion leads to further metabolic

adjustments in processes such as glycolysis, TCA cycle, amino acid transport and hypoxia, among others.

1.2.1 Aims

In the present study, we took a multi-level approach, where both the expression system and the strain were engineered (Figure 1.1). We evaluated different methods to increase the efficiency of protein entry into the secretory pathway by promoting co-translational translocation, not only through selection of the leader peptide but also by exploiting an alternative mechanism to promote SRP binding via the 3' untranslated region – a novel approach to enhance translocation. We also optimized the pathway using a variety of non-protein specific strategies, including expansion of the ER for improvement of the secretory pathway capacity, disruption of ERAD components for impaired protein degradation and addition of ER exit recognition sites. This resulted in an optimal plasmid harboring novel components and a series of strains with new interventions and novel combinations. When used together, the secretion of three different proteins from a variety of origins: a bacterial endoglucanase, a fungal β-glucosidase and a hybridoma single chain antibody fragment was substantially improved.

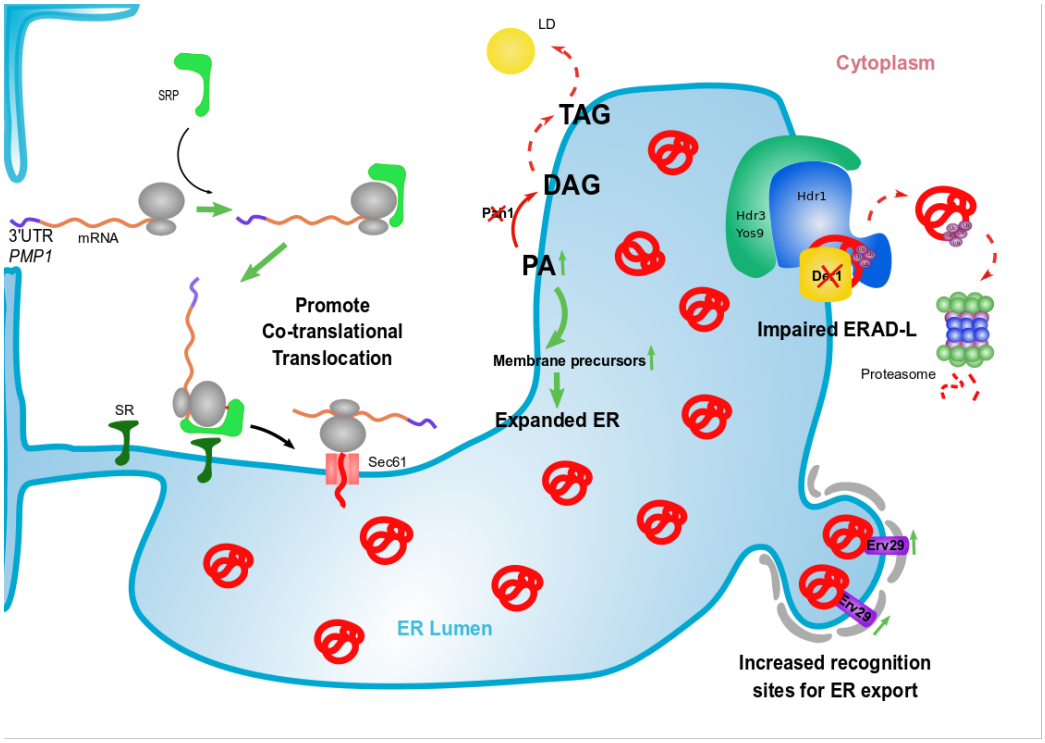

Figure 1.1. Overview of the secretory pathway engineering strategies explored in this study. Efficient entry into the endoplasmic reticulum was promoted through co-translational translocation. Recruitment and strong binding of the signal recognition particle (SPR) for ER targeting toward the SRP receptor (SR) was accomplished though engineering of the secretion signal and use of a novel terminator. Translocation and translation take place simultaneously thought the Sec61 translocon. The endoplasmic reticulum membrane was engineered via deletion of PAH1 to re-direct lipid flux from formation of lipid droplet (LD) - diacylglycerol (DAG) and triacylglycerol (TAG)- toward synthesis of membrane precursors. The machinery for retro-translocation and targeting to the proteasome was impaired via DER1 knock-out. Efficient ER exit and protein packing into COPII vesicles for further trafficking in the secretory pathway was enabled though overexpression of Erv29.

1.3 Materials and Methods

1.3.1 Strains and vectors

Oligonucleotides and gBlocks were ordered from Integrated DNA Technologies (San Diego, CA) and are described in Supplementary Materials Table S1.1. T4 DNA ligase, NEBuilder® HiFi DNA Assembly Master Mix, OneTaq® Quickload® DNA polymerase, and deoxynucleotides were bought from New England Biolabs (Ipswhich, MA). Restriction enzymes were from New England Biolabs or Thermo Fisher Scientific (Walthman, MA). KOD Hot Start DNA Polymerase was ordered from Millipore Sigma (Burlington, MA). All PCR-amplified sequences were confirmed via sequencing at Eaton Bioscience (San Diego, CA) or Genewiz (San Diego, CA).

Transformation of plasmids and linear dsDNA for integration was performed using Frozen-EZ Yeast Transformation II Kit from Zymo Research (Irvine, CA). Total yeast genomic DNA extraction followed the protocol described by Sambrook and Green (2012). The resulting plasmids and strains are summarized in Table 1.1.

To create plasmid p2m, the ubi-tagged *URA3* marker of the vector pUb (Leber et al., 2015) was swapped by the native *URA3* marker using restriction sites *PacI* and *NheI* and the amplification product of primers FW_URA3 and RV_URA3 from pJC742 (Choi and Da Silva, 2014). To create the plasmid pCA, the PCR product of FW_CEN/ARS and RV_CEN/ARS from pJC742 was Gibson-assembled (Gibson et al., 2009) to the ~6.7 kb fragment of the *EcoRI*-digested p2m. To generate pCAMFa-CelAt, p2mMFa-CelAt and pUbMFa-CelAt; the secretion peptide preproMFa fused to endoglucanase CelA from *C. thermocellum* and its native dockerin were amplified from the plasmid pAt (Tsai et al., 2010) using primers FW_CelAt and RV_CelAt and then cloned into pCA, p2m or pUB using *PmeI* and *RsrII* restriction sites. The forward primer adds a Kozak consensus sequence in front of the start codon to facilitate ribosome binding and

subsequent translation initiation (Kozak, 1981). Plasmids pCAOMFa-CelAt , pCAOrestMFa-CelAt, p2mOMFa-CelAt, p2mOrestMFa-CelAt, pUbOMFa-CelAt and pUbOrestMFa-CelAt were generated by Gibson Assembly of the gBlocks Ost1proMFa or Ost1proMFaREST (after amplification using FW_Ost1pro and RV_Ost1pro for introduction of the phosphate group) and *AarI* and *PmeI*-digested pCAMFa-CelAt, p2mMFa-CelAt and pUbMFa-CelAt. gBlocks also contained a Kozak a consensus sequence. The selection of codons for insertion of the REST sequence in gBlock Ost1proMFaREST was based on codon usage described by (Pechmann et al., 2014). Plasmids p2mMFa-BglDf and pUbOMFa-BglDf were constructed from the Gibson assembly of *ClaI* and *RsrII*-digestion products of p2mMFa-CelAt and pUbOMFa-CelAt, respectively, with the PCR product of primers FW_proMFa-BGlDf and RV_proMFa-BGlDf, using pBGLf (Tsai et al., 2010) as a template. A three-piece Gibson assembly was used to construct p2mMFa-4420mRFP and pUbOMFa-4420mRFP using i) the PCR product from FW_proMFa-4420 and RV_4420 ii) PCR product from FW_mRFP and RV_mRFP and iii) *ClaI* and *RsrII*-digested p2mMFa-CelAt or pUbOMFa-CelAt. The template for pieces i) and ii) was provided by Prof. Jered Haun (Haun and Hammer, 2008). To change terminators, the 3'untranslated regions of *PMP1* and *PMP2* were amplified from the yeast DNA genome, as described by (Chartron et al., 2016) using primers pairs FW_3UTR_tPMP1 + RV_3UTR_tPMP1, and FW_3UTR_tPMP2 + FW_3UTR_tPMP2 . The sequence used as t*PGK1* was chosen based on (Yamanishi et al., 2013) and was amplified from genomic DNA using FW_3UTR_tPGK1 and RV_3UTR_tPGK1. All terminators were cloned using restriction sites *XhoI* and *NheI*.

1.3.2 Construction of protospacer, CRISPR vector and donor DNA

Gene integration and deletion was performed using the MoClo Yeast Toolkit (Lee et al., 2015). Protospacer sequences were constructed by annealing equimolar quantities of primers (FW_gRNA_PHA1KO + RV_gRNA_PHA1KO or FW_gRNA_XI-3+ RV_gRNA_XI-3) using

duplex buffer (100 mM Potassium Acetate; 30 mM HEPES, pH 7.5). *BsmBI* Golden Gate Assembly of pYTK050 and annealed primers was used to generate gRNA. After adding connectors, the transcriptional unit was assembled into a multi-copy plasmid harboring a *URA3* auxotrophic marker and a cassette expressing Cas9 under the control of the medium strength promoter of *pRPL18B* (pYTK017).

The repair DNA used for knocking-out *PAH1* was created by PCR of the 20-bp overlapping sequences: FW_Donor_PAH1KO_full and RV_Donor_PAH1KO_fullORF. The template for Erv29 donor DNA was created by amplification from the genome using primers FW_ERV29 and RV_ERV29 and subsequent Gibson assembly with the *NotI*-linerarized plasmid pUbOFa-CelAt. This allowed for comparison of co-expression in vector system vs. integration. The *TEF1*p-Erv29-*CYC1*t repair cassette was created by amplification using FW_XI-3_Up_CYC1t and RV_XI-3_Down_TEF1. The high expression integration site was chosen based on (Mikkelsen et al., 2012).

Integrations were performed by co-transformation of 1 µg of Cas9/gRNA plasmid and 2.5-4 µg of linear donor DNA, as described by (Lee et al., 2015). Clones were screened via Colony PCR and positive colonies were confirmed by Sanger sequencing. Counter-selection of the Cas9/gRNA plasmid was performed using YPD 2% (20 g/L dextrose, 20 g/L peptone, 10 g/L yeast extract) with 1 mg/mL of 5-FOA.

1.3.3 Media and cultivation

Escherichia coli strain XL-1 blue was cultivated in Luria Bertani (LB) medium containing either 100 mg/ml of Ampicillin, 25 mg/mL of Chloramphenicol or 50 mg/mL Kanamycin, based on recommendations by Addgene. *S. cerevisiae* strains were grown in SDC-A (20 g/L dextrose, 5 g/L casamino acids, 5g/L ammonium sulfate, 1.7 g/L yeast nitrogen base without amino acids, 50 mg/L adenine) at 250 rpm and 30ºC.

For expression experiments, cells were inoculated from fresh SDC-A plates (with 20% agar) into 5 ml of liquid SDC-A and grown overnight. Cells were then transferred (initial OD_{600}=0.05) to fresh 5 ml of SDC-A and cultivated 18-20 h. This culture was used as the inoculum for the experimental cultures in 5 ml tubes (initial OD_{600}=0.05), which were grown for 24 h, 36 h, 48 h, 72 h or 96 h. For each sample, optical density was measured at 600 nm in a Shimadzu UV-2450 spectrophotometer (Columbia, MD), and the sample was centrifuged at x2500 g for 5 min. The activity or fluorescence of the supernatant was then analyzed.

1.3.4 Extracellular activity and fluorescence assays

The endoglucanase activity of the supernatant was measured using the *endo*-Cellulase Assay Kit CellG5 (Megazyme, Wicklow, Ireland) by mixing 6.25 µl of the supernatant with 6.25 µl of pre-equilibrated CELLG5 substrate in a clear 96-well plate (Corning, Corning NY). After incubation for 25 min at 37ºC, 187.6 µl of stopping solution were added, and absorbance was measured at 405 nm in a plate reader (SpectraMax M2, Molecular Devices, San Jose, CA). This protocol maintains the proportion of reagents advised in the manufacturer instructions. Samples were run at different dilutions to ensure linearity. Dilutions were prepared using a 100 mM sodium acetate buffer (pH=5.50). Blanks were determined using the supernatant from strains transformed with the empty vector (i.e., pCA, p2m, pUb).

The activity of β-glucosidase was determined by hydrolyzation of *p*-nitrophenyl-β-D-glucopyranoside (pNPG,Sigma-Aldrich, St. Louis, MO) by slight modification of the protocol described by (Strahsburger et al., 2017). An aliquot of 57.2 µl of supernatant was mixed with 28.5 µl of 5mM pNPG in a transparent 96-well plate (Corning, Corning NY). After incubation for 30 min at 30ºC, 114.3 µl of stopping solution were added, and absorbance was measured at 405 nm in the plate reader. Samples were run at different dilutions to ensure linearity. Dilutions were prepared using 100 mM sodium acetate buffer (pH=5.50). Blanks were determined using the

supernatant from strains transformed with the empty vector (i.e. pCA, p2m, pUb). Activity of the supernatant was measured at 48 h.

To determine levels of 4-4-20-mRP secreted, 200 µl of supernatant was placed in a 96-well Nunc black plate (Thermo Scientific, Waltham, MA). Fluorescence was measured using an excitation wavelength of 584 nm and emission wavelength of 612 nm in the plate reader. Blanks were determined using the supernatant from strains transformed with the empty vector (i.e., p2m, pUb). Fluorescence of the supernatant was evaluated at 96 h.

1.3.5 Statistical analysis

Statistical analysis was performed by one-way or two-way ANOVA using Post Hoc Tukey's test to account for multiple comparisons (variance is estimated from the whole set of data) (Tukey, 1949).

Table 1.1. Summary of Plasmids and Strains constructed for this study

Strain/Plasmid	**Description**	**Reference**
Strains		
BY4741	MATa *his*3Δ1 *leu*2Δ0 *met*15Δ0 *ura*3Δ0	Open Biosystems
BYΔ*pah1*	BY4741 *pah1*Δ	This study
BYErv29	BY4741 *XI-3::TEF1*p-*erv29-CYC1t*	This study
BYΔ*der1*	BY4741 *der1*::KanMx	Open Biosystems
BYΔ*der1*Δ*pah1*	BY4741 *der1*::KanMx *pah1*Δ	This study
BYΔ*der1*Δ*pah1*Erv29	BY4741 *der1*::KanMx *pah1*Δ *XI-3::TEF1*p-*erv29-CYC1*t	This study
BYAcc1m	BY4741 Δ*met*17::*PGK1*p-*acc1*^{S1157A}-*LEU2*	(Choi and Da Silva, 2014)
BYAcc1mΔ*pah1*	BY4741 Δ*met*17::*PGK1*p-*acc1*^{S1157A}-*LEU2 pah1*Δ	This study
BYAcc1mΔ*pah1*Δ*der1*Δ*pah1*	BY4741 Δ*met*17::*PGK1*p-*acc1*^{S1157A}-*LEU2 der1*Δ*pah1*Δ *XI-3::TEF1*p-*erv29-CYC1*t	This study
BYAcc1mΔ*pah1*Δ*der1*Δ*pah1* Erv29	BY4741 Δ*met*17::*PGK1*p-*acc1*^{S1157A}-*LEU2 pah1*Δ *XI-3::TEF1*p-*erv29-CYC1*t	This study
Plasmids		
pCA	C/A plasmid, two *TEF1* promoters, two *CYC1* terminators and *URA3* maker	This study
p2m	Yeast 2µ plasmid, two *TEF1* promoters, two *CYC1* terminators and *URA3* maker	This study
pUb	Yeast 2µ plasmid, two *TEF1* promoters, two *CYC1* terminators, ubi-tagged *URA3* selectable maker	Based on pXP842U-Bi (Leber et al., 2016)
pCAMFα-CelAt	pCA backbone. Promotes secretion of the endoglucanase CelA from *C. thermocellum* and its native dockerin using pre-pro-MFα signal peptide	This study

pCAOMFα-CelAt	pCA backbone. Promotes secretion of the endoglucanase CelA from *C. thermocellum* and its native dockerin using Ost1-pro-MFα signal peptide.	This study
pCAOrestMFα-CelAt	pCA backbone. Promotes secretion of the endoglucanase CelA from *C. thermocellum* and its native dockerin using Ost1-pro-MFα signal peptide with a REST sequence.	This study
p2mMFα-CelAt	p2m backbone. Promotes secretion of the endoglucanase CelA from *C. thermocellum* and its native dockerin using pre-pro-MFα signal peptide.	This study
p2mOFα-CelAt	p2m backbone. Promotes secretion of the endoglucanase CelA from *C. thermocellum* and its native dockerin using Ost1-pro-MFα signal peptide.	This study
p2mOrestFα-CelAt	p2m backbone. Promotes secretion of the endoglucanase CelA from *C. thermocellum* and its native dockerin using Ost1-pro-MFα signal peptide with a REST sequence.	This study
pUbMFα-CelAt	pUb backbone. Promotes secretion of the endoglucanase CelA from *C. thermocellum* and its native dockerin using pre-pro-MFα signal peptide.	This study
pUbOFα-CelAt	pUb backbone. Promotes secretion of the endoglucanase CelA from *C. thermocellum* and its native dockerin using Ost1-pro-MFα signal peptide.	This study
pUbOrestFα-CelAt	pUb backbone. Promotes secretion of the endoglucanase CelA from *C. thermocellum* and its native dockerin using Ost1-pro-MFα signal peptide with a REST sequence.	This study
pUbOFα-CelAt-*PMP1*t	pUb backbone with one *PMP1* terminator. Promotes secretion of the endoglucanase CelA from *C. thermocellum* and its native dockerin using Ost1-pro-MFα signal peptide.	This study
pUbOFα-CelAt-*PMP2*t	pUb backbone with one *PMP2* terminator. Promotes secretion of the endoglucanase CelA from *C. thermocellum* and its native dockerin using Ost1proMFα signal peptide.	This study
p2mMFα-BglDf	p2m backbone. Promotes secretion of the fungal protein b-glucosidase BglI from *T. aurantiacus* fused to the dockerin of *R. flavefaciens* using pre-pro-MFα signal peptide.	This study
pUbOFα-BglDf	pUb backbone. Promotes secretion of the fungal protein b-glucosidase BglI from *T. aurantiacus* fused to the dockerin of *R. flavefaciens* using Ost1-pro-MFα signal peptide.	This study
pUbOFα-BglDf-*PMP1*t	pUb backbone with one *PMP1* terminator. Promotes secretion of the fungal protein b-glucosidase BglI from *T. aurantiacus* fused to the dockerin of *R. flavefaciens* using Ost1-pro-MFα.	This study
pUbOFα-BglDf-*PMP2*t	pUb backbone with one *PMP2* terminator. Promotes secretion of the fungal protein b-glucosidase BglI from *T. aurantiacus* fused to the dockerin of *R. flavefaciens* using Ost1-pro-MFα.	This study
p2mMFα-4420mRFP	p2m backbone. Promotes secretion of the anti-fluorescein single-chain antibody derived from myeloma cells 4-4-20 fused to a fluorescent reporter mRFP derived from Discosima sp using pre-pro-MFα.	This study
pUbOFα-4420mRFP	pUb backbone. Promotes secretion of the anti-fluorescein single-chain antibody derived from myeloma cells 4-4-20 fused to a fluorescent reporter mRFP derived from Discosima sp using Ost1-pro-MFα.	This study
pUbOFα-4420mRFP-*PMP1*t	pUb backbone with one *PMP1* terminator. Promotes secretion of the anti-fluorescein single-chain antibody derived from myeloma cells 4-4-20 fused to a fluorescent reporter mRFP derived from Discosima sp using Ost1-pro-MFα.	This study
pUbOFα-4420mRFP-*PMP2*t	pUb backbone with one *PMP2* terminator. Promotes secretion of the anti-fluorescein single-chain antibody derived from myeloma cells 4-4-20 fused to a fluorescent reporter mRFP derived from Discosima sp using Ost1-pro-MFα.	This study

1.4 Results and Discussion

1.4.1 Engineering the expression system: copy number and secretion signal

Increases in plasmid copy number and promoter strength do not necessarily result in improved secretion levels (Ernst, 1986; Liu et al., 2012; Parekh et al., 1995). Different hypotheses have been proposed to explain this phenomena, such as saturation of the ER folding capacity (Parekh et al., 1995), poor translation efficiency due to high RNA turnover (Liu et al., 2012) or selection against cells populations with higher copy number (Ernst, 1986). However, little attention has been paid to the efficiency of the translocation step. It is known that the widely used secretion signal pre-pro-MFα1 undergoes post-translational translocation (Ng et al., 1996), a less efficient mode of entry into the secretory pathway. We sought to alleviate this bottleneck by promoting co-translational translocation via signal peptide engineering. Based on a 2014 study (Fitzgerald and Glick, 2014), the signal peptide of the alpha subunit from the oligosaccharyltransferase complex of the ER lumen (Ost1) was fused to the pro- region of the MFα1 leader sequence. The first section promotes co-translational translocation and is cleaved upon ER entry, while the latter harbors an ER export sequence that is cut in the late Golgi (Young and Robinson, 2014). Selection of the first 22 amino acid sequence of Ost1 was made based on SignalP 3.0 prediction (Bendtsen et al., 2004; Rakestraw et al., 2009). Supporting the use of Ost1 against other co-translational promoting leaders is its strong interaction with SRP (Pechmann et al., 2014).

We also evaluated whether a local slow-down of translation upon emergence of the secretion signal from the ribosomal tunnel would further promote SRP interaction (Pechmann et al., 2014) and result in increased extracellular levels. This would favor ER targeting against cytosolic elongation in the competition among these processes. To do this, we added a ‘REST’ sequence of six rare codons 34-40 amino acids (the approximate length of the ribosomal tunnel) downstream of the hydrophobic core of the signal. The latter was determined by computation of

the Kyte-Doolittle plot using the ExPASy server (Gasteiger et al., 2003). For all our initial experiments, the endoglucanase fused to its native dockerin (CelAt) was used as a reporter.

To find the optimal copy number and compare the secretion of an endoglucanase driven by the pre-proMFα, Ost1-proMFα and Ost1-proMFαREST leader sequences, a set of nine vectors were constructed (pCAMFα-CelAt, pCAOMFα-CelAt, pCAOrestMFα-CelAt, p2mMFα-CelAt, p2mOMFα-CelAt, p2mOrestMFα-CelAt, pUbMFα-CelAt, pUbOMFα-CelAt, and pUbOrestMFα-CelAt) and transformed into BY4741. Three copy number levels were explored: i) low copy using centromeric origin of replication, ii) high-copy 2μ vector, and iii) higher-copy by combining the 2μ origin of replication with a *URA3* auxotroph marker tagged with a ubiquitin/N-degron under the control of the weak promoter *KEX2*p (Chen et al., 2012).

Cells were grown in SDC-A for 24 h and optical density at 600 nm as well as activity of the supernatant after cell pelleting were measured. Figure 1.2 shows activity per cell of all the combinations explored. Overall, when using the centromeric plasmid, all leaders result in comparable levels of secretion. For the 2μ-based plasmid, pre-pro-MFα1 and Ost1-proMFαREST showed similar extracellular actives. However, secretion increased by up to 46% for p2mOMFα-CelAt (*p<0.05). The highest extracellular levels were observed when using pUb combined with the Ost1 signal.

Secretion driven by the pre-pro-MFα1 (yellow bars) did not show a statistically significant increase with copy number, in agreement with Parekh et al. (1995). In contrast, for the engineered peptide Ost1-pro-MFα, secretion did increase when changing from the C/A to the 2μ plasmids (blue bars), with up to a 2.7-fold increase for pUbOMFα-CelAt (***p<0.001) with respect to pCAOMFα-CelAt. When the Ost1-proMFαREST was used, changing from pCA to p2m did not result in statistically significant changes in secretion, but addition of the ubiquitin tag to the marker

did result in a 58.2% increase with respect to the centromeric plasmid (pink bars, *p<0.05). Introduction of the REST sequence, however did not improve secretion, but instead resulted in a 31% (*p<0.05) or 26% (*p<0.05) reduction when compared to the Ost1-pro-MFα in p2m and pUb respectively. This could be attributed to a decrease in mRNA stability due to the use of codons that had the least translational efficiency – based on the ratio of tRNA availability with respect to the demand for secretory proteins described by Pechmann et al., (2014) – for the design of the REST sequence. It has been shown that changing optimal codons for non-optimal codons results in destabilization of mRNA (Presnyak et al., 2015) and all the codons used for the REST sequence are considered non-optimal in that study.

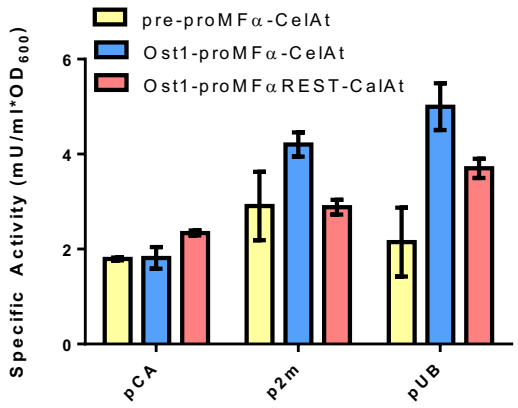

Figure 1.2. Effect of expression system on extracellular specific activity of bacterial endoglucanase CelAt. The different plasmid backbones utilized (pCA, p2m and pUB) are shown on the x-axis in order of increasing copy number. Different color of the bars show the secretion peptides studied: the native pre-proMFa (yellow) and engineered leaders Ost1-pro-MFα (blue) and Ost1-proMFαREST (pink). Error bars represent SEM of three biological replicates.

Improvements in secretion as copy number increased when using the engineered peptides suggest that translocation was indeed a bottleneck of the secretion process. Promoting co-translational translocation may alleviate it, leading to higher extracellular levels in the presence of higher mRNA copies. Based on these observations, we chose the pUb vector that incorporates the Ost1-pro-MFα secretion signal for further studies. A just published study supports our decision,

as this leader sequence was shown to promote efficient protein secretion in *Pichia pastoris* (Barrero et al., 2018).

1.4.2 Engineering the endoplasmic reticulum: dimensions, retro-translocation and exit

To alleviate secretory bottlenecks beyond translocation, we rationally engineered components of the yeast early secretory pathway, starting with the membrane of the endoplasmic reticulum. The gene *PAH1* encodes for a cytoplasmic phosphatidate (PA) phosphatase that is recruited to the ER membrane for synthesis of diacylglycerol (DAG) from phosphatidic acid (PA) (Figure 1.1). PA is localized in the ER lipid bilayer and is the precursor of the cell membrane phospholipids. Upon synthesis, DAG is transformed into triacylglycerol (TAG), the main component of lipid droplets (Fakas et al., 2011). Knocking-out *PAH1* results in impaired formation of lipid droplets, re-direction of lipid flux toward synthesis of membrane precursors and consequent proliferation of ER/nuclear membrane (Santos-Rosa et al., 2005). The deletion of this gene has successfully improved heterologous membrane protein expression in *Yarrowia lipolytica* (Guerfal et al., 2013) and has enhanced production of ER membrane-associated enzymes for triterpene synthesis in *S. cerevisiae* (Arendt et al., 2017). We thus hypothesized that ER membrane proliferation would be also beneficial for protein secretion by means of ER expansion and increased levels of lipids available for trafficking vesicle formation (Klein et al., 2014). Using CRISPR/Cas9, we deleted *PAH1* from BY4741 and transformed it with the plasmid pUbOMFα-CelAt. After growth for 96 h, optical density and extracellular activity were measured. As seen in Figure 1.3A, the BYΔ*pah1* strain increased endoglucanase secretion by 80% (***p<0.001). This intervention did not have significant effects on final cell density (Figure S1.1). This improvement in secretion can be due to both increased membrane precursors and attenuation of ER stress caused by membrane expansion (Schuck et al., 2009).

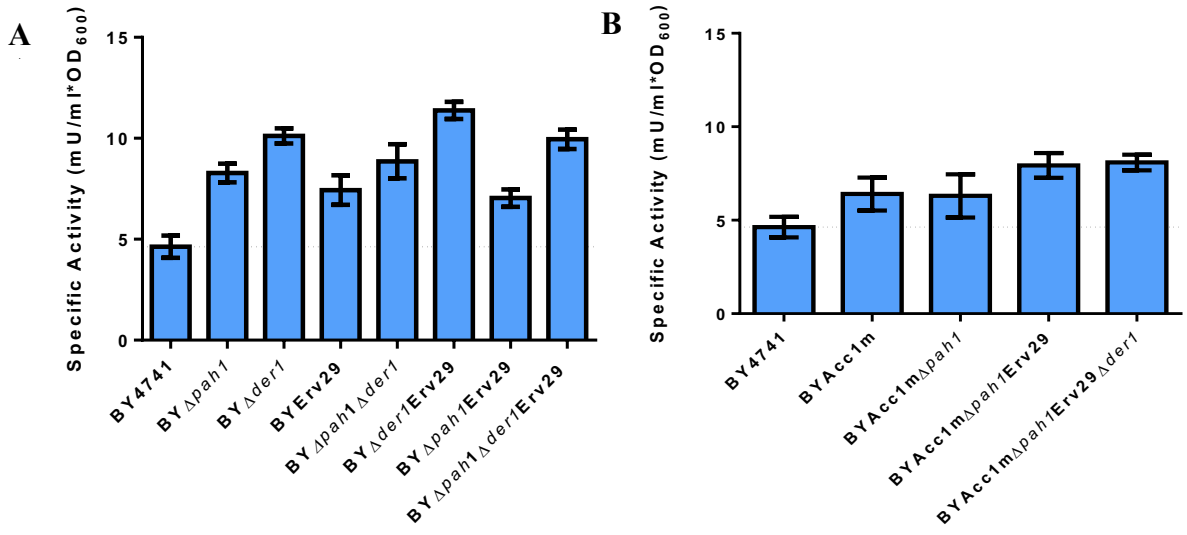

Figure 1.3. A) Secretion from different strain backgrounds transformed with the plasmid pUbOFα-CelAt at 96 h. B) Secretion from different strain backgrounds with Acc1m integrated and transformed with the plasmid pUbOFα-CelAt at 96 h. Results show average of endoglucanase extracellular specific activity. Error bars represent SEM of three biological repeats.

We also sought to further promote membrane proliferation via overexpression of the acetyl-CoA carboxylase mutant Acc1^{S1157A}(Acc1m); this mutation increases Acc1 activity, resulting in increased production of polyketides and fatty acids (Choi and Da Silva., 2014). However, this did not enhance secretion (Figure 1.3B). Acc1m not only causes changes in total lipid content, but also shifts lipid composition toward longer acyl-chains (Besada-Lombana et al., 2017; Hofbauer et al., 2014). This results in nuclear localization of Opi1, a transcriptional repressor of genes involved in the biosynthesis of phospholipid precursors (Hofbauer et al., 2014). Therefore, overexpression of the Acc1m may be negatively affecting our ER membrane expansion approach by reducing synthesis of membrane precursors – despite increasing total fatty acid content. Cues to the relevance of the role of Opi1 in secretion come from a report where its deletion led to expanded ER and improved extracellular production of full-chain antibodies (de Ruijter et al., 2016). It will be interesting to test in the future the effects on secretion of the combination of BYAcc1m and deletion of both *PAH1* and *OPI1*.

The genes responsible for ER-associated degradation (ERAD) machinery are upregulated when the quality control (QC) of the ER is activated, leading to retro-translocation to the cytoplasm and subsequent targeting to the proteasome (Travers et al., 2000a; Young and Robinson, 2014). Moreover, it has been reported that deletion of ERAD components constitutively activates a partial UPR response as a compensatory mechanism, resulting in a potential improvement of the ER folding capacity (Travers et al., 2000a). Activation of the UPR as a mechanism to enhance protein secretion is supported by reports where overexpression of the active form of Hac1 improved extracellular levels of some proteins (Payne et al., 2008; Valkonen et al., 2003).

Der1 is an ERAD-associated transmembrane protein in charge of initiating polypeptide export from the ER lumen to the cytoplasm (Mehnert et al., 2014). Moreover, its deletion leads to higher levels of UPR activation with respect to knock-out of other ERAD members (Travers et al., 2000a). Therefore, the deletion of Der1 was evaluated for increased secretion (Figure 1.1). The strain BYΔ*der1* was transformed with pUbOMFα-CelAt and extracellular activity of endoglucanase was evaluated at 96 h. Figure 1.3A shows that strain BYΔ*der1* increases the endoglucanase specific extracellular activity by 2.2-fold with respect to the baseline strain (***p<0.001). When this intervention was combined with deletion of *PAH1*, no further change was observed. Despite impairing an important cell function, deletion of *DER1* had no detrimental effects on cell growth (Figure S1.1). Partial activation of the UPR in strain BYΔ*der1* strain was confirmed by detection of the spliced form of Hac1 when CelAt is being overexpressed (Figure S1.2). This, along with a diminished retro-translocation may have led to the observed improvements in endoglucanase secretion.

Efficient trafficking from the ER to the Golgi complex takes place via COPII vesicles. Transmembrane receptors mediate interaction between the cargo inside the lumen and Sec24, localized on the cytoplasmic side of the ER (Bonifacino and Glick, 2004; Dancourt and Barlowe,

2010; Melero et al., 2018). The I-L-V motif present in the pro-MFα1 region is recognized by the ER multi-spanning transmembrane receptor Erv29, allowing efficient packing of the α-factor precursor into COPII vesicles (Otte and Barlowe, 2004). Disruption of *ERV29* gene results in accumulation of protein inside the ER and consequent absence of pre-pro-MFα-driven secretion (Fitzgerald and Glick, 2014; Huang et al., 2015). In order to ensure the presence of enough ER exit recognition sites, we constitutively overexpressed *ERV29* (Figure 1.1) via integration of an extra copy under the control of *TEF1*p in the high-expression site XI-3 (Mikkelsen et al., 2012). Resulting strains were then transformed with the pUbOFα-CelAt plasmid and extracellular endoglucanase activity was measured at 96 h. BYErv29 increases protein secretion by 60% (***p<0.001) with respect to the baseline strain (Figure 1.3A). Integration of the cassette *TEF1*p-Erv29-*CYC1*t was compared to episomal co-overexpression (using the same promoter and terminator) and showed 15% higher extracellular endoglucanase activity (Figure S1.3).

When Erv29 integration was combined with deletion of *PAH1* (BYΔ*pah1*Erv29), no significant improvements were observed. However, multiplexing with the *DER1* knock-out (BYΔ*der1*Erv29) showed the highest levels of endoglucanase secreted, with a 2.5-fold improvement with respect to the baseline strain (***p<0.001) (Figure 1.3A). Further strain engineering of the BYΔ*der1*Erv29 by including a *PAH1* deletion to create BYΔ*pah1*Δ*der1*Erv29 did not result in further improvement, but led to a 29% decreased secretion (***p<0.001). Addition of the Acc1m to these interventions did not improve secretion levels (Figure 1.3B).

1.4.3 Engineering the 3' untranslated region: an alternative mechanism of co-translational translocation

The choice of terminator is usually overlooked during the design stage of secretory strategies. However, these functional 3'UTR sequences are known to impact mRNA stability, mRNA abundance, and post-transcriptional processing (Yamanishi et al., 2013). Another

interesting role of some 3‘-untranslated regions (3’UTR) has been recently suggested via SRP-associated ribosome profiling. It was found that a fraction of RNCs destined to the secretory pathway were bound to SRP before emergence of the secretion signal (Chartron et al., 2016). This means that SRPs can be pre-recruited independently of the leader sequence. This is the case, for example, of co-translationally translocated proteins that are shorter than the ribosomal tunnel such as Pmp1 and Pmp2. Experimental evidence along with previous studies led to the conclusion that the 3’UTR played an important role in the SRP pre-recruitment process (Ast and Schuldiner, 2013; Chartron et al., 2016; Loya et al., 2008). It is important to note that the 3’UTR is not sufficient for SRP-mediated targeting, as binding of the leader peptide to the Srp54 hydrophobic groove is important during the co-translational translocation process (Chartron et al., 2016).

To test whether secretion benefits from SRP pre-recruitment, the *CYC1* terminator in plasmid pUBOFα-CelAt was changed to the 3’UTR sequences of *PMP1* or *PMP2* to create the plasmids pUbOFα-CelAt-*PMP1*t and pUbOFα-CelAt-*PMP2*t. These were transformed into the best-performing engineered strains, and the effect of these 3’UTRs was assessed by measuring extracellular activity after growth for 96 h.

The endoglucanase extracellular specific activity improved significantly when using the 3’UTR of *PMP1* and *PMP2* (Figure 1.4; green and red bars, respectively) relative to that from *CYC1* (blue bars). This was consistent for all six strains tested. For the baseline strain BY4741, a 2.3-fold increase (***p<0.001) and 3-fold increase (***p<0.001) were observed for *PMP2*t and *PMP1*t, respectively. Thus, the best performance was observed for the *PMP1*t and this trend was observed at 48 h and 96 h (Figure S1.4). The best-performing strain resulted from a combination of *PMP1*t with the knock-out of *DER1*, showing a 5.4-fold improvement (***p<0.001) with respect to BY4741 transformed with the original pUbOFα-CelAt. These results provide additional evidence supporting a translocation bottleneck.

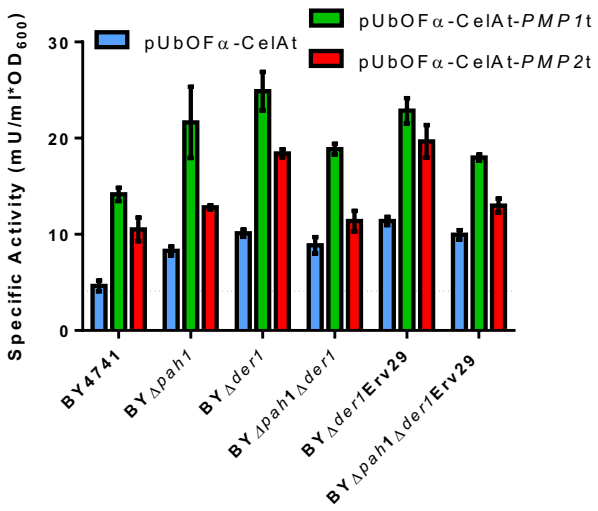

Figure 1.4. Secretion from different strain backgrounds transformed with the plasmid pUBOFa-CelAt (blue bars), pUBOFa-CelAt-tPMP2 (red bars) and pUBOFa-CelAt-tPMP1 (green bars). Results show average endoglucanase extracellular specific activity, and error bars represent SEM of three biological replicates.

Terminators influence other mRNA traits like stability, processing and translational efficiency. Thus, the positive changes observed may be partially due to improvements in these aspects. An interesting insight in this respect is provided by a genome-wide analysis of *S. cerevisiae*'s terminatome (Yamanishi et al., 2013). This study ranked the activity of 5302 terminator regions based on GFP fluorescence intensity under the control of the *TDH3* promoter, normalized to the signal provided by the *PGK1* terminator. Values reported for *CYC1*t, *PMP1*t and *PMP2*t were 0.556, 0.709 and 1.036 respectively, demonstrating enhanced expression with the membrane protein terminators. Therefore, we tested whether the use of a 3'UTR sequence from a non-secretory gene that shows higher terminator activity would also improve endoglucanase secretion. Interestingly, replacement of *CYC1*t in pUbOFα-CelAt by *PGK1*t led to decreased and inconsistent secretion with respect to *CYC1*t, as shown in Figure 1.5. This demonstrates how improved terminator activity does not necessarily correlate to improved secretion and supports the

partial functional role of the 3'UTR of *PMP1* and *PMP2* in the translocation process. To our knowledge, this is the first secretory engineering approach that takes advantage of this mechanism.

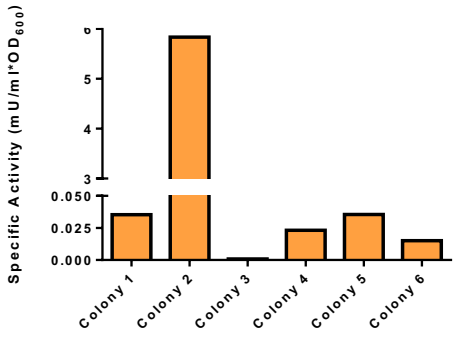

Figure 1.5. Extracellular specific activity of CelAt when *CYC1*t is changed to *PGK1*t in the plasmid pUbOFα-CelAt at 24 h. Up to six independent colonies were tested.

A summary of the most beneficial interventions identified in this study and the effects on endoglucanase extracellular specific activity are shown in Figure 1.6. Fold-changes are calculated with respect to the baseline strain transformed with the multi-copy plasmid p2mMFα-CelAt. The first step was to change the secretion peptide from pre-pro-MFα to Ost1-pro-MFα to promote a more efficient mode of entry into the secretory pathway. This combined with the use of the ubi-tagged *URA3* auxotrophic marker led to a 69% (***p<0.001) improvement. Additional tuning of the expression system to further improve co-translational translocation was accomplished through the use of *PMP1*t, providing a 5.1-fold increase (***p<0.001) in secretion levels. Finally, among the different approaches tested for strain engineering, impairment of the ERAD by deletion of *DER1* (combined with the optimal vector) resulted in an overall 9.1-fold change (***p<0.001) at 96 h. An enhancement of up to 11.5-fold for the same strain was observed at 48 h (Figure S1.5).

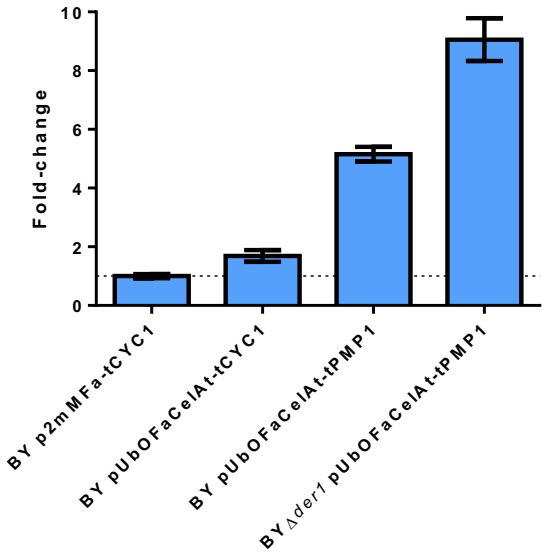

Figure 1.6. Summary of best-performing interventions. Fold-change improvements with respect to the baseline strain transformed with p2mMFα-CelAt at 96 h. Error bars represent SEM of three biological replicates.

1.4.4 Evaluating strategies for the secretion of alternate heterologous proteins

To test the general applicability of the approaches described above, we extended the study to other two proteins from different origins: a fungal β-glucosidase fused to a dockerin domain (BglDf) (Tsai et al., 2010) and a hybridoma single-chain antibody fragment C-tagged with a monomeric red fluorescent protein (4-4-20-mRFP) (Haun and Hammer, 2008). These were sub-cloned into p2mMFα-CelAt, pUbOFα-CelAt, pUbOFα-CelAt-*PMP1*t and pUbOFαCelAt-*PMP2*t by replacement of the endoglucanase gene. Extracellular activity and fluorescence were monitored at different time points. Figure 1.7 shows fluorescence and activities with respect to BY4741 transformed with p2mMFα-BglDf and p2mMFα-4420mRFP. Secretion of both proteins benefited from the effects of *PMP1*t, showing 3.2-fold (BglDf, ***p<0.001) and 2.1-fold (4-4-20, *p<0.05) increases when expressed in the pUb vector and fused to the engineered peptide (Figure 1.7., non-slashed bars)

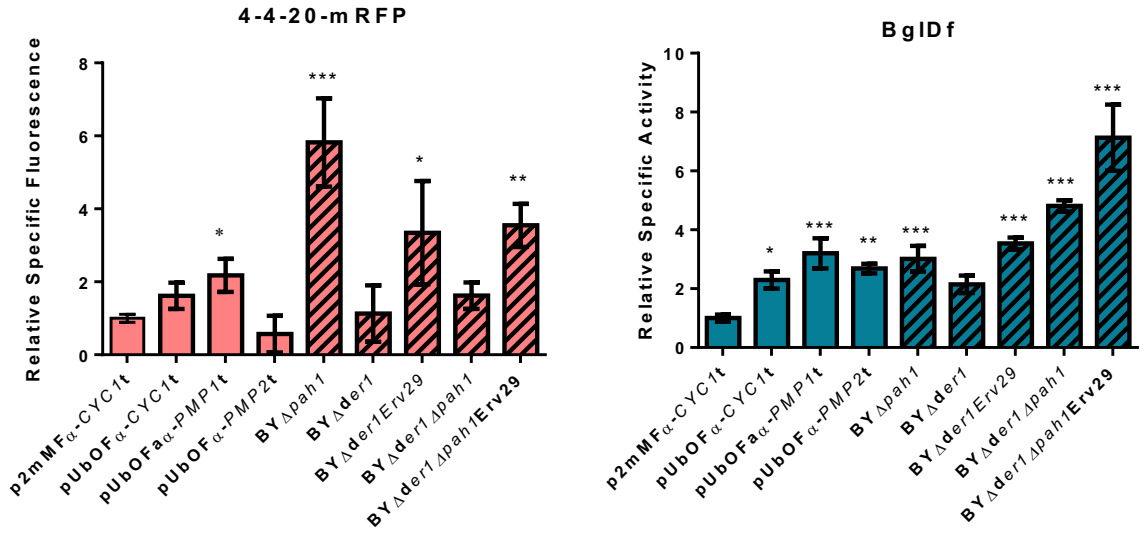

Figure 1.7. Secretion of heterologous proteins scFv 4-4-20-mRFP and β-glucosidase BglDf. A) Relative specific fluorescence of mRFP with respect to the signal of the baseline strain transformed with the plasmid p2mMFa-4420mRFP at 96 h. Fold-changes for BY4741 transformed with different expression systems are shown in pink non-slashed bars. Engineered strains transformed with pUbMFa-4420mRFP-tPMP1 are represented by pink slashed bars. B) Specific β-glucosidase activity relative to the baseline strain transformed with the plasmid p2mMFa-BglDf at 48 h. Fold-changes for BY4741 transformed with different expression systems are shown in dark blue non-slashed bars. Engineered strains transformed with pUbMFa-BglDf-tPMP1 are represented by dark blue slashed bars. Error bars represent SEM of three biological replicates. Statistical significance with respect to control (*p<0.05, **p<0.01, ***p<0.001).

For further study of secretion of the short fragment antibody tagged with the monomeric red fluorescent protein, the optimum vector pUbOFα-4420mRFP-*PMP1*t was then transformed into the engineered strains (Figure 1.7A, slashed bars). Strain BYΔ*pah1* had the highest extracellular relative specific fluorescence, with a 5.8-fold increase (***p<0.001) with respect to the original strain BY4741 carrying the plasmid p2mMFα-4420mRFP. Strain BYΔ*der1* alone did not have a significant impact, despite being the best-performing strain for CelAt. Interestingly, when combined with Erv29 to obtain strain BYΔ*der*1Erv29, a 4.3-fold improvement (**p<0.01) was observed. Knocking out *PAH1* from BYΔ*der1*Erv29 did not produce a further increase in fluorescence, as previously observed for CelAt (Figure 1.7A).

For evaluation of secretion of the fungal β-glucosidase, the optimum vector pUbOFa-BglDf-*PMP1*t was transformed into the same group of strains (Figure 1.7B, slashed bars). For this protein, strains BYΔ*der1* and BYΔ*pah1* showed similar extracellular specific activity to those observed for the baseline strain with the same vector. However, the combination of both interventions in the strain BYΔ*der1*Δ*pah1* increased secretion by 56% (**p<0.01) relative to BY4741 transformed with pUbOFa-BglDf-*PMP1*t, leading to a 4.8-fold increase (***p<0.001) relative to the baseline strain transformed with p2mMFα-BglDf. Further addition of the ER exit recognition sites to create BYΔ*der1*Δ*pah1*Erv29 resulted in an overall improvement of 7.1-fold (***p<0.001).

1.5 Conclusions

The three proteins evaluated benefited to different extents from the secretory pathway engineering strategies proposed herein. Using the bacterial endoglucanase (CelAt) as a reporter, we engineered the expression system by testing different origins of replication and different secretion peptides. The highest extracellular levels were detected using the engineered Ost1-pro-MFα leader sequence –which promotes co-translational translocation – along with a 2μ plasmid that has an N-degron in the *URA3* marker. This combination showed up to a 2.8-fold increase with respect to the native pre-pro-MFα, which did not show similars changes in CelAt secretion with copy number.

Once the optimal expression system was chosen, engineering of the endoplasmic reticulum by deletion of *PAH1*, *DER1* and overexpression of Erv29, led to 80%, 120% and 60% increases in secretion of CelAt relative to the baseline strain, respectively. When combining the *DER1* knock-out and Erv29 overexpression, a 2.5-fold improvement was observed. To further improve co-translational translocation, we took advantage of the 3'UTR-mediated SRP pre-recruitment. By changing our *CYC1* terminator to those of the short transmembrane proteins Pmp1 and Pmp2, we observed a 2.3-fold and a 3.0-fold increase of CelAt extracellular activity. This is the first report that takes advantage of this mechanism to engineer protein secretion. When combining the use of *PMP1*t in the optimal expression system with the deletion of *DER1*, an improvement of up to 11.5-fold of extracellular CelAt was observed with respect to the baseline strain using the pre-pro-MFα peptide.

Promoting co-translational translocation via the engineered peptide and *PMP1*t also proved beneficial for secretion of the two other proteins tested, a hybridoma single-chain antibody fragment 4-4-20-mRFP and a fungal β-glucosidase. These results indicate that translocation is a bottleneck of the secretion process and co-translational translocation can be used as a general

strategy to overcome it. Thus, the plasmid expression system pUbOMFα that harbors the *PMP1*t has the potential to be widely applicable and improve secretion of other proteins.

Once the optimal expression system was found, we proceeded to test it in different strain backgrounds. While deletion of *DER1* was the most beneficial for CelAt, the deletion of *PAH1* resulted in the best secretion of 4-4-20-mRFP with a 5.8-fold increase relative to the baseline strain and plasmid. For the fungal β-glucosidase, the best-performing strain was BYΔ*pah1*Δ*der1*Erv29, with an improvement of 7.1-fold relative to baseline strain and plasmid. All proteins benefited from the triple intervention strain BYΔ*pah1*Δ*der1*Erv29. This strain may be a candidate for secretion of other proteins as well.

1.6 References

Arendt P, Miettinen K, Pollier J, De Rycke R, Callewaert N, Goossens A. 2017. An endoplasmic reticulum-engineered yeast platform for overproduction of triterpenoids. *Metab. Eng.* **40**:165–175. http://dx.doi.org/10.1016/j.ymben.2017.02.007.

Ast T, Schuldiner M. 2013. All roads lead to Rome (but some may be harder to travel): SRP-independent translocation into the endoplasmic reticulum. *Crit. Rev. Biochem. Mol. Biol.* **48**:273–288.

Barlowe CK, Miller EA. 2013. Secretory protein biogenesis and traffic in the early secretory pathway. *Genetics* **193**:383–410.

Barrero JJ, Casler JC, Valero F, Ferrer P, Glick BS. 2018. An improved secretion signal enhances the secretion of model proteins from Pichia pastoris. *Microb. Cell Fact.*:1–13. https://link.springer.com/article/10.1186/s12934-018-1009-5?utm_source=researcher_app&utm_medium=referral&utm_campaign=MKEF_USG_Researcher_inbound.

Bendtsen JD, Nielsen H, Heijne G Von, Brunak S. 2004. Improved prediction of signal peptides : SignalP 3 . 0. *J. Mol. Biol.* **340**:783–795. http://www.ncbi.nlm.nih.gov/entrez/query.fcgi?cmd=Retrieve&db=PubMed&dopt=Citation&list_uids=15223320.

Besada-Lombana PB, Fernandez-Moya R, Fenster J, Da Silva NA. 2017. Engineering Saccharomyces cerevisiae fatty acid composition for increased tolerance to octanoic acid. *Biotechnol. Bioeng.* **114**:1531–1538.

Besada-Lombana PB, McTaggart TL, Da Silva NA. 2018. Molecular tools for pathway engineering in Saccharomyces cerevisiae. *Curr. Opin. Biotechnol.* **53**:39–49. http://dx.doi.org/10.1016/j.copbio.2017.12.002.

Bonifacino JS, Glick BS. 2004. The Mechanisms of Vesicle Budding and Fusion. *Cell* **116**:153–166.

Brake a J, Merryweather JP, Coit DG, Heberlein U a, Masiarz FR, Mullenbach GT, Urdea MS, Valenzuela P, Barr PJ. 1984. Alpha-factor-directed synthesis and secretion of mature foreign proteins in Saccharomyces cerevisiae. *Proc. Natl. Acad. Sci. U. S. A.* **81**:4642–4646.

Bukau B, Horwich AL. 1998. The Hsp70 and Hsp60 chaperone machines. *Cell* **92**:351–366.

Butz JA, Niebauer RT, Robinson AS. 2003. Co-expression of molecular chaperones does not improve the heterologous expression of mammalian G-protein coupled receptor expression in yeast. *Biotechnol. Bioeng.* **84**:292–304.

Chartron JW, Hunt KCL, Frydman J. 2016. Cotranslational signal-independent SRP preloading during membrane targeting. *Nature* **536**:224–8. http://dx.doi.org/10.1016/j.cell.2016.07.025%5Cnhttp://www.ncbi.nlm.nih.gov/pubmed/27565344%5Cnhttp://www.ncbi.nlm.nih.gov/pubmed/27487213%5Cnhttp://dx.doi.org/10.1016/j.cell.2016.07.024%5Cnhttp://www.ncbi.nlm.nih.gov/pubmed/27545349.

Chen Y, Partow S, Scalcinati G, Siewers V, Nielsen J. 2012. Enhancing the copy number of episomal plasmids in Saccharomyces cerevisiae for improved protein production. *FEMS Yeast Res.* **12**:598–607.

Chigira Y, Oka T, Okajima T, Jigami Y. 2008. Engineering of a mammalian O-glycosylation pathway in the yeast Saccharomyces cerevisiae: production of O-fucosylated epidermal growth factor domains. *Glycobiology* **18**:303–14. http://www.ncbi.nlm.nih.gov/pubmed/18252777.

Choi JW, Da Silva NA. 2014. Improving polyketide and fatty acid synthesis by engineering of the yeast acetyl-CoA carboxylase. *J. Biotechnol.* **187**:56–59. http://dx.doi.org/10.1016/j.jbiotec.2014.07.430.

Costa EA, Subramanian K, Nunnari J, Weissman JS. 2018. Defining the physiological role of SRP in protein-targeting efficiency and specificity. *Science (80-.).* **359**:689–692.

Covino R, Hummer G, Ernst R. 2018. Integrated Functions of Membrane Property Sensors and a Hidden Side of the Unfolded Protein Response. *Mol. Cell* **71**:458–467. https://doi.org/10.1016/j.molcel.2018.07.019.

Dancourt J, Barlowe C. 2010. Protein Sorting Receptors in the Early Secretory Pathway. *Annu. Rev. Biochem.* **79**:777–802. http://www.annualreviews.org/doi/10.1146/annurev-biochem-061608-091319.

Davison SA, den Haan R, van Zyl WH. 2016. Heterologous expression of cellulase genes in natural Saccharomyces cerevisiae strains. *Appl. Microbiol. Biotechnol.* **100**:8241–8254. http://dx.doi.org/10.1007/s00253-016-7735-x.

Ernst JF. 1986. Improved secretion of heterologous proteins by Saccharomyces cerevisiae : effects of promoter substitutions in alpha factor fusions. *DNA* **5**:483–492.

Fakas S, Qiu Y, Dixon JL, Han GS, Ruggles K V., Garbarino J, Sturley SL, Carman GM. 2011. Phosphatidate phosphatase activity plays key role in protection against fatty acid-induced toxicity in yeast. *J. Biol. Chem.* **286**:29074–29085.

Feyder S, De Craene J-O, Bär S, Bertazzi D, Friant S. 2015. Membrane Trafficking in the Yeast Saccharomyces cerevisiae Model. *Int. J. Mol. Sci.* **0067**:1509–1525.

Fitzgerald I, Glick BS. 2014. Secretion of a foreign protein from budding yeasts is enhanced by cotranslational translocation and by suppression of vacuolar targeting. *Microb. Cell Fact.* **13**:125. http://www.microbialcellfactories.com/content/13/1/125.

Gasteiger E, Gattiker A, Hoogland C, Ivanyi I, Appel RD, Bairoch A. 2003. ExPASy: The proteomics server for in-depth protein knowledge and analysis. *Nucleic Acids Res.* **31**:3784–3788.

Gibson DG, Young L, Chuang RY, Venter JC, Hutchison CA, Smith HO. 2009. Enzymatic assembly of DNA molecules up to several hundred kilobases. *Nat. Methods* **6**:343–345.

Guerfal M, Claes K, Knittelfelder O, De Rycke R, Kohlwein SD, Callewaert N. 2013. Enhanced membrane protein expression by engineering increased intracellular membrane production. *Microb. Cell Fact.* **12**:122. http://www.microbialcellfactories.com/content/12/1/122.

Hashimoto Y, Koyabu N, Imoto T. 1998. Effects of signal sequences on the secretion of hen lysozyme by yeast: construction of four secretion cassette vectors. *Protein Eng.* **11**:75–77.

Haun JB, Hammer D a. 2008. Quantifying nanoparticle adhesion mediated by specific molecular interactions. *Langmuir* **24**:8821–32. http://www.ncbi.nlm.nih.gov/pubmed/18630976.

Hegde RS, Bernstein HD. 2006. The surprising complexity of signal sequences. *Trends Biochem. Sci.* **31**:563–571.

Hofbauer HF, Schopf FH, Schleifer H, Knittelfelder OL, Pieber B, Rechberger GN, Wolinski H, Gaspar ML, Kappe CO, Stadlmann J, Mechtler K, Zenz A, Lohner K, Tehlivets O, Henry SA, Kohlwein SD. 2014. Regulation of gene expression through a transcriptional repressor that senses acyl-chain length in membrane phospholipids. *Dev. Cell* **29**:729–739.

Hou J, Tyo KEJ, Liu Z, Petranovic D, Nielsen J. 2012a. Metabolic engineering of recombinant protein secretion by Saccharomyces cerevisiae. *FEMS Yeast Res.* **12**:491–510.

Hou J, Tyo K, Liu Z, Petranovic D, Nielsen J. 2012b. Engineering of vesicle trafficking improves heterologous protein secretion in Saccharomyces cerevisiae. *Metab. Eng.* **14**:120–127. http://dx.doi.org/10.1016/j.ymben.2012.01.002.

Huang M, Bai Y, Sjostrom SL, Hallström BM, Liu Z, Petranovic D, Uhlén M, Joensson HN, Andersson-Svahn H, Nielsen J. 2015. Microfluidic screening and whole-genome sequencing identifies mutations associated with improved protein secretion by yeast. *Proc. Natl. Acad. Sci.* **112**:E4689–E4696. http://www.pnas.org/lookup/doi/10.1073/pnas.1506460112.

Huang M, Bao J, Hallström BM, Petranovic D, Nielsen J. 2017. Efficient protein production by yeast requires global tuning of metabolism. *Nat. Commun.* **8**. http://dx.doi.org/10.1038/s41467-017-00999-2.

Hwang J, Qi L. 2018. Quality Control in the Endoplasmic Reticulum: Crosstalk between ERAD and UPR pathways. *Trends Biochem. Sci.* **43**:593–605. https://doi.org/10.1016/j.tibs.2018.06.005.

Idiris A, Tohda H, Kumagai H, Takegawa K. 2010. Engineering of protein secretion in yeast: Strategies and impact on protein production. *Appl. Microbiol. Biotechnol.* **86**:403–417.

Klein T, Lange S, Wilhelm N, Bureik M, Yang TH, Heinzle E, Schneider K. 2014. Overcoming the metabolic burden of protein secretion in Schizosaccharomyces pombe - A

quantitative approach using13C-based metabolic flux analysis. *Metab. Eng.* **21**:34–45. http://dx.doi.org/10.1016/j.ymben.2013.11.001.

Kozak M. 1981. Possible role of flanking nucleotides in recognition of the aug initiator codon by eukaryotic ribosomes. *Nucleic Acids Res.* **9**:5233–5252.

Kurjan J, Herskowitz I. 1982. Structure of a yeast pheromone gene (MF alpha): a putative alpha-factor precursor contains four tandem copies of mature alpha-factor. *Cell* **30**:933–943.

Leber C, Choi JW, Polson B, Silva NA Da. 2016. Disrupted Short Chain Specific b - Oxidation and Improved Synthase Expression Increase Synthesis of Short Chain Fatty Acids in Saccharomyces cerevisiae **113**:895–900.

Leber C, Polson B, Fernandez-Moya R, Da Silva NA. 2015. Overproduction and secretion of free fatty acids through disrupted neutral lipid recycle in Saccharomyces cerevisiae. *Metab. Eng.* **28**:54–62.

Lee ME, DeLoache WC, Cervantes B, Dueber JE. 2015. A Highly Characterized Yeast Toolkit for Modular, Multipart Assembly. *ACS Synth. Biol.* **4**:975–986.

Liu Z, Tyo KEJ, Martínez JL, Petranovic D, Nielsen J. 2012. Different expression systems for production of recombinant proteins in Saccharomyces cerevisiae. *Biotechnol. Bioeng.* **109**:1259–1268.

Loya A, Pnueli L, Yosefzon Y, Wexler Y, Ziv-Ukelson M, Arava Y. 2008. The 3'-UTR mediates the cellular localization of an mRNA encoding a short plasma membrane protein. *RNA* **14**:1352–1365.

Mandon EC, Trueman SF, Gilmore R. 2013. Protein Translocation across the Rough Endoplasmic Reticulum. *Cold Spring Harb. Perspect. Biol.* **5**:303–368.

Matlack KES, Misselwitz B, Plath K, Rapoport TA. 1999. BIP acts as a molecular ratchet during posttranslational transport of prepro-α factor across the ER membrane [2]. *Cell* **97**:553–564.

Mehnert M, Sommer T, Jarosch E. 2014. Der1 promotes movement of misfolded proteins through the endoplasmic reticulum membrane. *Nat. Cell Biol.* **16**:77–86. http://dx.doi.org/10.1038/ncb2822.

Melero A, Chiaruttini N, Karashima T, Riezman I, Funato K, Barlowe C, Riezman H, Roux A. 2018. Lysophospholipids Facilitate COPII Vesicle Formation. *Curr. Biol.* **28**:1950–1958.e6.

Mikkelsen MD, Buron LD, Salomonsen B, Olsen CE, Hansen BG, Mortensen UH, Halkier BA. 2012. Microbial production of indolylglucosinolate through engineering of a multi-gene pathway in a versatile yeast expression platform. *Metab. Eng.* **14**:104–111. http://dx.doi.org/10.1016/j.ymben.2012.01.006.

Nagel KM. 2018. Introduction to Biologic and Biosimilar Product Development and Analysis. Ed. Karen M Nagel. Cham: Springer International Publishing. AAPS Introductions in the Pharmaceutical Sciences. http://link.springer.com/10.1007/978-3-319-98428-5.

Ng DTW, Brown JD, Walter P. 1996. Signal sequences specify the targeting route to the endoplasmic reticulum membrane. *J. Cell Biol.* **134**:269–278.

Nyathi Y, Wilkinson BM, Pool MR. 2013. Co-translational targeting and translocation of proteins to the endoplasmic reticulum. *Biochim. Biophys. Acta - Mol. Cell Res.* **1833**:2392–2402. http://dx.doi.org/10.1016/j.bbamcr.2013.02.021.

Otte S, Barlowe C. 2004. Sorting signals can direct receptor-mediated export of soluble proteins into COPII vesicles. *Nat. Cell Biol.* **6**:1189–1194.

Parekh R, Forrester K, Wittrup D. 1995. Multicopy overexpression of bovine pancreatic trypsin inhibitor saturates the protein folding and secretory capacity of saccharomyces cerevisiae. *Protein Expr. Purif.*

Payne T, Hanfrey C, Bishop AL, Michael AJ, Avery S V, Archer DB. 2008. Transcript-specific translational regulation in the unfolded protein response of Saccharomyces cerevisiae. *FEBS Lett.* **582**:503–9. http://www.ncbi.nlm.nih.gov/pubmed/18206654.

Pechmann S, Chartron JW, Frydman J. 2014. Local slowdown of translation by nonoptimal codons promotes nascent-chain recognition by SRP in vivo. *Nat. Struct. Mol. Biol.* **21**:1100–1105.

Presnyak V, Alhusaini N, Chen YH, Martin S, Morris N, Kline N, Olson S, Weinberg D, Baker KE, Graveley BR, Coller J. 2015. Codon optimality is a major determinant of mRNA stability. *Cell* **160**:1111–1124. http://dx.doi.org/10.1016/j.cell.2015.02.029.

Rakestraw JA, Sazinsky SL, Piatesi A, Antipov E, Wittrup KD. 2009. Directed evolution of a secretory leader for the improved expression of heterologous proteins and full-length antibodies in Saccharomyces cerevisiae. *Biotechnol. Bioeng.* **103**:1192–1201.

Rapoport TA, Li L, Park E. 2017. Structural and Mechanistic Insights into Protein Translocation. *Annu. Rev. Cell Dev. Biol.* **33**:369–390. http://www.annualreviews.org/doi/10.1146/annurev-cellbio-100616-060439.

Robinson AS, Hines V, Wittrup KD. 1994. Protein Disulfide Isomerase Overexpression Increases Secretion of Foreign Proteins in Saccharomyces cerevisiae. *Bio/Technology* **12**:381–384. http://www.nature.com/doifinder/10.1038/nbt0494-381.

de Ruijter JC, Koskela E V., Frey AD. 2016. Enhancing antibody folding and secretion by tailoring the Saccharomyces cerevisiae endoplasmic reticulum. *Microb. Cell Fact.* **15**:1–18.

Sakai A, Shimizu Y, Hishinuma F. 1988. Isolation and characterization of mutants which show an oversecretion phenotype in Saccharomyces cerevisiae. *Genetics* **119**:499–506.

Sambrook J, Green MR. 2012. Molecular Cloning: A Laboratory Manual. Ed. Micahel R Green, J Sambrook 4th Erditi. Cold Spring Harbor. Vol. 1 1-2028 p.

Santos-Rosa H, Leung J, Grimsey N, Peak-Chew S, Siniossoglou S. 2005. The yeast lipin Smp2 couples phospholipid biosynthesis to nuclear membrane growth. *EMBO J.* **24**:1931–1941. http://emboj.embopress.org/cgi/doi/10.1038/sj.emboj.7600672.

Schmidt FR. 2004. Recombinant expression systems in the pharmaceutical industry. *Appl. Microbiol. Biotechnol.* **65**:363–372.

Schuck S, Prinz W a., Thorn KS, Voss C, Walter P. 2009. Membrane expansion alleviates endoplasmic reticulum stress independently of the unfolded protein response. *J. Cell Biol.* **187**:525–536.

Sheng J, Flick H, Feng X. 2017. Systematic optimization of protein secretory pathways in Saccharomyces cerevisiae to increase expression of hepatitis B Small Antigen. *Front. Microbiol.* **8**:1–10.

Srikrishnan S, Chen W, Da Silva NA. 2013. Functional assembly and characterization of a modular xylanosome for hemicellulose hydrolysis in yeast. *Biotechnol. Bioeng.* **110**:275–285.

Strahsburger E, de Lacey AML, Marotti I, DiGioia D, Biavati B, Dinelli G. 2017. In vivo assay to identify bacteria with β-glucosidase activity. *Electron. J. Biotechnol.* **30**:83–87. https://doi.org/10.1016/j.ejbt.2017.08.010.

Tang H, Bao X, Shen Y, Song M, Wang S, Wang C, Hou J. 2015. Engineering protein folding and translocation improves heterologous protein secretion in Saccharomyces cerevisiae. *Biotechnol. Bioeng.* **9999**:n/a-n/a. http://doi.wiley.com/10.1002/bit.25596.

Travers KJ, Patil CK, Wodicka L, Lockhart DJ, Weissman JS, Walter P. 2000a. Functional and genomic analyses reveal an essential coordination between the unfolded protein response and ER-associated degradation. *Cell* **101**:249–258.

Travers KJ, Patil CK, Wodicka L, Lockhart DJ, Weissman JS, Walter P, Francisco S. 2000b. Functional-and-Genomic-Analyses-Reveal-an-Essential-Coordination-between-the-Unfolded-Protein-Response-and-ER-Associated-Degradation_2000_Cell.pdf **101**:249–258.

Tsai SL, Goyal G, Chen W. 2010. Surface display of a functional minicellulosome by intracellular complementation using a synthetic yeast consortium and its application to cellulose hydrolysis and ethanol production. *Appl. Environ. Microbiol.* **76**:7514–7520.

Tsai SL, Oh J, Singh S, Chen R, Chen W. 2009. Functional assembly of minicellulosomes on the Saccharomyces cerevisiae cell surface for cellulose hydrolysis and ethanol production. *Appl. Environ. Microbiol.* **75**:6087–6093.

Tukey JW. 1949. Comparing Individual Means in the Analysis of Variance. *Biometrics* **5**:99. https://www.jstor.org/stable/3001913?origin=crossref.

Tyo KE, Liu Z, Petranovic D, Nielsen J. 2012. Imbalance of heterologous protein folding and disulfide bond formation rates yields runaway oxidative stress. *BMC Biol* **10**:16.

Valkonen M, Penttilä M, Saloheimo M. 2003. Effects of inactivation and constitutive expression of the unfolded- protein response pathway on protein production in the yeast Saccharomyces cerevisiae. *Appl. Environ. Microbiol.* **69**:2065–72.

Wang BD, Chen DC, Kuo TT. 2001. Characterization of a Saccharomyces cerevisiae mutant with oversecretion phenotype. *Appl. Microbiol. Biotechnol.* **55**:712–720.

Wang T-Y, Huang C-J, Chen H-L, Ho P-C, Ke H-M, Cho H-Y, Ruan S-K, Hung K-Y, Wang I-L, Cai Y-W, Sung H-M, Li W-H, Shih M-C. 2013. Systematic screening of glycosylation- and trafficking-associated gene knockouts in Saccharomyces cerevisiae identifies mutants with improved heterologous exocellulase activity and host secretion. *BMC Biotechnol.* **13**:71. http://www.pubmedcentral.nih.gov/articlerender.fcgi?artid=3766678&tool=pmcentrez&rendertype=abstract.

Wu X, Rapoport TA. 2018. Mechanistic insights into ER-associated protein degradation. *Curr. Opin. Cell Biol.* **53**:22–28. https://linkinghub.elsevier.com/retrieve/pii/S0955067418300048.

Yamanishi M, Ito Y, Kintaka R, Imamura C, Katahira S, Ikeuchi A, Moriya H, Matsuyama T. 2013. A genome-wide activity assessment of terminator regions in saccharomyces cerevisiae provides a “terminatome” toolbox. *ACS Synth. Biol.* **2**:337–347.

Young CL, Robinson AS. 2014. Protein folding and secretion: Mechanistic insights advancing recombinant protein production in S. cerevisiae. *Curr. Opin. Biotechnol.* **30**:168–177. http://dx.doi.org/10.1016/j.copbio.2014.06.018.

Chapter 2

Development of an Extracellular Glucose Sensor for Substrate-Dependent Surface Display of Cellulases

2.1 Abstract

Efficient lignocellulosic biomass hydrolysis into fermentable sugars is key for the economic viability of production of biofuels and biorenewable platform molecules from second-generation feedstocks. A promising approach consists of merging the saccharification of lignocellulose into fermentable sugars and the production of the desired chemical (e.g. ethanol, medium chain fatty acids, triacetic acid lactone, etc.) into a single step. This is known as Consolidated Bioprocessing (CBP). CBP can be accomplished by hydrolysis of hemicellulose and cellulose via display of a xylanosome and a cellulosome. To achieve complete saccharification without wasting valuable resources, it is desired to design a consortium with the ability to secrete enzymes depending on the carbon source available. We have developed an extracellular glucose sensor that would enable the display of the cellulosome enzymes only in the presence of the cellulosic fraction of lignocellulose by leveraging cellulose-dependent signal amplification. Our initial design was based on the *HXT1* promoter. After characterization of its glucose-responsiveness, we engineered the *HXT1*p by changing its core to that of the strong *THD3*p. This led to an increase in expression levels of up to 81%. We proceeded to demonstrate glucose-mediated display of an enzyme by anchoring the β-glucosidase Bgl1 – the enzyme responsible for the last step of cellulose hydrolysis into glucose – to the surface of *S. cerevisiae*. This system was optimized by re-directing fatty acid pools from lipid droplet synthesis toward formation of membrane precursors via *PAH1* knock-out. This resulted in an up to 4.24-fold improvement with respect to the baseline strain. Finally, we observed cellobiose-dependent signal amplification, with increases in enzymatic activity between 55% and 91% when 2% cellobiose was added.

2.3 Introduction

The shift from oil-based chemical and fuel platforms to bio-based ones requires raw materials to sustain cell growth. Lignocellulosic biomass is the most abundant renewable source and can be sustainably obtained from agricultural residues, minimizing the conflict between food and chemical production (Hadar, 2013; Lopes, 2015). Lignocellulose comprises 90% of the plant cell wall (Faraco, 2013) and, depending on the source, has variable percentages of cellulose (38-50%), hemicellulose (23-32%) and lignin (15-25%). These components form a three-dimensional polymeric structure that plays a key role in the plant's structure and rigidity (Figure 2.1). Cellulose is a non-branched homopolymer of glucose units linked by β-(1→4) glycosidic bonds (Weifu Lee, 2013). These long linear chains associate into a highly stable nanometer-scale crystalline fiber by establishing hydrogen bonds. Formation of these interactions hinder the flexing of the polymeric chains that must occur during hydrolysis. In contrast, hemicellulose is a branched heteropolymer and does not form fibril structures. Its composition varies among species but is primarily formed of xylans, a backbone of β-(1→4)-glycosidic-linked xylose. Side-chains can be other pentoses such as arabinose or hexoses like glucose, galactose or mannose.

Fermentable sugars are found in the hemicellulose and cellulose fractions of lignocellulose, comprising between 75-85% of the total mass (Weifu Lee, 2013). However, the crystalline structure of cellulose results in the recalcitrance of lignocellulosic biomass to hydrolysis. This hinders a more extensive application of this abundant natural resource, primarily due to the elevated costs of the enzymes required for obtaining fermentable sugars (Tsai et al., 2009; Tsai et al., 2010). Moreover, the heteropolymeric nature of hemicellulose and low fermentability by most industrial microorganisms reduce the profitable use of this fraction (Gírio et al., 2010).

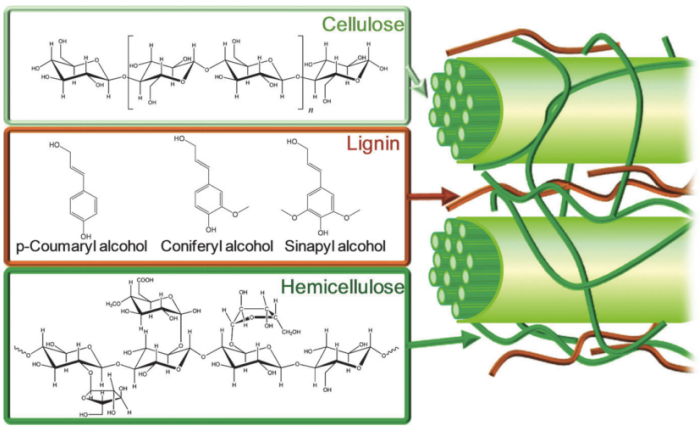

Figure 2.1. Lignocellulose structure and composition (Alonso et al., 2012).

The enzymes in charge of degrading cellulose via hydrolysis of β-(1→4) bonds are called cellulases and are divided into two different classes: endoglucanases and cellobiohydrolases (Weifu Lee, 2013). Endoglucanases are capable of hydrolyzing internal bonds in cellulose, acting preferably on amorphous zones. Their action generates new terminal ends, where cellobiohydrolases are able to act. The main product of this reaction is the disaccharide cellobiose, which can be transformed into two glucose by the action of a β-glucosidase (Pérez et al., 2002). The glucose formed after the series of these catalytic reactions is then available to the cells for synthesis of desired chemicals and fuels. Traditionally, cellulose saccharification and fermentation are performed as two separate processes. However, in order to reduce the cost of biorenewables production from cellulose, a novel strategy known as Consolidated Bioprocessing (CBP) has been developed (Lynd et al., 2005). CBP merges the transformation of cellulosic substrate into glucose and the fermentation process into a single step. This is accomplished by engineering the microorganism in charge of the chemical synthesis to also produce and secrete cellulolytic enzymes, alleviating the need for dedicated and separate enzyme production (Weifu Lee, 2013). One attractive candidate is the yeast *Saccharomyces cerevisiae*, due to its regular use in industry, the large number of molecular tools available, and the vast knowledge of its genome.

A promising approach towards the development of a CBP microorganism is the display of a cellulosome on the surface of the producing strain (Fan et al., 2012; Goyal et al., 2011; Tsai et al., 2009; Tsai et al., 2010; Tsai et al., 2013). The cellulosome is a structured enzyme complex present on the cell surface of many anaerobic bacteria that maximizes catalytic efficiency of cellulose hydrolysis based on its high level of enzyme-substrate synergy. The fibrillar protein scaffoldin is the principal component of the cellulosome and consists of at least one cellulose-binding domain (CBD) and repeating cohesins domains (Figure 2.2A). Each cohesin is docked with a particular cellulase tagged with the corresponding dockerin domain via a high affinity protein-protein interaction that is species specific (Doi and Kosugi, 2004; Tsai et al., 2013).

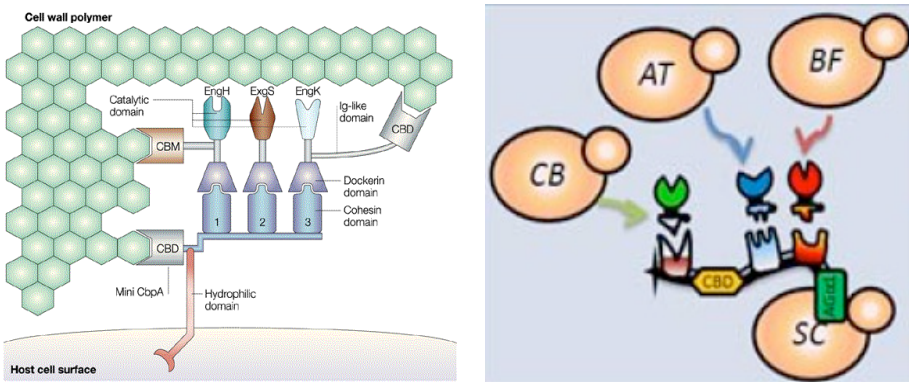

Figure 2.2. A) Cellulosome structure (Doi and Kosugi, 2004) B) yeast consortium approach for surface assembly of cellulosome (Goyal et al., 2011).

Over the past decade, many approaches to the development of a CBP microorganism for ethanol production have focused on the display of cellulosomes on the surface of *S. cerevisiae*. Work by our collaborators Tsai *et al*. (2009) showed that hydrolysis of cellulose using a synthetic cellulosome was more efficient than that of free enzymes, providing evidence of cellulosome synergistic effect. Further studies have developed the idea of a yeast consortium (Goyal et al., 2011), in which various yeast strains expressing different cellulases tagged with dockerin domains from different species were grown along with yeast expressing scaffoldins (Figure 2.2B). In that study, it was shown that control over the initial population played a key role in ethanol

productivity, obtaining ethanol yield changes of two-fold by simply fine-tuning cell population and enzyme ratio. This clearly indicates that secretion of enzymes should be finely regulated to attain maximal efficiency.

Based on the cellulosome approach, further advances in hemicellulose degradation have been made in our group. Srikrishnan *et al*. (2012) published the display of a functional xylanosome for the degradation of hemicellulose. Dockerin-tagged endoxylanase, β-xylosidase and acetylxylan esterase were assembled on the surface of *S.cerevisiae* using a scaffoldin with modular dockerins and a xylose-binding domain. This system was able to perform saccharification of birchwood xylan and presented higher degradation than free xylanases, demonstrating again the enzyme-enzyme and enzyme-substrate synergistic effect of these structures (Srikrishnan et al., 2013).

In order to improve CBP microorganisms for the production of biofuels and biorenewable platform molecules using the lignocellulose fermentable fraction as carbon source, we have focused on the development of an extracellular glucose sensor for controlled cellulase secretion. To achieve complete saccharification of fermentable lignocellulosic biomass, it is desired to develop cells with the ability to secrete enzymes depending on the carbon source accessible. This way, secretion of cellulases would occur when cellulose is available, while hemicellulases would be preferentially displayed when hemicellulose is the substrate present. To control cellulase secretion, our objective was to develop an extracellular glucose sensor based on a GPCR transduction cascade.

The natural adaptation of cellulosome composition to the environment has been reported for *Clostridium thermocellum*, an anaerobic thermophilic bacterium that has the highest cellulose utilization rate. Proteomic analysis has shown that *C. thermocellum* grown in cellulose presents higher levels of cellulosome enzymes and these are downregulated when cells grow in cellobiose (Gold and Martin, 2007). This phenomena has also been observed in other cellulolytic

microorganisms such as *Clostridium cellulolyticum* and *Clostridium cellulovorans* (Han et al., 2005).

The mechanism by which *C.thermocellum* is able to sense the extracellular composition of polymers was elucidated by Nataf *et al.* (2010) and involved σ factors (proteins required for the initiation of RNA synthesis in bacteria) and their repressors, anti-σ factors. It was found that some σ factors show specific intracellular interaction with transmembrane proteins having an extracellular carbohydrate-binding module that interacts with polysaccharides. In the absence of a substrate, this transmembrane protein will strongly interact with the σ factor and, therefore, the cellulosome component that is regulated by this σ factor will not be transcribed. In contrast, when the binding domain interacts with a polysaccharide, a conformational change in the intracellular domain occurs and the σ factor is released, promoting initiation of RNA synthesis of the cellulosome component that it regulates.

Yeast also possess the ability to sense multiple cues of nutrient availability in order to coordinate uptake, metabolism and regulatory networks required for cell fitness. For instance, in media where both galactose and glucose are present, galactose catabolism is repressed until glucose is exhausted (Escalante-Chong et al., 2015). This is due to the fact that glucose is the preferred carbon source in eukaryotic cells, including yeast. For this reason, cells have developed multiple glucose sensing systems, involving hexokinases, glucokinases, glucose carrier homologues and glucose repressors, among other proteins (Rolland et al., 2001). One of the glucose regulatory mechanisms exploited for metabolic engineering purposes is the use of glycolytic promoters (transcription depends on the presence of glucose and drops when it is depleted) for control of gene expression. The most widely used often belong to the glycolytic pathway, but there are many others that regulate other cellular functions. Some examples are: *PGK1*p, which controls expression of phosphoglycerate kinase; *PDG1*p for pyruvate

descarboxylase, and *ADH1*p for alcohol dehydrogenase, among many others (Da Silva and Srikrishnan, 2012). However, these regulation systems involve proteins and regulatory networks that sense intracellular concentrations of glucose, which do not necessarily reflect the extracellular composition.

One of the tools that yeast has for sensing extracellular cues are integral membrane G protein-coupled receptors (GPCRs) (Figure 2.3). The GPCR Gpr1 receptor is the one in charge of interacting with extracellular glucose (Rolland et al., 2002). It has seven transmembrane domains that are coupled to the G protein Gpa2 in the intracellular domain. When glucose is not bound to Gpr1, Gpa2 forms a complex with Rgs2, a regulator of heterodimeric G-protein that is responsible for stimulating the intrinsic GTPase activity of Gpa2, facilitating the formation of the inactive GDP-bound Gpa2 (Figure 2.3) (Versele et al., 1999). Upon binding to extracellular glucose, Gpr1 directs the formation of the GTP-bound active form of Gpa2 and adenylate cyclase Cyr1 is now able to interact with it. Glucose metabolism has also been shown to activate Ras proteins, which stimulate Cyr1 along with Gpa2. It is thought that Ras proteins are responsible for control of basal adenylate cyclase activity and the association of Gpa2 in response with Ras2 might enhance the responsiveness of Cyr1 stimulation by the GPCR system. Increasing levels of cAMP result in activation of protein kinase A (PKA) by binding of the cAMP to the regulatory subunit Bcy1. This interaction triggers the dissociation of the active kinase catalytic subunits Tpk1, Tpk2 or Tpk3 (Busti et al., 2010; Gancedo, 2008; Horák, 2013; Rolland et al., 2001). All three isoforms of PKA are now able to phosphorylate the hexose transporter repressor Rgt1, interrupting its interaction with the *HXT1* promoter and thus allowing gene transcription. PKA phosphorylation is sterically hindered by co-repressor Mth1 (Jouandot et al., 2011). Thus, full activation does not take place until disassociation of the repression complex, comprised of Rgt1, Std1, Mth1 and Ssn6-Tup1 (Jouandot et al., 2011; Roy et al., 2014). This is accomplished in two steps: i) glucose-mediated

targeting of Sdt1 and Mth1 to the proteasome via Snf3 and Rgt2 phosphorylation, and ii) destabilization of Rgt1 and Ssn6-Tup1 interactions due to PKA phosphorylation (Jouandot et al., 2011; Roy et al., 2014). This process allows differential transcriptional control of different hexose transporter (HXT) genes as a function of glucose concentration. At low levels, Mth1 is degraded but Rgt1 is not fully phosphorylated. This allows transcription of high affinity hexose transporters such as *HXT2*. At high glucose levels when Rgt1 is fully phosphorylated due to strong induction of PKA, Mth1 is still degraded but this time there is full induction of high glucose-induced HXT genes such as *HXT1* (Kim and Johnston, 2006).

Due to the fact that *HXT1* complete induction is regulated by the GPCR Gpr1, we will use this promoter as an extracellular glucose sensor by fusing it to dockerin-tagged cellulases (Figure 2.3). Detection of extracellular glucose will enable selective display of cellulases, only in the presence of the cellulosic fraction of lignocellulose via establishment of a positive-feedback loop (Figure 2.4). This process is primed by low levels of cellulase secretion triggered by the presence of glucose derived from de-lignification pretreatments such as wet oxidation (Klinke et al., 2002). When cellulose is present, these initially secreted cellulases will lead to depolymerization into its monomers, thus increasing glucose concentration. This rise in glucose is expected to escalate as more cellulases are secreted and cellulose degradation progresses, leading to full induction of the *HXT1* promoter.

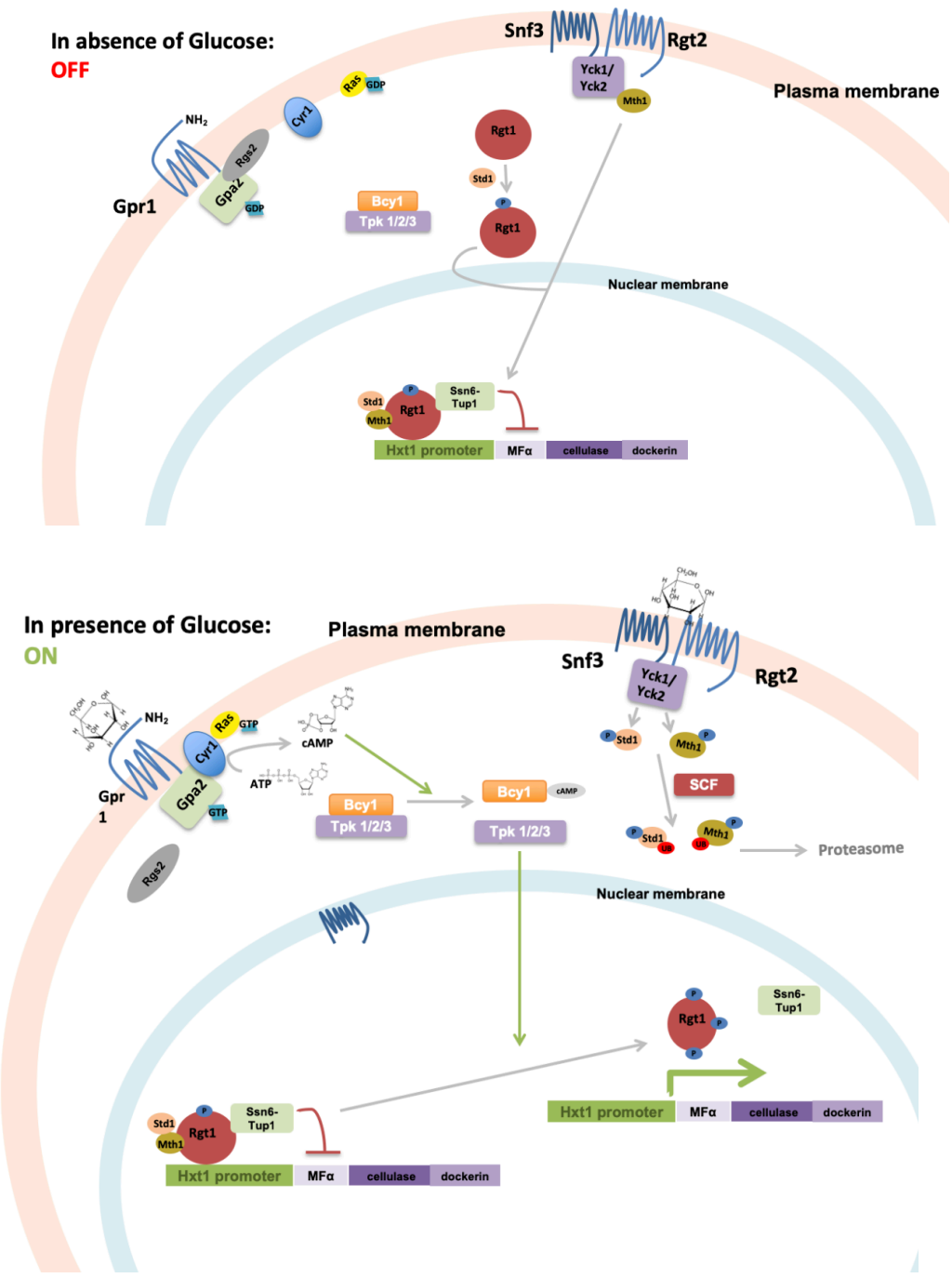

Figure 2.3. Extracellular glucose induction of *HXT1* promoter fusions to dockerin-tagged cellulases.

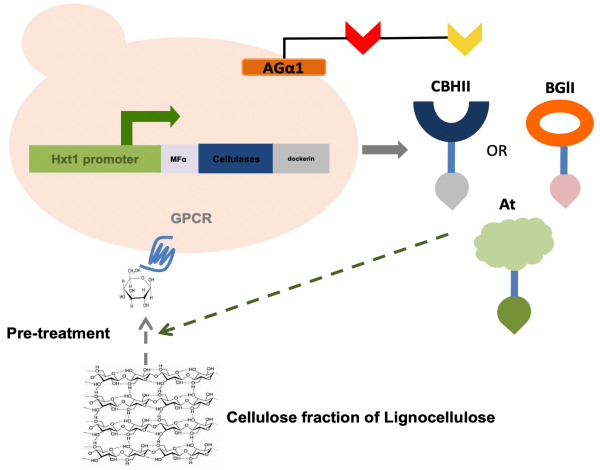

Figure 2.4. The selective display of cellulases in the presence of cellulose is triggered by residual glucose derived from lignocellulose pre-treatment process and a subsequent positive feedback loop that amplifies cellulase expression for complete cellulose degradation.

A series of examples of signal amplification by means of engineered positive feedback loops have been described in the literature. However, these approaches are different from the present study, as in most cases the positive feedback loop is based on the use of a promoter sequence that drives transcription of: i) its own activator and ii) the gene encoding for the output to be amplified (Matsu-Ura et al., 2018; Ryo et al., 2017; Williams et al., 2017). For instance, expression of cellulases in the filamentous fungi *Neurospora crassa* is driven by the transcription factor Clr2. The promoter *CBH1*p is also activated by Clr2. Therefore, when expression of Clr2 is driven by *CBH1*p, there is a 50-78% increase in cellulase expression (Matsu-Ura et al., 2018) due to amplification of Clr2 levels. In our approach, signal amplification is conditioned by the presence of cellulose.

2.3.1 Aims

The overall goal of this work was to improve CBP microorganisms for the production of biofuels and biorenewable platform molecules using the lignocellulose fermentable fraction as carbon source. To achieve complete saccharification, it is desired to design cells with the ability to secrete enzymes depending on the carbon source available. We have developed an extracellular

glucose sensor that will enable the display of cellulosome enzymes, only in the presence of the cellulosic fraction of lignocellulose. This is possible by leveraging cellulose-dependent signal amplification. To this end, we characterized the native *HXT1* promoter by measuring activation kinetics, expression levels as a function of glucose concentration, and the effect of galactose on its expression. We then proceeded to improve transcription levels via promoter engineering. Finally, to demonstrate the glucose-mediated display of enzymes (and thus potential application for cellulosome) enabled by our sensor, the engineered promoter was used to drive the surface display of the enzyme responsible for the last catalytic step of cellulose degradation. Strain engineering was used to improve the display, and cellobiose-dependent signal amplification was demonstrated.

2.4 Materials and Methods

2.4.1 Strains

'Ultracompetent' *Escherichia coli* strain XL1-Blue prepared using the Inoue Method (Sambrook and Green, 2012) were used for cloning and Golden Gate Assemblies. *Saccharomyces cerevisiae* strains used are listed in Table 2.1.

Table 2.1. List of Strains

Strain	**Description**	**Reference**
BY4741	MATa *his*3Δ1 *leu*2Δ0 *met*15Δ0 *ura*3Δ0	Open Biosystems
BYΔ*pah1*	BY4741 *pah1*Δ	Chapter 1

2.4.2 Construction of strains and expression vectors

Basic molecular biology protocols were based on Sambrook and Green (2012). Oligonucleotides were from Integrated DNA Technologies (San Diego, CA) and are described in Supplementary Materials Table S2.1. T4 DNA ligase, NEBuilder® HiFi DNA Assembly Master Mix, OneTaq® Quickload® DNA polymerase, restriction enzymes and deoxynucleotides were from New England Biolabs (Ipswhich, MA). KOD Hot Start DNA Polymerase was from Millipore Sigma (Burlington, MA). All PCR-amplified sequences were confirmed by Sanger sequencing analysis, either at Eaton Bioscience (San Diego, CA) or Genewiz (San Diego, CA).

Transformation of plasmids and linear dsDNA for integrations were performed using Frozen-EZ Yeast Transformation II Kit from Zymo Research (Irvine, CA). Total yeast genomic DNA extraction for PCR template and integration checking was performed using the protocol described by Sambrook and Green (2012).

Two sets of plasmids were constructed using different approaches: i) for secretion studies, generated either via cloning or Gibson Assembly (Gibson et al., 2009) and ii) for surface display studies, constructed via Golden Gate Assembly using the MoClo Yeast Toolkit (Lee et al., 2015).

Secretion plasmids are shown in Table 2.2 and were based on the vector pJC842 (Choi and Da Silva, 2014). The 750 base pairs upstream of the *HXT1* gene were amplified by PCR using primer pair FW_HXT1+RV_HXT1 and cloned into pJC842, replacing the existing *ADH2* promoter using *NotI* and *PmeI* restriction sites. The dockerin-tagged endoglucanase and β-glucosidase were amplified using primers FW_MFalpha+RV_CelA and FW_MFalpha+ RV_Bglf and templates At and the BGLf (Tsai et al., 2010) plasmids, kindly provided by Prof. Wilfred Chen (University of Delaware). The forward primer adds a Kozak consensus sequence in front of the start codon to facilitate ribosome binding and subsequent translation initiation. PCR products were cloned downstream of the *HXT1* promoter using restriction sites *PmeI* and *RsrII*. To generate the sequence of the minimal promoter core 'Core1' described by (Redden and Alper, 2015), primer pairs FW_HXT1Core1+ RV_HXT1Core, which contain a 20 bp overlap, were amplified using KOD to generate the 'Core 1 piece'. Then, the *HXT1* promoter variants were generated via Gibson Assembly between two PCR products that contain a 25 bp overlap: i) core sequence using either FW_HXT1THD3core+RV_HXT1THD3core or 'Core1 piece' and ii) FW_HXT1engBackbone + RV_HXT1engBackbone. The final plasmids are shown in Table 2.2.

Table 2.2. Plasmids constructed for secretion studies.

Plasmid	**Description**	**Reference**
pJC842	Multi-copy plasmid	(Choi and Da Silva, 2014)
pJC842-HXT1p	Multi-copy plasmid, harboring the *HXT1* promoter and *CYC1* terminator	This study
pJC842-HXT1p-CelAt	pJC842-HXT1p directing secretion of the endo-β-1,4-glucanase CelA from *C.thermocellum* with its native dockerin using the pre-pro-MFa.	This study

pJC842-HXT1p-BglDf	pJC842-HXT1p directing secretion of the β-glucosidase Bgl1 from *T.aurantiacus* fused with a dockerin from *R.flavefaciens* using the pre-pro-MFa.	This study
pJC842-HXT1^{core1}p-CelAt	pJC842-pHXT1-CelAt where the core sequence of *HXT1*p has been changed by the minimal 'Core1' described by (Redden and Alper, 2015)	This study
pJC842-HXT1^{core1}p-BglDf	pJC842-pHXT1-BglDf where the core sequence of *HXT1*p has been changed by the minimal 'Core1' described by (Redden and Alper, 2015)	This study
pJC842-HXT1^{THD3core}p-CelAt	pJC842-pHXT1-CelAt where the core sequence of *HXT1*p has been substituted by that of the strong *THD3* promoter.	This study
pJC842-HXT1^{THD3core}p-BglDf	pJC842-pHXT1-BglDf where the core sequence of *HXT1*p has been substituted by that of the strong *THD3* promoter.	This study

For surface display experiments, we used the MoClo Yeast Toolkit described by (Lee et al., 2015). We designed the parts described in Table 2.3, as they were not present in the original Toolkit: *HXT1*^{TDH3core}p, Aga1, Aga2, pre-proMFa, Aga-α and Bgl1. Bgl1 contained several internal BsmBI recognition sites, which were eliminated by a four-piece Gibson Assembly of the PCR products from: i) FW_BglDfSDM_Piece1 + RV_ BglDfSDM_Piece1 ii) FW_ BglDfSDM_Piece2 + RV_ BglDfSDM_Piece2 iii) FW_ BglDfSDM_Piece3 + RV_ BglDfSDM_Piece3, and iv) FW_ BglDfSDM_Piece4 + RV_ BglDfSDM _Piece4, using pJC842-pHXT1-BglDf as a template. Once it was confirmed that none of the templates contained either BsmBI or BsaI restriction sites, the PCR products of *HXT1*^{TDH3core}p (from primers FW_pHXT1_YTK2 +RV_pHXT1_YTK2 using pJC842-pHXT1^{THD3core}-CelAt as a template), Aga1 (FW_Aga1_YTK3+RV_Aga1_YTK3, from genomic DNA), Aga2 (FW_Aga2_YTK3a+ RV_Aga2_YTK3a, from genomic DNA), pre-pro-MFα (FW_prepoMFa_YTK3a+ RV_prepoMFa_YTK3a from At), Aga-α (FW_AgaAlpha_4a+RV_AgaAlpha_4a, from genomic DNA) and Bgl1 (FW_Bgl1 _YTK3b+RV_Bgl1_NoDockerin_YTK3b, from the Gibson assembly) were assembled to the Part Plasmid Entry Vector of the Yeast Toolkit (pYT001) using BsmBI-mediated Golden Gate assembly. This resulted in the generation of parts described in Table 2.3.

Table 2.3. List of Yeast Toolkit parts created for this study

Part Created	**Description**	**Reference**
pYTKNAD203	Hxt1 TDH3 core	This study
pYTKNAD3A01	Aga2	This study
pYTKNAD3A02	pre-pro-MFα	This study
pYTKNAD301	Aga1	This study
pYTKNAD3B01	Bgl1	This study
pYTKNAD4A01	Aga-α	This study
ConLSr	Reversed pYTL002 connector: changes orientation of transcriptional unit	Dr. Richard Que
ConR1r	Reversed pYTK067 connector: changes orientation of transcriptional unit	Dr. Richard Que

Golden Gate assembly of transcriptional units (TU) was performed using BsaI-HFv2 and the parts described in Table 2.4. Pre-assembly of the plasmid Multi-TU was possible by elimination of the final digestion step of the protocol. Finally, multi-transcriptional units were assembled using BsmBI. All resulting plasmids are described in Table 2.4.

Table 2.4. List of plasmids assembled using Golden Gate.

Plasmid	**Part 1**	**Part2**	**Part 3A**	**Part 3B**	**Part 4A**	**Part 4B**	**Part 5**	**Part 6**	**Part 7**	**Part 8**
Aga-alpha	pYTK003 ConL1	pYTKNAD203	pYTKNAD3A02	pYTKNAD4A01	pYTK57 mTurq2	pYTK066 *THD1*t	pYTK072 ConRE	pYTK064 *URA3*	pYTK082 2μ	pYTK083 Amp^R-ColE1
Aga1 TU	pYTK003 ConL1	pYTKNAD203	pYTKNAD301		pYTK056 *THD1*t		pYTK072 ConRE	pYTK095 Amp^R-ColE1 with GFP dropout		
Aga2-mTurquoise TU	ConLSr	pYTKNAD203	pYTKNAD3A01	pYTK044 mTurquoise2	pYTK056 *THD1*t		ConR1r	pYTK095 Amp^R-ColE1 with GFP dropout		
Aga2-Bgl1-mTurquoise TU	ConLSr	pYTKNAD203	pYTKNAD3A01	pYTKNAD3B01	pYTK57 mTurq2	pYTK066 *THD1*t	ConR1r	pYTK095 Amp^R-ColE1 with GFP dropout		

Multi-TU	pYTK 008 ConLS'	pYTK047 GFP Dropout	pYTK 073 ConR E'	pYTK 064 *URA3*	pYTK 082 2μ	pYTK 084 Kan^R-ColE1
Aga1-Aga2	Multi-TU BsmBI-assembled with Aga1TU and Aga2-mTurquoise2 TU					
Bgl1-mTurquoise2	Multi-TU BsmBI-assembled with Aga1TU and Aga2-Bgl1-mTurquoise2 TU					

2.4.3 Media and cultivation

E.coli was cultivated in Luria Bertani (LB) medium containing either 100 mg/ml of Ampicillin, 25 mg/mL of chloramphenicol, or 50 mg/mL kanamycin, based on recommendations by Addgene.

For expression experiments, cells were inoculated from fresh SDC-A plates (20 g/L dextrose, 5 g/L casamino acids, 5g/L ammonium sulfate, 1.7 g/L yeast nitrogen base without amino acids, 50 mg/L adenine, 20% agar) into 5 ml of liquid SGC-A 0.5% (5 g/L galactose, 5 g/L casamino acids, 5g/L ammonium sulfate, 1.7 g/L yeast nitrogen base without amino acids, 50 mg/L adenine, 20% agar) and grown overnight. This culture was used as the inoculum (initial OD_{600}=0.05). If not explicitly stated, cultivations were performed in 5 ml glass culture tubes at 30ºC and 250 rpm.

2.4.4 Rapid activation kinetics

After inoculation, cells were grown in 50 ml of SGC(A) with 2% galactose for 20 h. Samples (5 ml) were collected for measurement at t=0. Glucose was then added to a final concentration of 2% and samples were harvested every 30 min for ~3 hours. Immediately after collection, phosphoric acid swollen cellulose (PASC) was added to a final concentration of 0.3%(w/v) and the supernatant was incubated for 24 h at 30ºC before HPLC analysis.

2.4.5 HPLC analysis of PASC degradation, cellobiose, glucose and ethanol

Samples were centrifuged at 3000xg for 10 minutes at 4°C. The supernatant (20 µL) was analyzed on a Shimadzu HPLC (Prominence UFLC) using an Aminex HPX-42A column (BioRad) heated at 80ºC. Oligosaccharide separation is accomplished by a combination of size exclusion and ligand exchange mechanisms. Analytes were detected via changes in refractive index using a Shimadzu RID-10A detector. Water was used as an eluent at a flow rate of 0.4 mL min^{-1}.

2.4.6 Activity assay of secreted endoglucanase using CELLG5

The endoglucanase activity of the supernatant was measured using the *endo*-Cellulase Assay Kit CellG5 (Megazyme, Wicklow, Ireland) by mixing 6.25 µl of the supernatant with 6.25 µl of pre-equilibrated CELLG5 substrate in a clear 96-well plate (Corning, Corning NY). After incubation for 25 min at 30ºC, 187.6 µl of stopping solutions were added, and absorbance was measured at 405 nm in a plate reader (SpectraMax M2, Molecular Devices, San Jose, CA). This protocol maintains the proportion of reagents advised in the manufacturer instructions. Samples were run at different dilutions to ensure linearity.

2.4.7 Activity assay of secreted β-glucosidase using pNPG

The activity of β-glucosidase was determined by hydrolyzation of *p*-nitrophenyl-β-D-glucopyranoside (pNPG, Sigma-Aldrich, St. Louis, MO) by minor modification of the protocol described by Strahsburger et al. (2017). An aliquot of 57.2 µl of supernatant was mixed with 28.5 µl of 5 mM pNPG in a transparent 96-well plate (Corning, Corning NY). After incubation for 30 min at 37ºC, 114.3 µl of stopping solution were added, and absorbance was measured at 405 nm in a plate reader. Samples were run at different dilutions to ensure linearity. Dilutions were prepared using 100 mM sodium acetate buffer (pH=5.50).

2.4.8 Whole-cell activity assay of surface displayed β-glucosidase using pNPG

Samples were centrifuged at x2000g and cells re-suspended in sodium acetate buffer (100 mM sodium acetate, pH=5.0) to a final OD_{600}=10. Aliquots of 62.5µl of the cell suspension at OD_{600}=10 were mixed with 62.5 µl of water and 42.8 µl of 5 mM pNPG, and incubated in the in a microplate shaker at 30 ºC for 15 min. Cells were then pelted at x3500g for 10 min and 85.7 µl of the supernatant was placed into a 96-well clear-bottom microplate using a multichannel pipette, where 114.4 µl of the stopping solution (2% (w/v) Tris-base Buffer (pH=9.0) was then added. Absorbance was measured at 405 nm in a plate reader.

2.4.9 Fluorescence of surface displayed mTurquoise2

Samples were centrifuged at x2000g and cells re-suspended in water to a final OD_{600}=10. Fluorescence of 200 µl of cells was measured in a microplate reader using λ_{ex}=444 nm and λ_{em}=538 nm. To correct for pipetting errors, the OD_{600} was measured to correct for potential deviations in number of cells added to each well.

2.4.10 Statistical analysis

Statistical analysis consisted of either one-way ANOVA followed by t-test using Bonferroni corrections to account for multiple comparisons or two-way ANOVA using Post Hoc Tukey's test to account for multiple comparisons (the variance is estimated from the whole set of data).

2.5 Results and Discussion

2.5.1 Evaluation of *HXT1* promoter as glucose sensor

To develop an extracellular glucose sensor that will enable the display of cellulosome enzymes only in the presence of the cellulosic fraction of lignocellulose, we used the *HXT1* promoter to drive secretion of dockerin-tagged cellulases. The 760 base pairs upstream of the *HXT1* coding sequence were selected as the promoter. This decision was based on functional studies of glucose dependency previously reported (Ferrer-Martínez et al., 2004). We corroborated the presence of Rgt1 recognition sites in this region using the Eukaryotic Promoter Data Base Search Motif Tool (Cavin Périer et al., 1998). It identified at least five Rgt1 binding sites (***p<0.001) at positions -185, -302, -357, -408, and -438 relative to the transcriptional start site (TSS) – which is 39 bp upstream the start codon of *HXT1*. Once selected, this promoter sequence was cloned upstream of cellulases tagged C-terminally with dockerins and N-terminally with the pre-proMFα leader (to direct secretion) in a 2μ-based plasmid. Cells transformed with these multi-copy plasmids were grown in 0.5% galactose with increasing glucose concentrations and cellulase secretion was measured after 24 h.

Specific extracellular activities of BglDf and CelAt following exposed to different glucose concentrations are shown in Figure 1.5. The *HXT1* promoter enabled increased cellulase expression as glucose concentration rose, showing promise for the desired application. Differences in secretion between the lowest glucose concentration evaluated (0.5%) and the highest (3%) are 2.50-fold for BglDf (*p<0.05) and 15.6-fold for CelAt (***p<0.001). Comparing these secretion profiles to those of the strong constitutive *PGK1* promoter (Supplementary Material Figure S2.1) corroborates that increased specific activity is not solely due to carbon availability. This will also be further discussed below.

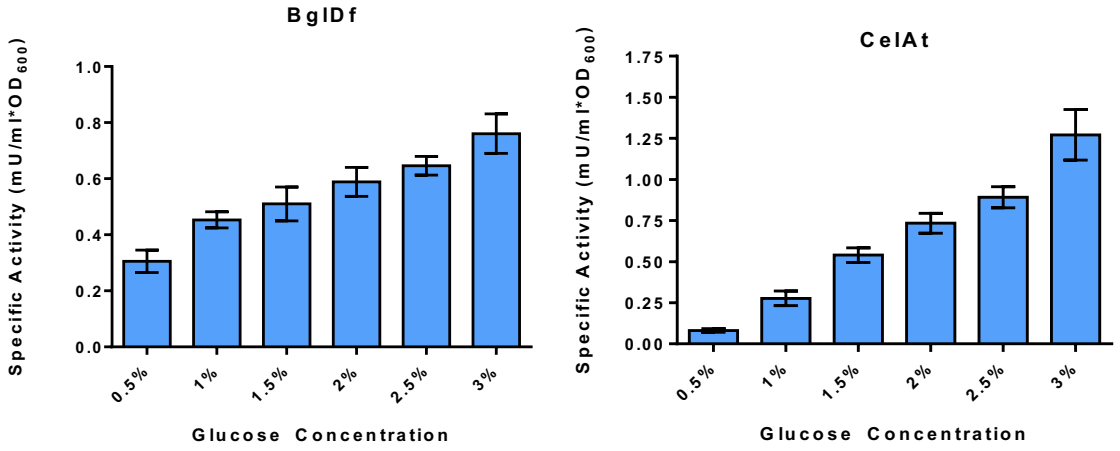

Figure 2.5. Extracellular activity of BglDf and CelAt as a function of glucose concentration. Both proteins are under transcriptional control of the *HXT1* promoter. Activity of endoglucanase was determined via CELLG5 colorimetric assay and activity of β-glucosidase was quantified using pNPG. Error bars represent SEM of three biological repeats.

Another important aspect is the specificity of the promoter to glucose versus galactose. It has been previously reported that the repressor Rgt1 binds to the *HXT1* regulatory sequence in cells grown in galactose, but not glucose, resulting in a 100-fold difference in induction levels (Kim and Johnston, 2006). Thus, we compared cellulase secretion of cells grown in ether 2% glucose or 2% galactose.

As shown in Figure 2.6, extracellular activity of BglDf is only detected when glucose is present in the media (**p<0.01). In contrast, very low levels of CelAt are detected, albeit at a level an order of magnitude lower. Although this could be attributed to non-enzymatic hydrolysis of PASC, the signal is higher than that of the control (which was subtracted) and potential leakiness of the promoter cannot be ruled out. Differences in secretion efficiency, enzyme activity, or sensitivity of the detection methods could explain why BglDf is not detected in 2% galactose, unlike CelAt.

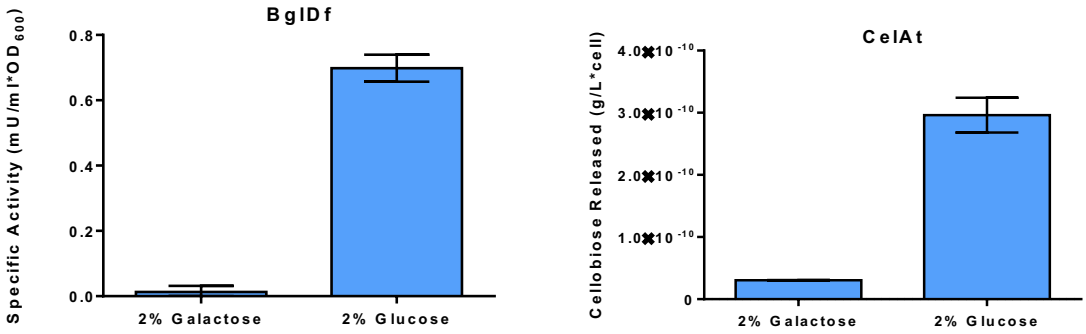

Figure 2.6. Extracellular activity of BglDf and CelAt in presence of 2% galactose and 2% glucose. The signal from the 'Empty Vector' was used as a control and subtracted. Activity of endoglucanase was determined via PASC hydrolysis and activity of β-glucosidase was quantified using pNPG. Error bars represent SEM of three biological repeats.

An additional advantage of using the *HXT1* promoter is its rapid transcriptional activation upon exposure to glucose. This has been previously described in a study where the kinetics of different glucose-induced proteins were interrogated (Kuttykrishnan et al., 2010). Their results showed that mRNA levels of *HXT1* reached a maximum in only 50 min after exposure to 2% glucose, but levels started to rise before 25 min. In order to verify this behavior, cells were grown in 2% galactose for 20 hours before addition of 2% glucose. Cellulase activity in the supernatant was then assessed at 0 min, 30 min, 60 min, 90 min, and 120 min after glucose supplementation in order to determine activation kinetics. In this case, activity was measured by quantification of the amount of cellobiose released when the supernatant was incubated with phosphoric acid swollen cellulose (PASC). Cellobiose release was chosen due to interference of high glucose levels on the CELLG5 activity assay (Figure S2.2). Results in Figure 2.7 show that endoglucanase activity was detected at 30 min, the first timepoint evaluated after glucose addition. These results are in accordance with the transcriptional kinetic profile reported in the literature (Kuttykrishnan et al., 2010) and indicate that the system will rapidly respond to the presence of glucose.

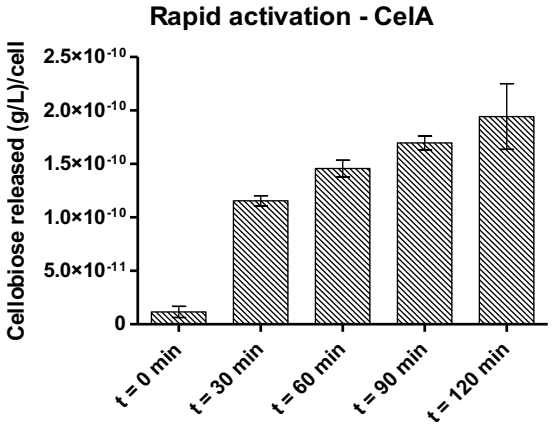

Figure 2.7. Glucose sensor rapid activation. Presence of extracellular endoglucanase is detected 30 min after glucose addition. Error bars represent SEM of three biological repeats.

2.5.2 Promoter architecture and engineering the *HXT1* promoter

In addition to the regulatory sequence, consisting of upstream activating or repressing sequences (UAS or URS), promoters also require the presence of a minimal structure that recruits RNA polymerase II and other general transcription factors to favor proper loading of the pre-initiation complex (Portela et al., 2017; Redden and Alper, 2015). This sequence is called the 'core' of the promoter and it comprises the region between the TATA box and the TSS. It is thought to primarily affect promoter strength and translation initiation.

To increase the strength of the *HXT1* promoter, we evaluated the effect of two different core sequences on extracellular levels of BglDf and CelAt. One core sequence corresponds to that of the strong *TDH3* promoter and the other to a minimal synthetic 'Core1' described by Redden and Alper (2015). The 78 bp sequence comprised between the TATA box and the TSS of the native *HXT1* promoter was substituted either by the corresponding 103 bp of the *TDH3* promoter (*HXT1*$^{\text{TDH3core}}$p) or the 38 bp of the 'Core1' sequence (*HXT1*$^{\text{Core1}}$p). For the latter, the TSS used corresponds to that of the *TDH3* promoter. We identified the TATA box and TSS using Eukaryotic Promoter Data Base Search Motif Tool (Cavin Périer et al., 1998). The 5' untranslated region between the TSS and the start codon was not changed with respect to the wild type *HXT1*p.

Once promoter variants were constructed, they were substituted for *HXT1*p in plasmids pJC842-pHXT1-CelAt and pJC842-pHXT1-BglDf to create pJC842-pHXT1^{core1}-CelAt, pJC842-pHXT1^{THD3core}-CelAt, pJC842-pHXT1^{core1}-BglDf, and pJC842-pHXT1^{THD3core}-BglDf. These plasmids were transformed into BY4741 and grown at increasing glucose concentrations, as described above. Activity of the enzymes secreted to the medium was evaluated after 24 h. For BglDf (Figure 2.8A), at low glucose concentrations (0.5% and 1%) there are no statistically significant difference between activities per cell between the HXT1^{THD3core}p and the wild type promoter; however, differences in secretion between *HXT1*^{TDH3core}p and *HXT1*^{Core1}p were significant. For the *HXT1*^{TDH3core}p, at 1.5% glucose, 81.0% more β-glucosidase activity (***p<0.001) was measured relative to the non-engineered promoter. At the highest glucose concentration evaluated (3%), levels of extracellular BglDf activity were 31.8% higher (**p<0.01) for *HXT1*^{TDH3core}p. There are no statistically significant differences between β-glucosidase levels driven by *HXT1*^{Core1}p and *HXT1*p throughout the glucose concentrations evaluated. Growth across the different biological replicates for cells using *HXT1*^{Core1}p varied considerably, as shown by the size of the error bars in Figure S2.3.

For the endoglucanase CelAt (Figure 2.8B), the *HXT1*^{Core1}p showed lower activity across all glucose concentrations evaluated, with 69.4% (***p<0.001, for 3%) to 85.1% (*p<0.05, for 0.5%) reductions relative to the native promoter. The *HXT1*^{TDH3core}p did not show statistically significant differences in specific activities at 0.5% and 1% glucose relative to *HXT1*p. However, at higher glucose concentrations, the *HXT1*^{TDH3core}p gave the highest extracellular activity. When glucose concentration was 2.5%, the maximum difference between *HXT1*^{TDH3core}p and *HXT1*p was observed, with a 73.0% increase (***p<0.001).

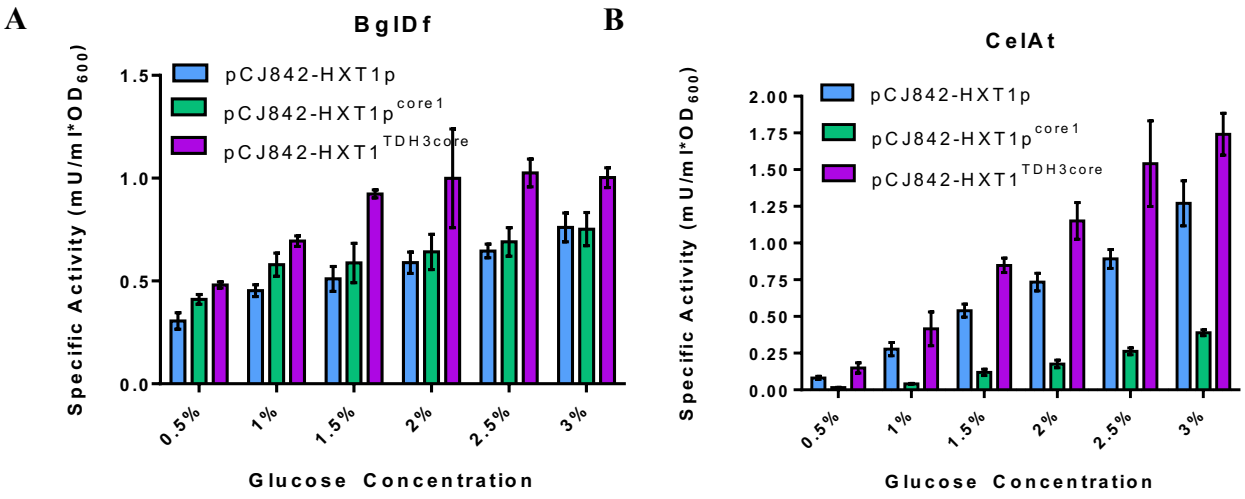

Figure 2.8. Specific extracellular activity of A) BglDf and B) CelAt as a function of glucose concentration. Proteins are under the transcriptional control of: the wild type *HXT1* promoter (blue bars) or engineered promoters that have the minimal core sequence described by Redden and Alper (2015) (green bars) and the core of *TDH3* promoter (purple bars). Activity of endoglucanase was determined via CELLG5 colorimetric assay and activity of β-glucosidase was quantified using pNPG. Error bars represent SEM of three biological repeats.

Overall, *HXT1*^{TDH3core}p provides the biggest increment in specific signal between the lowest and the highest glucose concentration tested. This is potentially beneficial, as improved enzyme expression and secretion at higher concentrations –when glucose concentration rises due to the presence of cellobiose– will enable a more efficient cellobiose degradation, while maintaining similar expression to that of the native promoter at lower glucose percentages. This was an unexpected (but welcomed) result, as previous reports showed increased basal expression using *YGP1*p when its core was substituted by that of the *TDH3* promoter (Rajkumar et al., 2016). This difference in results may be due to their selection of the full 150 bp upstream the *TDH3* gene, which includes not only the TSS and the TATA box but also the 5' untranslated region (5'UTR). In our constructs, the 5'UTR remained constant across promoters.

The different effects of the use of *HXT1*^{Core1}p when placed upstream of BglDf and CelAt were also interesting. For BglDf there were no significant differences in specific activity relative

to the wild type promoter. In contrast, CelAt levels were considerably diminished by the use of this core sequence. This indicates that caution needs to be taken when translating an engineered promoter approach from one protein to another.

2.5.3 Surface display of β-glucosidase

To demonstrate glucose-mediated display of enzymes (and thus potential application on a cellulosome) enabled by our sensor, we focused on the last catalytic step of cellulose degradation: the conversion of cellobiose into glucose. To this end, a fusion of β-glucosidase and a fluorescent protein was displayed on the surface of the yeast. The fluorescent reporter served as a detection method to verify expression of the construct. Surface display is expected limit the extent of product inhibition by rapidly importing glucose into the cell (Tsai et al., 2009).

A wide range of yeast surface display technologies are currently available, but the most extensively used are those related to the adhesion of opposite mating type haploid cells during mating: a-agglutinin and α-agglutinin (Kondo and Ueda, 2004). In both cases, proteins are transported to the outside of the plasma membrane and then anchored to the outermost surface via β-glucan covalent bonds (Teparic and Mrsa, 2016; Walker, 2014). To use the α-agglutinin-based system, the desired protein is fused to a secretion peptide (such as pre-pro-MFα) at the N-terminus and to the C-terminal sequence of Sag1 at the C-terminus. The last 960 bp of Sag1 encodes the glycosyl-phosphatidyl inositol (GPI) anchor. For a-agglutinin, there are two protein subunits, Aga1 and Aga2, which are bound through two disulfide bonds (Boder and Wittrup, 1997). The core Aga1 subunit serves as surface GPI anchor and, for biotechnological applications, is usually chromosomally expressed under the control of the *GAL1-10* promoter in the strain EBY100 (Kondo and Ueda, 2004). The Aga2 subunit can be N-terminally or C-terminally fused to the target protein for surface display and its expression is also usually controlled by the *GAL1-10* promoter.

We compared these two surface display approaches to determine which expression system would be more beneficial for our application. To this end, the classic a-agglutinin system was adapted into a bigenic multi-copy plasmid that co-overexpresses both subunits under the control of the *HXT1*^{TDH3core}p. A similar plasmid-based mode of expression has been successfully implemented for surface display of EGFP and EtMic2 proteins without the need of EBY100 or an engineered host cell (Sun et al., 2014). The α-agglutinin system was expressed in a single-gene multi-copy plasmid.

Comparison of the systems was performed using surface expression of the fluorescent reporter mTurquoise2 using plasmids pAga1-Aga2 and pAga-alpha. Cells were grown on galactose for 24 h, then harvested by centrifugation and in media containing 3% glucose. Cells were then incubated at 30ºC and fluorescence was monitored at 0 min, 30 min, 60 min and 90 min. The signal was normalized by cell density and the fluorescence per cell measured for an empty plasmid was subtracted to account for cell autofluorescence caused by products of glucose metabolism (Maslanka et al., 2018).

The mTurquoise2 fluorescence with time after glucose supplementation for the Aga1-Aga2 and Aga-alpha systems is shown in Figure 2.9. Initially, the Aga1-Aga2 system (blue bars) shows high basal fluorescence, indicating potential leakiness of the promoter. This basal signal does not start to rise until 60 and 90 min (**p<0.01). In contrast to the Aga1-Aga2, no signal is observed at t=0 for the Aga-alpha system (gray bars). A similar progression is then seen, where fluorescence increase begins at 60 min (*p<0.05). The signal is lower across all timepoints, which could be attributed either to a less efficient surface display or a discrepancy in fluorescent protein localization, aggregation or inactivation as a consequence of the different tagging modes of the two systems (i.e., N-terminal or C-terminal) (Stadler et al., 2013). Based on the results in Figure 2.9, we chose Aga1-Aga2 for surface display. For our final application, ensuring the maximal

signal amplification in the presence of cellulose will be more important than the basal expression level.

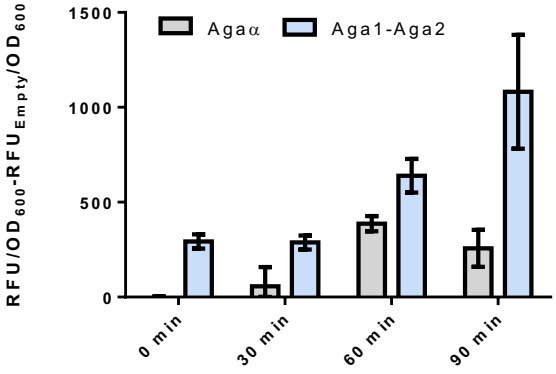

Figure 2.9. Comparison of two different systems of surface display based on α-agglutinin (Agaα) and a-agglutinin (Aga1-Aga2). Specific fluorescence of mTurquoise2 with time after re-suspension in media containing 3% glucose. Error bars represent SEM of three biological repeats.

We then evaluated the signal and the time profile of the β-glucosidase fused to mTurquoise2. Using the same experimental conditions as described above, it was observed that there is no statistical difference between the two, mTurquoise2 alone or fused to β-glucosidase, for all timepoints evaluated (Figure 2.10). Moreover, the *HXT1*^{TDH3core}p was able to drive surface display of the enzyme after 45 min of glucose addition.

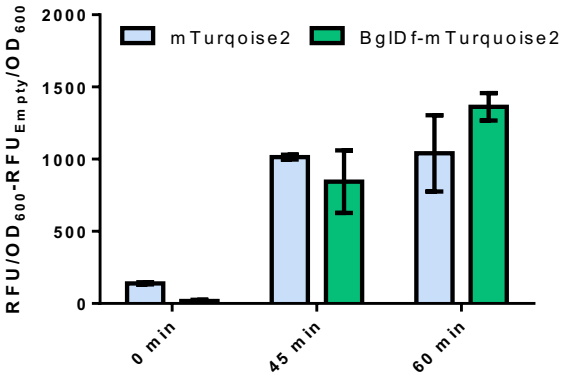

Figure 2.10. Comparison of mTurquoise2 and BglI fused to mTurquoise2 displayed on surface of yeast using the a-agglutinin-based expression system. Specific fluorescence vs. time after resuspension in medium containing 3% glucose. Error bars represent SEM of three biological repeats.

To further optimize this system, we tested whether deletion of *PHA1* would enable signal amplification by improving surface display. The gene *PAH1* encodes for a cytoplasmic phosphatidate (PA) phosphatase that is recruited to the ER membrane for synthesis of diacylglycerol (DAG) from phosphatidic acid (PA). Knocking-out *PAH1* results in impaired formation of lipid droplets, re-direction of lipid flux toward synthesis of membrane precursors and consequent proliferation of the ER/nuclear membrane (Santos-Rosa et al., 2005). The deletion of this gene has successfully improved heterologous membrane protein expression in *Yarrowia lipolytica* (Guerfal et al., 2013), has enhanced production of ER membrane-associated enzymes for triterpene synthesis in *S. cerevisiae* (Arendt et al., 2017) and has increased cellulase secretion (Chapter 1). We inoculated BY4741 and BYΔ*pah1* transformed with plasmid pBgl1-mTurquoise2 in 0.5% SGC(A) media containing either 0% or 3% glucose. Fluorescence and surface activity of cells were measured after 20 h of growth. In the absence of glucose, both cell types displayed similar fluorescence signals (Figure 2.11A) and enzymatic activity (Figure 2.11B). When glucose was included, BYΔ*pah1* showed 34.2% higher fluorescence (*p<0.05) and 43.7% higher activity (***p<0.001) relative to BY4741. Glucose induction resulted in a 73% increase in fluorescence for BY4741 (**p<0.01) and a 85% increase for BYΔ*pah1* (**p<0.001) relative to levels in galactose medium. Bgl1 activity increased 16.2-fold for BY4741 (***p<0.001) and 17.3-fold for BYΔ*pah1* (***p<0.001) upon glucose induction. These results show that cells with the engineered ER had a higher signal gain relative to BY4741. Activity also provided a more sensitive mode of measurement, as changes in signal were more pronounced than for fluorescence. For this reason, we will focus on activity measurements and fluorescence will only be used as a trend indicator that is later corroborated by activity.

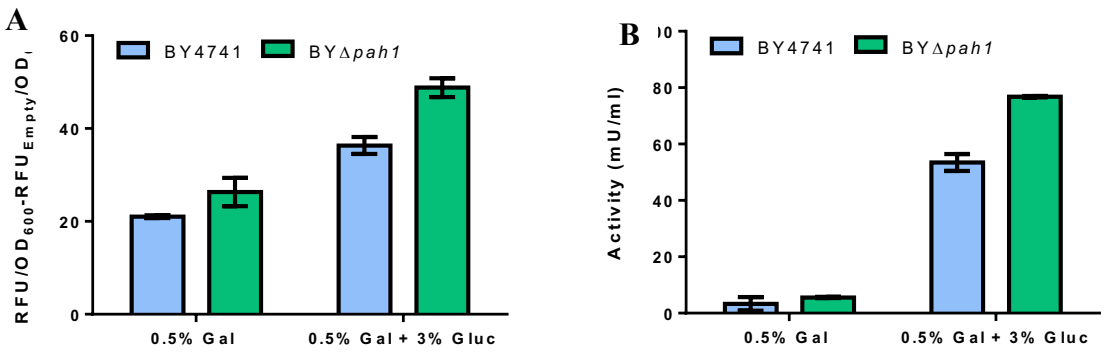

Figure 2.11. A) Fluorescence and B) β-glucosidase activity for yeast strains BY4741 and BY*Δpah1* (OD_{600}=10) displaying a fusion of β-glucosidase and mTurquoise2 using the a-agglutinin-based system. Error bars represent SEM of *n*=3.

To examine the effect of cell engineering on the glucose dose-response profile, both cell types were inoculated from plates into 0.5% SGC(A), grown overnight and inoculated into increasing concentrations of glucose. To ensure that an increase in signal is not due to higher availability of carbon, carbon concentration was kept constant at 3% (w/v) across groups by galactose supplementation. As an example, when activity and fluorescence are evaluated at a glucose concentration of 0.5%, 2.5% galactose was also added to the medium. Activity and fluorescence were evaluated at 24 h. Results are shown in Figure 2.12.

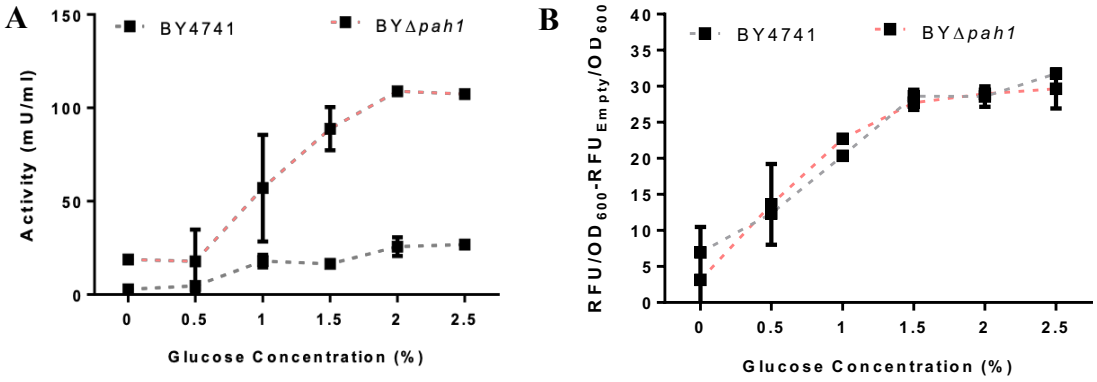

Figure 2.12. Change in A) activity and B) fluorescence with glucose concentration at 24 h for BY4741 (gray) and BY*Δpah1*(pink) strains displaying a fusion of β-glucosidase and mTurquoise2 using the a-agglutinin-based system. Error bars represent SEM of three biological repeats.

When comparing the activity vs. glucose concentration profile for strains BY4741 and BYΔ*pah1* (Figure 2.12A), no significant changes were observed at 0.5%. However, at 1% glucose, higher activities are measured for the BYΔ*pah1* culture (*p<0.05). At glucose concentrations of 1.5% and higher, BYΔ*pah1* shows a significant increase in activity with respect to BY4741, displaying up to a 4.24-fold improvement at 2%, thus corroborating the trend observed in Figure 2.11. This result also indicates great promise for increased efficiency of cellulose degradation when the strain BYΔ*pah1* is used for displaying the cellulosome. In contrast to what is observed for activity, fluorescence (Figure 2.12B) does not show significant differences among strains at any glucose concentration. This could be due to lack of sensitivity of the fluorescent reporter, as indicated by the previous experiment (Figure 2.11), where differences in activity between the 'OFF' and 'ON' state were 17.3-fold, while changes in fluorescence were only 85%. Therefore, the next studies focused on activity measurements. Based on the results shown in Figure 2.12A, we selected BYΔ*pah1* for the remaining experiments.

2.5.4 Positive feedback loop for glucose-induced cellobiose degradation

The overall aim of this study was to develop a method to selectively display cellulases in the presence of the cellulose fraction of lignocellulosic feedstock. The strategy was that residual glucose derived from the pre-treatment process would prime this process by triggering low amounts of cellulase secretion. The initial secreted cellulases would lead to cellulose depolymerization, resulting in increased glucose concentration. This rise in glucose would escalate as more cellulases are secreted and cellulose degradation progresses, triggering a positive feedback loop that leads to full induction of the promoter.

To test whether signal rises as cellobiose concentration increases, strain BYΔ*pah1* transformed with the plasmid pBgl1-mTurquoise2 – which displays a β-glucosidase-mTurquoise2 fusion on the surface of the cell using the a-agglutinin system – was inoculated from plates into

0.5% SGC(A) and grown overnight. Cells were inoculated in fresh medium containing 1% glucose for induction. At approximately 20 h, increasing concentrations of cellobiose were added and activity was measured at 28 h, 52 h, 74 h and 97 h after addition. Separation of enzyme induction and substrate addition was used as a precaution, as β-glucosidase catalytic activity is inhibited at high concentrations of substrate and product (Bohlin et al., 2013; Parry et al., 2001). After growing for ~20 h, glucose is expected to be depleted based on previous studies with strain BY47471-pJC842-pHXT1-CelAt (Figure S2.5). For the final application, we do not anticipate that this will be an issue, as the cellobiose released by the action of the endoglucanase and cellobiohydrolase is not expected to accumulate. However, in the present simplified system where only the final step of hydrolysis is evaluated, cellulose is substituted by cellobiose.

Activity increased with time as cellobiose was degraded (Figure 2.13A). Differences between the control (gray line) and groups where cellobiose was added (blue lines) became apparent at 52 h, and were more pronounced at 97 h. Figure 2.13B shows a comparison of activity at 97 h, where there is an increase of 74.7% (*p<0.05), 84.7% (**p<0.01) and 91.0% (**p<0.01) between groups where cellobiose is equal or higher than 1% relative to the control. These results corroborate that there is an increase in sensor induction levels in the presence of cellobiose, suggesting a possible positive feedback loop. Despite this, differences in activities among samples where cellobiose was added are not statistically significant. This experiment will need to be repeated increasing the number of biological repeats and running a control where no induction takes place in order to improve the robustness of the results.

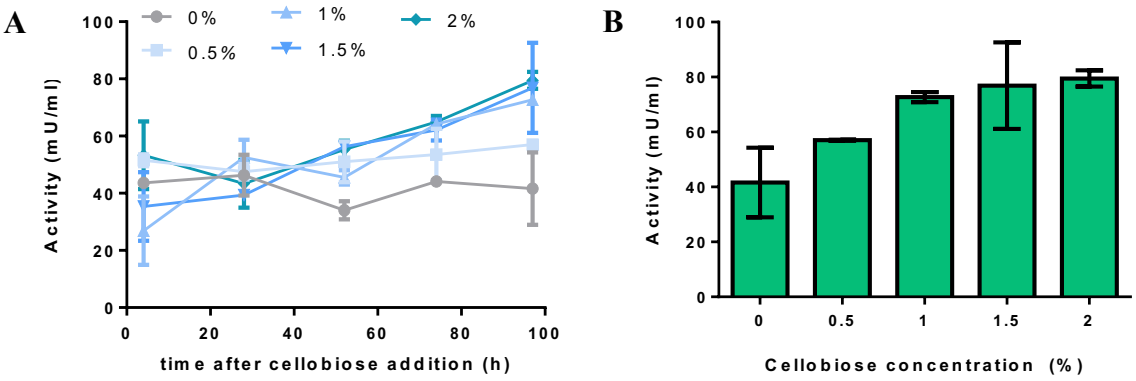

Figure 2.13. A) Progression of activity with time after addition of increasing cellobiose concentrations. Darker shades of blue indicate increasing levels of cellobiose. Gray line corresponds to the control with no cellobiose. B) Differences in activity observed at increasing cellobiose concentrations evaluated after 97 h of cellobiose addition. Cells were induced at t=0 min with 1% glucose and increasing amounts of cellobiose were added at t~20 h. Error bars represent SEM of two biological repeats.

To determine the extent of cellobiose degradation, generation of fermentation products, and the extent of cellobiose trans-glycosylation (Bohlin et al., 2013) at 97 h, the samples (Figure 2.13B) were analyzed via high performance liquid chromatography (HPLC). Levels of cellobiose, glucose, cellotriose, and ethanol were measured and compared to those observed for cells transformed with an 'empty plasmid'. The glucose concentration detected via HPLC is shown in Figure 2.14A. Levels of glucose present in the media were greater than zero for the empty plasmid and could be a consequence of non-enzymatic cellobiose hydrolyzation. However, the levels are low, as there is only between 0.02 and 0.05 g of glucose formed for every gram of cellobiose added. Cellobiose concentrations depicted in Figure 2.14B demonstrate lack of cellobiose uptake in the absence of β-glucosidase (as expected). In contrast, there is no cellobiose peak when the enzyme is displayed on the surface, indicating 100% conversion. As seen in Figure 2.14C, part of the cellobiose is converted to cellotriose via trans-glycosylation. This process is known to be catalyzed by β-glucosidases at high substrate concentrations (Bohlin et al., 2013), which could explain the increase in cellotriose at the highest cellobiose concentration evaluated (*p<0.05) and

why this peak is not observed in the 'empty plasmid' group. Finally, Figure 2.14D shows that production of ethanol increases as more cellobiose is added, but only when there is enzyme expression; ethanol remains constant across cellobiose concentrations for the control with the empty plasmid. At 2% cellobiose, ethanol levels reach 10.3 g/L when the β-glucosidase is displayed, in comparison to the 2.6 g/L observed for the control cells. These results demonstrate the feasibility of applying of our system for simultaneous saccharification and fermentation, induced by endogenous molecules of the system.

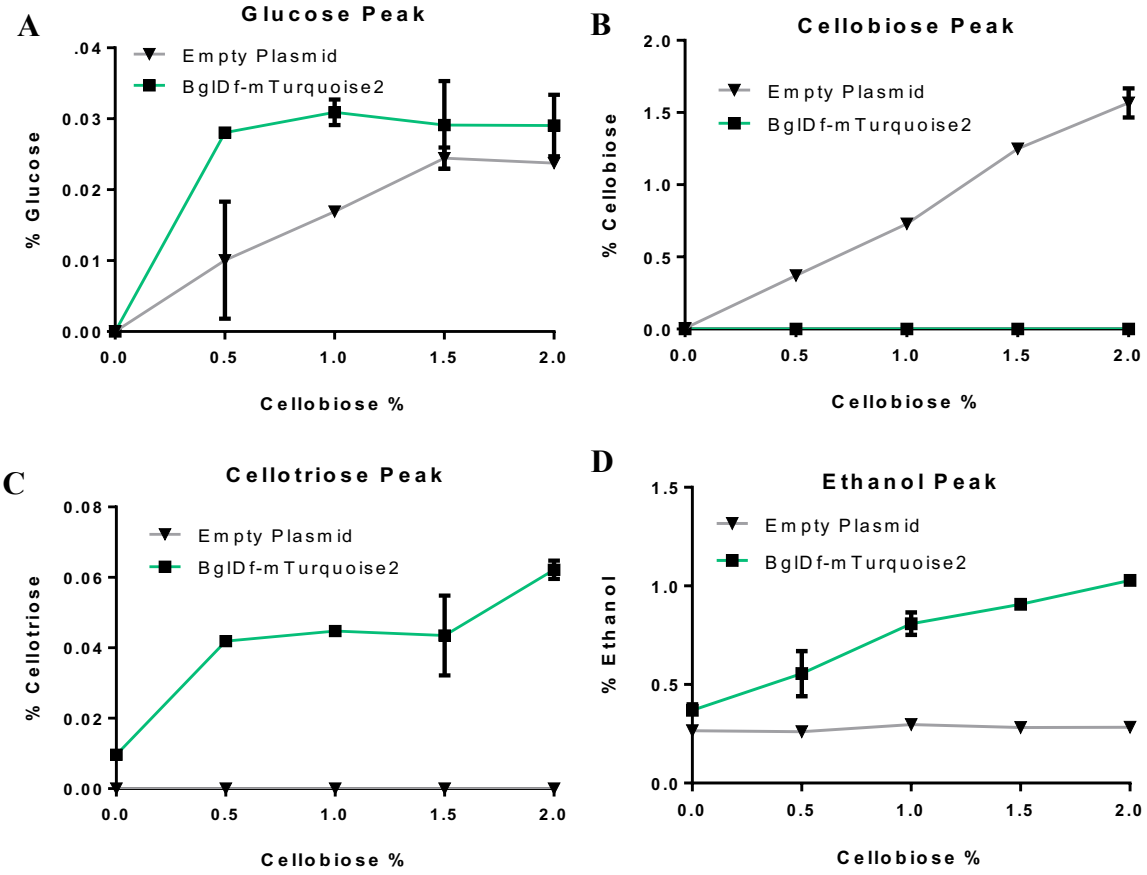

Figure 2.14. Levels of A) glucose B) cellobiose C) cellotriose and D) ethanol of strains transformed with empty plasmid (control, gray lines) and Bgl1-mTurquoise2 plasmid (green lines) and grown with increasing % cellobiose added. Cells were induced at t=0 min with 1% glucose and increasing amounts of cellobiose were added at t~20 h. Cells were cultured for 97 h after cellobiose addition and the supernatant was analyzed via HPLC. Error bars represent SEM of two biological repeats.

The next aim was to determine the glucose concentrations that would trigger increased cellulase activity in the presence of cellobiose. This will determine the levels necessary to prime the positive feedback loop. We inoculated strain BYΔ*pah1* transformed with the Bgl1-mTurquoise2 plasmid in 0.5% SGC(A) supplemented with 0%, 0.5%, 1%, 1.25%, 1.5% and 2% glucose, and after ~20 h of growth we added either water or 1% cellobiose. Activity was tested 100 h after cellobiose addition.

As seen in Figure 2.15, 0.5% of glucose does not trigger an increase in activity when cellobiose is present. However, at 1% and 1.25% glucose, activity increased by 29.8% and 28.2% (*p<0.05), respectively. At higher concentrations, no improvement was observed, potentially due to signal saturation, as the sensor is out of the linear range (Figure S2.4). These results should be corroborated in the future by running additional biological replicates, testing intermediate glucose concentrations and keeping total carbon concentration constant at the time of inoculation.

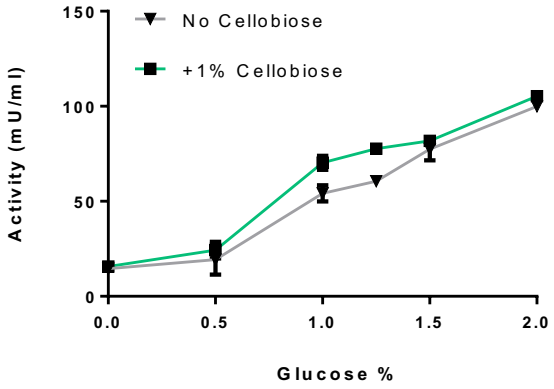

Figure 2.15. Enzymatic activity as function of glucose added either in absence (gay lines) or presence of 1% cellobiose (green lines) for strain BYΔ*pah1* transformed with the Bgl1-mTurquoise2 plasmid. Samples were incubated for 100 h after cellobiose addition. Error bars represent SEM of two biological replicates.

Despite the need for further investigation, our results show that at glucose concentrations of approximately 1% there is an amplification of the signal in presence of cellobiose. Signal amplification at 1% is further increased from 29.8% to 55.8% when cellobiose concentration was

shifted from 1% to 2% (Figure 2.16). Although very preliminary, these results corroborate the trend observed in Figure 2.13, where there is a rise in activity as a function of cellobiose concentration.

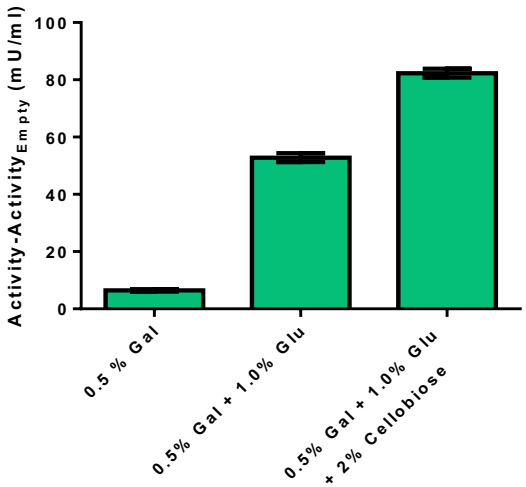

Figure 2.16. Whole-cell activity of cells induced with 0% or 1% glucose at t=0, and grown for ~20 h before addition of water or 2% cellobiose. Error bars represent SEM of three biological replicates.

2.6 Conclusions

In this study, we have developed and characterized a sensor that drives protein expression in response to increasing glucose in the media. Our initial approach was based on the *HXT1*p, the expression of which is triggered by the PKA cascade in response to the extracellular glucose detected by the GPCR Gpr1. We improved this sensor by changing the core of the promoter to that of the strong *THD3*p. This led to an increase in levels of extracellular β-glucosidase and endoglucanase activity by up to 81% and 73% in the presence of 1.5% and 2% glucose, respectively, while maintaining equivalent activity as the native promoter at lower glucose concentrations.

The main application for this glucose sensor will be the selective display of cellulases in the presence of the cellulose fraction of lignocellulosic biomass. This will be enabled by priming of the system with low glucose concentrations that are present as a consequence of pre-treatment processes. In the presence of cellulose, this signal will be amplified, triggering more cellulase secretion to allow complete saccharification. To model and demonstrate the feasibility of this approach, we focused on the last step of cellulose hydrolysis and displayed β-glucosidase on the surface of the cell. Characterization of this system showed increased expression with glucose concentration. By engineering the cell via deletion of *PAH1*, we were able to improve enzyme display, resulting in up to a 4.24-fold signal gain with respect to the wild type strain. To our knowledge, this is the first report that demonstrates how the *PAH1* knock-out improves surface display of GPI-anchored proteins. We have also observed that there is amplification of the signal due to the presence of cellobiose with increases in enzymatic activity between 55% and 91% when 2% cellobiose is added. Preliminary results suggest amplification may increase as cellobiose levels increases. However more experiments are required to confirm this. We have also demonstrated

that our system is capable of 100% cellobiose conversion, with increasing production of ethanol as initial cellobiose concentration increased.

2.7 Future directions

The preliminary data needs to be confirmed by repeating experiments with the modifications indicated in the text. In addition, there should be further assessment of other aspects of the study, including the evaluation of the effect of *PAH1* deletion on the transcriptional regulation of *HXT1* ^{THD3core}p. Processes such as the PKA signaling cascade could be affected, as Gpr1 is a membrane protein and BYΔ*pah1* shows proliferation of membrane structures. This could be tested using a cytoplasmic reporter under the control of HXT1^{THD3core}p. If the reporter signal in BYΔ*pah1* is different than that for BY4741, it would indicate that strain engineering has an effect on *HXT1* ^{THD3core}p transcriptional regulation, as increases in signal would be independent of surface display or protein secretion of the reporter. Other aspects such as potential interference of xylose or other hemicellulose monomers, and leakiness of the *HXT1*^{TDH3core}p should also be considered. Finally, it would be interesting to compare the efficiency of cellobiose degradation with our system to that of other inducible promoters that will not generate the positive feedback loop, such as *GAL1*p. For this study, it would be necessary to find the galactose concentration that leads to an equivalent level of expression as observed at glucose 'priming' concentrations.

Another potential application of this glucose sensor is the dynamic regulation of gene expression for proteins that negatively affect protein secretion and cellulosome assembly, but where gene deletion results in growth defects. This is the case for *PMT5* and *MNN10*, involved in protein glycosylation (Wang et al., 2013). To diminish their expression only when cellulases are secreted, we propose to down-regulate *PMT5* and *MNN10* using CRISPRi (Zalatan et al., 2015) by controlling the transcription of dCas9-Mxi1 using the *HXT1*^{TDH3core}p. Targeting of dCas9-Mxi1 protein to the genes will be enabled by co-expression with an optimal *PMT5*/ *MNN10* targeting gRNA.

2.8 References

Alonso DM, Wettstein SG, Dumesic J a. 2012. Bimetallic catalysts for upgrading of biomass to fuels and chemicals. *Chem. Soc. Rev.* **41**.

Arendt P, Miettinen K, Pollier J, De Rycke R, Callewaert N, Goossens A. 2017. An endoplasmic reticulum-engineered yeast platform for overproduction of triterpenoids. *Metab. Eng.* **40**:165–175. http://dx.doi.org/10.1016/j.ymben.2017.02.007.

Boder ET, Wittrup KD. 1997. Yeast surface display for screening combinatorial polypeptide libraries. *Nat. Biotechnol.* **15**:553–557. http://www.nature.com/doifinder/10.1038/nbt0697-553.

Bohlin C, Praestgaard E, Baumann MJ, Borch K, Praestgaard J, Monrad RN, Westh P. 2013. A comparative study of hydrolysis and transglycosylation activities of fungal β-glucosidases. *Appl. Microbiol. Biotechnol.* **97**:159–169.

Busti S, Coccetti P, Alberghina L, Vanoni M. 2010. Glucose signaling-mediated coordination of cell growth and cell cycle in Saccharomyces Cerevisiae. *Sensors* **10**:6195–6240.

Cavin Périer R, Junier T, Bucher P. 1998. The Eukaryotic Promoter Database EPD. *Nucleic Acids Res.* **26**:353–7. https://academic.oup.com/nar/article-lookup/doi/10.1093/nar/gkw1069.

Choi JW, Da Silva NA. 2014. Improving polyketide and fatty acid synthesis by engineering of the yeast acetyl-CoA carboxylase. *J. Biotechnol.* **187**:56–59. http://dx.doi.org/10.1016/j.jbiotec.2014.07.430.

Doi RH, Kosugi A. 2004. Cellulosomes: plant-cell-wall-degrading enzyme complexes. *Nat. Rev. Microbiol.* **2**:541–551.

Escalante-Chong R, Savir Y, Carroll SM, Ingraham JB, Wang J, Marx CJ, Springer M. 2015. Galactose metabolic genes in yeast respond to a ratio of galactose and glucose. *Proc. Natl. Acad. Sci.* **112**:1636–1641. http://www.pnas.org/lookup/doi/10.1073/pnas.1418058112.

Fan L-H, Zhang Z-J, Yu X-Y, Xue Y-X, Tan T-W. 2012. Self-surface assembly of cellulosomes with two miniscaffoldins on Saccharomyces cerevisiae for cellulosic ethanol production. *Proc. Natl. Acad. Sci.* **109**:13260–13265.

Faraco V ed. 2013. Lignocellulose Conversion. Berlin: Springer-Verlag 21-39 p. http://link.springer.com/10.1007/978-3-642-37861-4.

Ferrer-Martínez A, Riera A, Jiménez-Chillarón JC, Herrero P, Moreno F, Gómez-Foix AM. 2004. A glucose response element from the S. cerevisiae hexose transporter HXT1 gene is sensitive to glucose in human fibroblasts. *J. Mol. Biol.* **338**:657–667.

Gancedo JM. 2008. The early steps of glucose signalling in yeast. *FEMS Microbiol. Rev.* **32**:673–704.

Gibson DG, Young L, Chuang RY, Venter JC, Hutchison CA, Smith HO. 2009. Enzymatic assembly of DNA molecules up to several hundred kilobases. *Nat. Methods* **6**:343–345.

Gírio FM, Fonseca C, Carvalheiro F, Duarte LC, Marques S, Bogel-Łukasik R. 2010. Hemicelluloses for fuel ethanol: A review. *Bioresour. Technol.* **101**:4775–4800. http://dx.doi.org/10.1016/j.biortech.2010.01.088.

Gold ND, Martin VJJ. 2007. Global view of the Clostridium thermocellum cellulosome revealed by quantitative proteomic analysis. *J. Bacteriol.* **189**:6787–6795.

Goyal G, Tsai S-L, Madan B, DaSilva N a, Chen W. 2011. Simultaneous cell growth and ethanol production from cellulose by an engineered yeast consortium displaying a functional mini-cellulosome. *Microb. Cell Fact.* **10**:89. http://www.microbialcellfactories.com/content/10/1/89.

Guerfal M, Claes K, Knittelfelder O, De Rycke R, Kohlwein SD, Callewaert N. 2013. Enhanced membrane protein expression by engineering increased intracellular membrane production. *Microb. Cell Fact.* **12**:122. http://www.microbialcellfactories.com/content/12/1/122.

Hadar Y. 2013. Sources for Lignocellulosic Raw Materials for the Production of Ethanol. In: Faraco, V, editor. *Lignocellul. Conversion. Enzym. Microb. Tools Bioethanol Prod.* Berlin: Springer-Verlag, pp. 21–38.

Han SO, Yukawa H, Inui M, Doi RH. 2005. Effect of carbon source on the cellulosomal subpopulations of Clostridium cellulovorans. *Microbiology* **151**:1491–1497.

Horák J. 2013. Regulations of sugar transporters: insights from yeast. *Curr. Genet.*:1–31.

Jouandot D, Roy A, Kim JH. 2011. Functional dissection of the glucose signaling pathways that regulate the yeast glucose transporter gene (HXT) repressor Rgt1. *J. Cell. Biochem.* **112**:3268–3275.

Kim J-H, Johnston M. 2006. Two glucose-sensing pathways converge on Rgt1 to regulate expression of glucose transporter genes in Saccharomyces cerevisiae. *J. Biol. Chem.* **281**:26144–26149.

Klinke HB, Ahring BK, Schmidt AS, Thomsen AB. 2002. Characterization of degradation products from alkaline wet oxidation of wheat straw. *Bioresour. Technol.* **82**:15–26.

Kondo A, Ueda M. 2004. Yeast cell-surface display - Applications of molecular display. *Appl. Microbiol. Biotechnol.* **64**:28–40.

Kuttykrishnan S, Sabina J, Langton LL, Johnston M, Brent MR. 2010. A quantitative model of glucose signaling in yeast reveals an incoherent feed forward loop leading to a specific, transient pulse of transcription. *Proc. Natl. Acad. Sci. U. S. A.* **107**:16743–16748.

Lee ME, DeLoache WC, Cervantes B, Dueber JE. 2015. A Highly Characterized Yeast Toolkit for Modular, Multipart Assembly. *ACS Synth. Biol.* **4**:975–986.

Lopes MSG. 2015. Engineering biological systems toward a sustainable bioeconomy. *J. Ind. Microbiol. Biotechnol.* **42**:813–38.

Lynd LR, Van Zyl WH, McBride JE, Laser M. 2005. Consolidated bioprocessing of cellulosic biomass: An update. *Curr. Opin. Biotechnol.* **16**:577–583.

Maslanka R, Kwolek-Mirek M, Zadrag-Tecza R. 2018. Autofluorescence of yeast Saccharomyces cerevisiae cells caused by glucose metabolism products and its methodological implications. *J. Microbiol. Methods* **146**:55–60. https://linkinghub.elsevier.com/retrieve/pii/S0167701218300514.

Matsu-Ura T, Dovzhenok AA, Coradetti ST, Subramanian KR, Meyer DR, Kwon JJ, Kim C, Salomonis N, Glass NL, Lim S, Hong CI. 2018. Synthetic Gene Network with Positive Feedback Loop Amplifies Cellulase Gene Expression in Neurospora crassa. Research-article. *ACS Synth. Biol.* **7**:1395–1405.

Nataf Y, Bahari L, Kahel-Raifer H, Borovok I, Lamed R, Bayer E a, Sonenshein AL, Shoham Y. 2010. Clostridium thermocellum cellulosomal genes are regulated by extracytoplasmic polysaccharides via alternative sigma factors. *Proc. Natl. Acad. Sci. U. S. A.* **107**:18646–18651.

Parry NJ, Beever DE, Owen E, Vandenberghe I, Van Beeumen J, Bhat MK. 2001. Biochemical characterization and mechanism of action of a thermostable beta-glucosidase purified from Thermoascus aurantiacus. *Biochem. J.* **353**:117–127.

Pérez J, Muñoz-Dorado J, De La Rubia T, Martínez J. 2002. Biodegradation and biological treatments of cellulose, hemicellulose and lignin: An overview. *Int. Microbiol.* **5**:53–63.

Portela RMC, Vogl T, Kniely C, Fischer JE, Oliveira R, Glieder A. 2017. Synthetic Core Promoters as Universal Parts for Fine-Tuning Expression in Different Yeast Species. *ACS Synth. Biol.* **6**:471–484.

Rajkumar AS, Liu G, Bergenholm D, Arsovska D, Kristensen M, Nielsen J, Jensen MK, Keasling JD. 2016. Engineering of synthetic, stress-responsive yeast promoters. *Nucleic Acids Res.* **44**.

Redden H, Alper HS. 2015. The development and characterization of synthetic minimal yeast promoters. *Nat. Commun.* **6**:7810. http://www.nature.com/doifinder/10.1038/ncomms8810.

Rolland F, Winderickx J, Thevelein JM. 2002. Glucose-sensing and-signalling mechanisms in yeast. *{FEMS} yeast Res.* **2**:183–201.

Rolland F, Winderickx J, Thevelein JM. 2001. Glucose-sensing mechanisms in eukaryotic cells. *Trends Biochem. Sci.* **26**:310–317.

Roy A, Jouandot D, Cho KH, Kim JH. 2014. Understanding the mechanism of glucose-induced relief of Rgt1-mediated repression in yeast. *FEBS Open Bio* **4**:105–111.

Ryo S, Ishii J, Matsuno T, Nakamura Y, Matsubara D, Tominaga M, Kondo A. 2017. Positive Feedback Genetic Circuit Incorporating a Constitutively Active Mutant Gal3 into Yeast GAL Induction System. *ACS Synth. Biol.* **6**:928–935.

Sambrook J, Green MR. 2012. Molecular Cloning: A Laboratory Manual. Ed. Micahel R Green, J Sambrook 4th Erditi. Cold Spring Harbor. Vol. 1 1-2028 p.

Santos-Rosa H, Leung J, Grimsey N, Peak-Chew S, Siniossoglou S. 2005. The yeast lipin Smp2 couples phospholipid biosynthesis to nuclear membrane growth. *EMBO J.* **24**:1931–1941. http://emboj.embopress.org/cgi/doi/10.1038/sj.emboj.7600672.

Da Silva NA, Srikrishnan S. 2012. Introduction and expression of genes for metabolic engineering applications in Saccharomyces cerevisiae. *FEMS Yeast Res.* **12**:197–214.

Srikrishnan S, Chen W, Da Silva NA. 2013. Functional assembly and characterization of a modular xylanosome for hemicellulose hydrolysis in yeast. *Biotechnol. Bioeng.* **110**:275–285.

Stadler C, Rexhepaj E, Singan VR, Murphy RF, Pepperkok R, Uhlén M, Simpson JC, Lundberg E. 2013. Immunofluorescence and fluorescent-protein tagging show high correlation for protein localization in mammalian cells. *Nat. Methods* **10**:315–323. http://www.nature.com/articles/nmeth.2377.

Strahsburger E, de Lacey AML, Marotti I, DiGioia D, Biavati B, Dinelli G. 2017. In vivo assay to identify bacteria with β-glucosidase activity. *Electron. J. Biotechnol.* **30**:83–87. https://doi.org/10.1016/j.ejbt.2017.08.010.

Sun H, Wang T, Zhang J, Liu Q, Wang L, Chen P, Wang F, Li H, Xiao Y, Zhao X. 2014. Display of heterologous proteins on the Saccharomyces cerevisiae surface display system using a single constitutive expression vector. *Biotechnol. Prog.* **30**:443–450.

Teparic R, Mrsa V. 2016. Overview of systems and techniques for surface display of recombinant proteins in yeast S . cerevisiae. *Appl. Food Biotechnol.* **3**:3–14. http://journals.sbmu.ac.ir/afb/article/view/9457.

Tsai SL, DaSilva N a, Chen W. 2013. Functional display of complex cellulosomes on the yeast surface via adaptive assembly. *ACS Synth. Biol.* **2**:14–21.

Tsai SL, Goyal G, Chen W. 2010. Surface display of a functional minicellulosome by intracellular complementation using a synthetic yeast consortium and its application to cellulose hydrolysis and ethanol production. *Appl. Environ. Microbiol.* **76**:7514–7520.

Tsai SL, Oh J, Singh S, Chen R, Chen W. 2009. Functional assembly of minicellulosomes on the Saccharomyces cerevisiae cell surface for cellulose hydrolysis and ethanol production. *Appl. Environ. Microbiol.* **75**:6087–6093.

Versele M, De Winde JH, Thevelein JM. 1999. A novel regulator of G protein signalling in yeast, Rgs2, downregulates glucose-activation of the cAMP pathway through direct inhibition of Gpa2. *EMBO J.* **18**:5577–5591.

Walker JM. 2014. Yeast Metabolic Engineering. Ed. Valeria Mapelli. New York, NY: Springer New York. Vol. 1152 Chapter 8 p. Methods in Molecular Biology. http://link.springer.com/10.1007/978-1-4939-0563-8.

Wang T-Y, Huang C-J, Chen H-L, Ho P-C, Ke H-M, Cho H-Y, Ruan S-K, Hung K-Y, Wang I-L, Cai Y-W, Sung H-M, Li W-H, Shih M-C. 2013. Systematic screening of glycosylation- and trafficking-associated gene knockouts in Saccharomyces cerevisiae identifies mutants with improved heterologous exocellulase activity and host secretion. *BMC Biotechnol.* **13**:71. http://www.pubmedcentral.nih.gov/articlerender.fcgi?artid=3766678&tool=pmcentrez&rendertype=abstract.

Weifu Lee J ed. 2013. Advanced biofuels and bioproducts. New York: Springer Science+ Bussiness Media.

Williams TC, Xu X, Ostrowski M, Pretorius IS, Paulsen IT. 2017. Positive-feedback, ratiometric biosensor expression improves high-throughput metabolite-producer screening

efficiency in yeast. *Synth. Biol.* **2**:1–13. https://academic.oup.com/synbio/article/2962546/Positive-feedback,.

Zalatan JG, Lee ME, Almeida R, Gilbert LA, Whitehead EH, La Russa M, Tsai JC, Weissman JS, Dueber JE, Qi LS, Lim WA. 2015. Engineering complex synthetic transcriptional programs with CRISPR RNA scaffolds. *Cell* **160**:339–350. http://dx.doi.org/10.1016/j.cell.2014.11.052.

Chapter 3

Engineering *Saccharomyces cerevisiae* Fatty Acid Composition for Increased Tolerance to Octanoic Acid

3.1 Abstract

Biorenewable chemicals such as short and medium chain fatty acids enable functional or direct substitution of petroleum-derived building blocks, allowing reduction of anthropogenic greenhouse gases while meeting market needs of high-demand products like aliphatic alcohols and alpha olefins. However, producing these fatty acids in microorganisms can be challenging due to toxicity issues. Octanoic acid (C8) can disrupt the integrity of the cell membrane in yeast, and exogenous supplementation of oleic acid has been shown to help alleviate this. We recently engineered the Saccharomyces cerevisiae enzyme acetyl-CoA carboxylase by replacing serine residue 1157 with alanine to prevent deactivation by phosphorylation. Expression of $Acc1^{S1157A}$ in S. cerevisiae resulted in an increase in total fatty acid production, with the largest increase for oleic acid. In this study, we evaluated the effect of this modified lipid profile on C8 toxicity to the yeast. Expression of $Acc1^{S1157A}$ in S. cerevisiae BY4741 increased the percentage of oleic acid 3.1- and 1.6-fold in the absence and presence of octanoic acid challenge, respectively. Following exposure to 0.9mM of C8 for 24h, the engineered yeast had a 10-fold higher cell density relative to the baseline strain. Moreover, overexpressing $Acc1^{S1157A}$ allowed survival at C8 concentrations that were lethal for the baseline strain. This marked reduction of toxicity was shown to be due to higher membrane integrity as an 11-fold decrease in leakage of intracellular magnesium was observed. Due to the increase in oleic acid, this approach has the potential to reduce toxicity of other valuable bioproducts such as shorter chain aliphatic acids and alcohols and other membrane stressors. In an initial screen, increased resistance to n-butanol, 2-propanol, and hexanoic acid was demonstrated with cell densities 3.2-, 1.8-, and 29-fold higher than the baseline strain, respectively.

3.3 Introduction

The use of renewable raw materials in lieu of petroleum-based feedstocks has become increasingly important not only for political, energetic, and economic reasons but also due to environmental concerns (Carlson, 2011; Demski et al., 2014; Lopes, 2015; Perlack et al., 2005). Higher levels of greenhouse gases derived from fossil fuel consumption have been related to climate change, affecting sea levels, thermohaline circulation, and coral reefs (Liao et al., 2016). Moreover, the extraction process and utilization of fossil fuels can contaminate water and air (Chen et al., 2015). In response to these threats, there is an increasing incentive for the production of biofuels and biobased chemicals (Schwartz et al., 2016). Microbial production of short and medium chain fatty acids, such as octanoic acid, has the potential to functionally replace molecules derived from petroleum for synthesis of aliphatic alcohols (Gunukula et al., 2016) and high-demand monomers for synthesis of polyolefins (Polyolefin Comonomers-World Markets, 2005-2015). However, biological production of fatty acids such as octanoic acid (C8) is hindered by the toxic effects on the microbial cell factories (Jarboe et al., 2013; Sandoval and Papoutsakis, 2016).

Inhibition of cell growth by fatty acids is the consequence of multiple factors including triggering of oxidative stress, dysfunctional regulation of internal turgor pressure, lipid peroxidation, membrane trafficking, and disruption of mitochondrial, vacuolar, and plasma membrane organization (Casal et al., 2008; Mira et al., 2010; Piper et al., 2001; Wojtczak and Więckowski, 1999). For octanoic acid, the effects on the plasma membrane are considered the main mechanism of microbial growth inhibition. When the yeast *Saccharomyces cerevisiae* was challenged with octanoic acid, transcriptome analysis showed activation of genes related to regulation of iron and phosphate starvation (Liu et al., 2013). Supplementation of the medium with Fe^{2+}, Fe^{3+} or KH_2PO_4 did not mitigate the toxicity of C8 and had no impact on cell growth, suggesting that membrane integrity had been compromised, causing leakage of these essential

nutrients and triggering the observed starvation transcriptional response (Liu et al., 2013). Cabral et al. (2001) reported that disruption of the *S. cerevisiae* cell membrane organization by octanoic acid dissipated the trans-membrane proton motive force, triggering activation of H^+-ATPase to restore pH homeostasis. The negative effects on the cell membrane are likely due to octanoic acid retention; nearly 80% of the carboxylic acid remains in the cell wall fraction after 3h of exposure, dropping to values between 30% and 50% after 12 h (Borrull et al., 2015).

To cope with membrane-related stresses such as changes in temperature, osmotic stress and exposure to membrane-damaging substances, microorganisms can modulate their membrane composition to maintain function, integrity, stability and fluidity (Arneborg et al., 1995; Bui et al., 2015; Hazel and Eugene Williams, 1990; Prashar et al., 2003; Rodríguez-Vargas et al., 2007; You et al., 2003). In general, an increase in saturated fatty acids promotes membrane stability to solvents and high temperatures due to the establishment of more van der Waals interactions, while introduction of a cis-unsaturation impacts membrane fluidity. Longer chain length can provide higher stability and rigidity (Sandoval and Papoutsakis, 2016). Adding exogenous oleic acid (C18:1) to the media was shown to mitigate the toxic effects of octanoic acid (Liu et al., 2013) and acetaldehyde (Matsufuji et al., 2008) on the yeast cells. Expressing the enzymes insect acyl coenzyme A Δ9 Z-desaturase (TniNPVE) and rat elongase 2 (rELO2) increased the fraction of oleic acid from 14.9% to 32% and from 29% to 44%, respectively (Yazawa et al., 2011; You et al., 2003). This resulted in improved tolerance when cells were challenged with ethanol, *n*-butanol, n-propanol, and 2-propanol. However, in the study by Liu et al. (2013), expression of TniNPVE failed to increase oleic acid levels enough to provide tolerance against octanoic acid. In two recently published studies, overexpression of the native Δ9-fatty acid desaturase Ole1 increased the fraction of oleic acid from 23% to approximately 30%, and increased membrane stability (Fang et al., 2017; Nasutution et al., 2017). Based on the changes in fatty acid composition, it was

hypothesized that modification of membrane rigidity activates the cell's stress response mechanism leading to increased proton efflux, diminished membrane damage and lower levels of ROS (Nasutution et al., 2017). Higher oleic acid levels were also found to ameliorate cadmium-related stresses by promoting cytoplasmatic membrane stability via inhibition of lipid peroxidation (Fang et al., 2017). These studies demonstrate that modulation of fatty acid composition results in increased membrane stability.

Our laboratory recently engineered the *S. cerevisiae* acetyl-CoA carboxylase enzyme to prevent Snf1-mediated deactivation, and thus increase the synthesis of polyketides following glucose depletion (Choi and Da Silva, 2014). This entailed identifying a critical serine residue (1157) and replacing it with alanine ($Acc1^{S1157A}$). In addition to improving polyketide titers, this strain showed a 3-fold increase in production of total fatty acids. Interestingly oleic acid was the predominant acyl chain with levels 7.3-fold higher than the baseline strain (representing a 2.3-fold increase in the percentage of oleic acid).

3.3.1 Aims

In the current study, we evaluated how the increased proportion of oleic acid due to expression of $Acc1^{S1157A}$ mitigates the toxic effects of octanoic acid. The fatty acid profiles of the baseline and engineered strain in the presence and absence of octanoic acid were measured. We then determined the viability of the cells at increasing concentrations of C8, and studied the effects of the increased synthesis of oleic acid on membrane integrity upon exposure to lethal C8 concentrations. This is the first report where endogenous synthesis of oleic acid was able to provide tolerance against octanoic acid. The results will be important for increasing titers of octanoic acid produced in *S. cerevisiae* (Leber and Da Silva, 2014). The increased tolerance to *n*-butanol, 2-propanol, and hexanoic acid observed demonstrates potential application when producing other toxic biobased chemicals that disrupt the yeast membrane.

3.4 Materials and Methods

3.4.1 Yeast and bacterial strains

Saccharomyces cerevisiae BY4741 (*MATa his3Δ1 leu2Δ0 met15Δ0 ura3Δ0)* (Brachmann et al., 1998) was used as the base yeast strain. A copy of the gene for $Acc1^{S1157A}$ (acetyl-CoA carboxylase with the mutation S1157A) under transcriptional control of the *S. cerevisiae PGK1* promoter and *CYC1* terminator, was integrated into the genome as described by Choi and Da Silva (2014). This new strain is designated BY4741-ACC1m.

3.4.2 Media and cultivation

Cells were inoculated from -80°C stock and grown in 5 mL of YPD non-selective complex medium (20 g/L dextrose, 20 g/L peptone, 10 g/L yeast extract) for 14-16 h. The cells were then transferred (initial OD_{600}=0.05) to 5 mL of SDC-A,U medium (20 g/L dextrose, 5 g/L casamino acids, 5g/L ammonium sulfate, 1.7 g/L yeast nitrogen base without amino acids, 50 mg/L adenine, 20 mg/L uracil) and incubated for 10-12 h. This culture was used as the inoculum for the subsequent tube and flask cultures (initial OD_{600}=0.05) in SDC-A,U supplemented with either octanoic acid (from a 100 mM stock in 70% ethanol, as previously described (Liu et al., 2013)) or an equivalent amount of 70% ethanol for the control cultures. Maximum concentration of ethanol did not exceed 1% (v/v), a concentration at which there is no detectable effect on yeast growth (Cabral et al., 2001). For all conditions studied, media was buffered using 100 mM MES (2-(4-Morpholino) ethane Sulfonic Acid) and pH was adjusted to 5.5 before inoculation in order to prevent the effect of pH variations due to addition of octanoic acid. All cells were cultivated at 30°C in a 250 rpm agitated shaker, and growth was monitored by optical density measurements at 600 nm in a Shimadzu UV-2450 spectrophotometer (Columbia, MD). For the other stressors, buffered media was supplemented with hexanoic or decanoic acid using 2 M and 100 mM stock

solutions in 70% ethanol, respectively. Ethanol, *n*-butanol and 2-propanol were directly supplemented to the media.

Determination of octanoic acid Minimal Inhibitory Concentration (MIC) was performed using the broth macrodilution method described by Narendranath et al. (2001). Biological triplicates were exposed to concentrations of 3 mM, 2.5 mM, 1.5 mM, 1.25 mM and 0.75 mM at pH=5.5. The octanoic acid stock in 70% ethanol was prepared at 300 mM to maintain final ethanol concentration below 1%. MIC was defined as the smallest concentration of acid that inhibited growth for a period of 72 h.

3.4.3 Fatty acid extraction analysis

Yeast cells were grown in 250 ml of media buffered with 100 mM MES in the absence or presence of 0.7 mM and 1.5 mM octanoic acid at pH=5.50. At OD_{600}=1, the cells were harvested by centrifugation (2000g, 4°C, 10 min) to obtain the same cell mass for each culture. Fatty acid extraction, methylation, and quantification via GC-MS were performed as described by Leber et al. (2015) using nonadecanoic acid as an internal standard. Fatty acid percentages are given on a mass basis.

3.4.4 Membrane leakage quantification

The membrane leakage protocol was based on previously described work by Prashar et al. (2003) and Liu et al. (2013). Cells were grown in 25 ml of SDC-A,U medium in 150 mL Erlenmeyer flasks at 30°C and 250 rpm. When OD_{600} reached 1.0, cells were harvested by centrifugation and washed twice with NaCl solution (0.9% w/v, pH=5.50). The cells were then resuspended in 4 ml of the same NaCl solution and supplemented with either 1 ml of a 7.5 mM octanoic acid solution (prepared from the 100 mM octanoic acid stock solution in 70% ethanol) to achieve a final concentration of 1.5 mM while maintaining pH at 5.50, or the equivalent amount of ethanol solution (for the controls). In all cases, ethanol concentration was kept at <1% (v/v).

After incubation in the presence of the acid for 25 min at 30°C, the cells were centrifuged at 17,000g for 5 min at 4°C and the magnesium content of the supernatant was determined via fluorescence using the cell impermeable pentapotassium salt of the molecular probe Magnesium Green™ (ThermoFisher Scientific, M3733, Eugene, OR). Fluorescence at λ_{em}=531 nm was measured by excitation at λ_{ex}=506 nm in Costar Black 384-well or Nunc 96-well plates using a fluorometer with temperature control at 25°C (SpectraMax M2, Molecular Devices, Sunnyvale, CA). The concentration of magnesium was determined using the equation below (Szmacinski and Lakowicz, 1996) by running standards for calculation of K_D and F_{max} at each experimental condition (0.9% NaCl pH=5.50 with and without 1.5 mM octanoic acid). Reported values correspond to the difference in measured Mg^{2+} concentration per cell between exposed and unexposed, as previously reported by Prashar et al. (2003). Mg^{2+} concentration was determined by the change in fluorescence observed at t=25 min with respect to t=0 min upon exposure to octanoic acid. A minimum of six biological replicates (with three readings per replicate) were performed for each condition.

$$[A] = K_D \frac{F - F_{min}}{F_{max} - F}$$

3.4.5 Statistical analysis

Statistical analysis consisted of either t-test or a two-way ANOVA followed by t-test using Bonferroni corrections to account for multiple comparisons (Rice, 1989).

3.5 Results and Discussion

3.5.1 Effects of expression of Acc1 mutant on cell lipid composition

The enzyme Acc1 catalyzes the conversion of acetyl-CoA to malonyl-CoA, a key step in the synthesis of polyketides and fatty acids. In prior work, we engineered the yeast Acc1 to prevent deactivation via phosphorylation of the serine residue 1157 (Choi and Da Silva, 2014). The prolonged and higher activity of the Acc1^{S1157A} enzyme led to approximately threefold increases in both the polyketide 6-methylsalicylic acid and native fatty acids, with the most dramatic change in fatty acid composition observed for oleic acid. We thus integrated a copy of this mutant *ACC1* gene into *S. cerevisiae* strain BY4741 (BY4741-ACC1m) and the fatty acid composition was compared to the original baseline strain.

Strains BY4741 and BY4741-ACC1m were cultivated in buffered SDC-AU medium, and collected in early exponential phase. Intracellular fatty acid levels were then measured via GC-MS following methylation. The most abundant fatty acids in *S. cerevisiae* are palmitic (C16:0), palmitoleic (C16:1), stearic (C18:0), and oleic (C18:1) acids, comprising more than 96% of total fatty acids (Augustyn, 1989; Liu et al., 2013; Prashar et al., 2003). The fatty acid profile of the baseline BY4741 strain was consistent with these reports, with 57% palmitoleic acid, 15% palmitic acid, 26% oleic acid and 2% stearic acid (Figure 3.1A). The engineered BY4741-ACC1m strain had a significantly different lipid profile, consisting of 8% palmitoleic acid, 3% palmitic acid, 79% oleic acid, and 10% stearic acid. Comparison of the two shows a 3.1-fold increase in the oleic acid fraction for strain BY4741-ACC1m, with a simultaneous 7.6-fold decrease in the palmitoleic acid fraction. This trend is also observed for saturated palmitic and stearic acids, where C16 fraction decreases while C18 increases. The increase in the percentage of oleic acid was significantly greater than that observed for the strain used in our initial Acc1^{S1157A} study. Overall, the changes in fatty acid composition resulted in a 7.8% increase in the average length of the fatty acid chains

(Figure 3.1B). This has been linked to increased stability and rigidity of the membrane in bacteria (Sandoval and Papoutsakis, 2016) and has been reported in octanoic-acid adapted *S. cerevisiae* cells (Liu et al., 2013). This increase in average lipid length was accompanied by an increase in total fatty acid content, as previously observed (Choi and Da Silva, 2014).

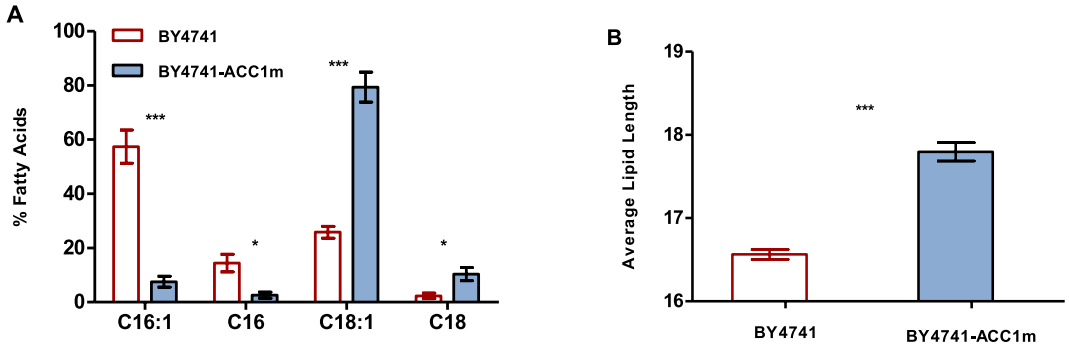

Figure 3.1. Fatty acid profiles. (A) Fatty acid percentages of C16:1, C16, C18:1 and C18 for *S. cerevisiae* strains BY4741 (open bars) and BY4741-ACC1m (filled bars) and (B) average lipid length of both strains. Results show average and SEM of biological triplicates (*p<0.05 and ***p<0.001, relative to baseline strain).

Longer average fatty acid chain length has also been observed in other studies expressing Acc1^{S1157A}. Hofbauer et al. (2014) showed that a higher activity resulting from the serine mutation leads to an increased production of malonyl-CoA and higher ratio of C18 to C16 fatty acids. Interestingly, when the Acc1-specific inhibitor Soraphen A was added, this trend was reversed. Moreover, Zhou et al. (2016) observed increased synthesis of longer chain fatty acids when Acc1^{S1157A,S659A} was overexpressed. In *in vitro* studies on the *S. cerevisiae* fatty acid synthase (Hori et al., 1987), fatty acids with longer average lipid lengths were obtained when acetyl-CoA is limiting and there is an excess of malonyl-CoA.

3.5.2 Resistance against octanoic acid toxicity

Supplementation of oleic acid to the media has been reported by Liu et al. (2013) to alleviate octanoic acid toxicity in *S. cerevisiae* by incorporation into the cell's membrane as a defense mechanism against this membrane-damaging compound. However, engineering the yeast

to increase endogenous oleic acid levels (by expressing TniNPVE) only increased the C18:1 fraction by 9%, insufficient to mitigate membrane damage. Our strain BY4741-ACC1m expressing the modified Acc1 enzyme substantially altered the fatty acid profile in the cell and increased the percentage of oleic acid by more than threefold to 79% percent of total fatty acids. Thus, we examined whether this increase is able to provide resistance against octanoic acid toxicity.

Strains BY4741-ACC1m and BY4741 (control) were cultured in buffered SDC-A,U medium supplemented with increasing concentrations of octanoic acid. Cell optical density (OD) was measured at 24 h and 36 h (Figure 3.2). At 24 h, the greatest difference in cell growth was observed in the medium containing 0.9 mM C8, with a 10-fold higher OD when $Acc1^{S1157A}$ was expressed. The concentration of 0.7 mM C8 was not completely inhibitory for the base strain, and a 3.2-fold increase in cell growth was observed for the engineered BY4741-ACC1m. The highest concentration screened (1.5 mM C8) showed similar inhibitory effects for both strains, with no significant difference in growth. At 36 h (Figure 3.2B), the greatest difference in cell density was observed at 1.2 mM C8, with a 19-fold improvement for the strain expressing $Acc1^{S1157A}$. At the highest concentration screened (1.5 mM), cell density was augmented 3.7-fold.

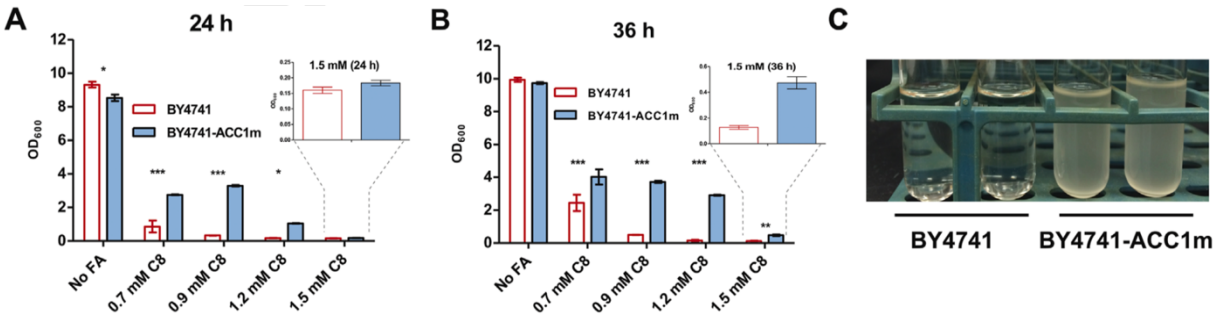

Figure 3.2. Effect of 0.7 mM, 0.9 mM, 1.2 mM and 1.5 mM octanoic acid on cell density (OD_{600}) of BY4741 (open bars) and BY4741-ACC1m (filled bars) at (A) 24 h and (B) 36 h. Results represent average and SEM of three biological replicates. C) Tube cultures (after 80 h) of BY4741 and BY4741-ACC1m exposed to 1.5 mM octanoic acid (*p<0.05, **p<0.01, ***p<0.001, relative to baseline strain).

These results demonstrate that the strain expressing $Acc1^{S1157A}$ can survive at concentrations up to 1.5 mM (Figure 3.2C), while the maximum tolerance of the baseline strain is 0.7-0.9 mM. Exposing the cells to higher concentration of octanoic acid allowed determination of a Minimal Inhibitory Concentration (MIC). The resulting MIC for the baseline strain was 1.25 mM, while for the engineered strain it was 2.5 mM (where MIC was defined as the smallest concentration of acid that inhibited growth for a period of 72 h). Liu *et al.* (2013) reported growth rates lower than 0.025 h^{-1} at 0.8 mM and 1 mM for BY4741, an observation that is consistent with these results. Moreover, Figure 3.2 shows that expression of $Acc1^{S1157A}$ does not have a detrimental effect on cell growth, with cell density of the engineered strain only 10% lower than the base strain at 24 h in C8-free medium and with no statistically significant difference at 36 h. This indicates that there is no significant metabolic burden with our approach.

3.5.3 Fatty acid composition and cell growth for cells exposed to octanoic acid

Expression of the enzyme $Acc1^{S1157A}$ resulted in a 3.1-fold increase in the percentage of oleic acid relative to the baseline strain in the absence of an octanoic challenge (Figure 3.1). It has been reported that *S. cerevisiae* modifies its membrane composition upon exposure to octanoic acid. Thus, we compared the lipid profile and cell growth rate for BY4741 and BY4741-ACC1m in the presence of octanoic acid. We chose the level of supplemented C8 to have a significant effect on cell survival, but still allow enough growth for sufficient cell harvesting for fatty acid analysis. Using this rationale, we exposed the cells to 0.7 mM octanoic acid. Three independent colonies of the baseline and engineered strains were grown in buffered SDC-A,U medium containing 0.7 mM octanoic acid. Cells were collected by centrifugation in early exponential phase, intracellular fatty acids were extracted, and methylated, and fatty acid content was analyzed via GC-MS.

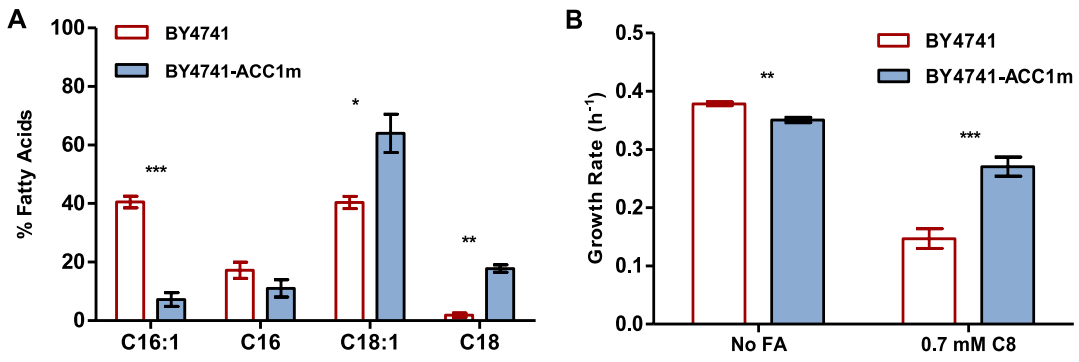

Figure 3.3. Fatty acid percentages and growth rates for BY4741 and BY4741-ACC1m in the presence of 0.7 mM octanoic acid. (A) Fatty acid fractions in early exponential phase and (B) Cell growth rates for BY4741 and BY4741-ACC1m in the presence of 0.7 mM octanoic acid. Results show average for biological replicates (n=3 for fatty acid profile and n=4 for growth rate). Error bars represent SEM (*p<0.05, **p<0.01, ***p,0.001, relative to baseline strain).

The fatty acid profiles in the presence of 0.7 mM octanoic acid are shown in Figure 3.3A. Comparison of the two strains shows that the C18:1 fraction is 1.6-fold higher in BY4741-ACC1m, while the C16:1 fraction is 5.6-fold greater in BY4741. For saturated fatty acids, the percentage of C18 is 9.6 times higher in the engineered strain, while differences in C16 are not significant. A comparison of Figure 3.3A with Figure 3.1A shows that for the base strain BY4741, upon exposure to 0.7 mM of octanoic acid, the percentage of palmitoleic acid decreased by 17% ($p<0.01$), while the oleic acid increased by 14% ($p<0.01$), reaching 40% of total fatty acids. Changes in individual saturated fatty acid fractions were not significant. This is in accordance with Liu *et. al* (2013), where cells pre-exposed to 0.8 mM octanoic acid and then challenged again with 0.8 mM C8 showed a significant drop in palmitoleic content, while oleic acid levels increased. These adapted cells showed improved membrane integrity, indicating that this change in membrane composition could be an adaptation mechanism to cope with membrane-associated octanoic acid stress. For the engineered strain BY4741-ACC1m, there is a 15% reduction in the fraction of oleic acid ($p<0.001$) and a higher proportion of palmitic and stearic acids, shifting from 2% to 11% and from 10% to 18% ($p<0.05$) respectively.

We measured growth rates for the two strains to assess the effect of the changes in membrane composition on cell resistance to C8 toxicity. In the absence of C8, cell growth rate for BY4741-ACC1m was only 7% lower than that for BY4741, indicating that there is no significant metabolic burden associated with expression of $Acc1^{S1157A}$ (Figure 3.3B). During cultivation in the presence of 0.7 mM C8, growth rate was 84% higher for the engineered strain, demonstrating increased tolerance to the octanoic acid.

As seen in Figure 3.2, cells expressing $Acc1^{S1157A}$ were able to grow (albeit poorly) in octanoic acid at concentrations of up to 1.5 mM. To determine whether there is further modification of cell lipid composition at increasing levels of C8, BY4741-ACC1m was grown in the presence of 1.5 mM octanoic acid and the fatty acid profile was analyzed (Figure 3.4). Membrane composition remained constant with increasing C8 concentration. This finding, along with the decreased viability of cells at 1.5 mM C8, shows that our approach to control the homeoviscous response to counteract membrane damage is limited, processes such as oxidative stress (Legras et al., 2010) are simultaneously taking place and inducing octanoic acid toxicity.

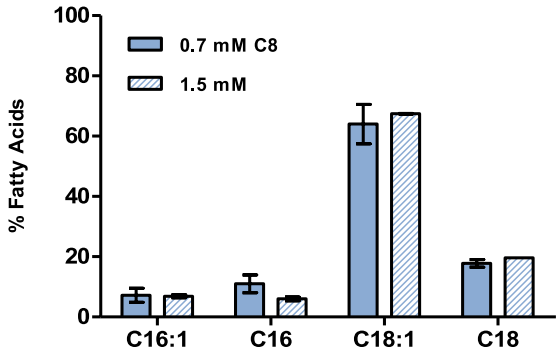

Figure 3.4. Fatty acid composition of BY4741-ACC1m at OD_{600}=1 during cultivation in medium containing 0.7 mM C8 (n=3 biological replicates, filled) and 1.5 mM C8 (n=2, hatched bars). Error bars represent SEM.

3.5.4 Analysis of changes in average lipid length and percentage of saturated fatty acids

The biophysical properties of the membrane bilayer depend on the structure of the fatty acid chains (Zhang and Rock, 2008) and their interactions (Marguet et al., 2006), and analysis of average lipid length and percentage of saturated fatty acids provides a general assessment of membrane properties. Our experiments show that the average lipid length of the baseline strain increased 1.6% when grown in 0.7 mM octanoic acid, shifting from 16.5 to 16.8 (Figure 3.5A). Changes in BY4741 are in accordance with Liu *et al.* (2013), where increasing doses of octanoic acid resulted in increased average lipid length, indicating that this is one of the cell's mechanisms to cope with C8 stress. In contrast, no significant change was observed for BY4741-ACC1m in the C8-containing medium; a higher average lipid length of 17.6 was observed in both media relative to the baseline strain.

Exposure to octanoic acid also resulted in no significant change in the percentage of saturated fatty acids for BY4741 (Figure 3.5B). However, addition of 0.7 mM C8 increased the proportion of saturated acyl chains by 16% in BY4741-ACC1m. This was due to an increase in levels of saturated stearic acid and palmitic acid with a simultaneous decrease in oleic acid (palmitoleic acid levels remain constant). In the absence of the octanoic acid, the engineered strain had 3.8% less saturated fatty acids than the baseline, while exposure to C8 reversed this trend, making the saturated content 9.7% higher for BY4741-ACC1 relative to BY4741.

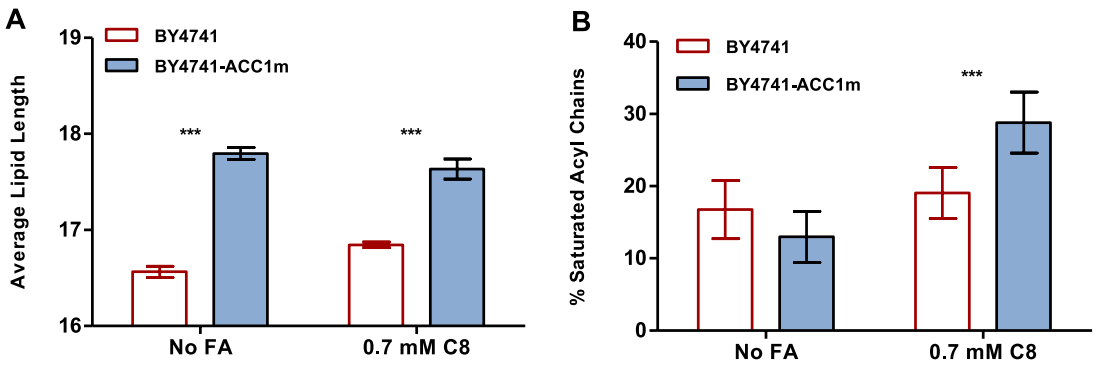

Figure 3.5. Average lipid length and percent of saturated fatty acid chains in absence and presence of 0.7 mM octanoic acid for *S. cerevisiae* strains BY4741 (open bars) and BY4741-ACC1m (filled bars). Results show average and SEM of biological triplicates (**p<0.01, ***p<0.001, relative to baseline strain).

Overall, overexpression of $Acc1^{S1157A}$ increased average lipid length and percent of saturated fatty acids upon exposure to 0.7 mM of octanoic acid. Generally, short acyl chains provide higher fluidity to the membrane, while an increasing proportion of longer chains results in stability and rigidity by increasing the tendency of the aliphatic tails to interact with each other (Sandoval and Papoutsakis, 2016). Introduction of a *cis*-unsaturation results in local decrease of membrane order at the vicinity of the double bond. This decrease in order is accompanied by the insertion of a rigid element that diminishes the range of conformations available to an otherwise flexible chain, resulting in a bend in the aliphatic chain (Hazel and Williams, 1990; Marguet et al., 2006). In contrast, saturated fatty acids tend to form ordered structures with low permeability by packing tightly together through van der Waals interactions (Sandoval and Papoutsakis, 2016; Zhang and Rock, 2008). Therefore, an increase in the proportion of saturated fatty acid is expected to lead to higher stability and lower permeability of the membrane in the presence of octanoic acid.

Based on the increased membrane stability and lower permeability derived from the combination of these changes, we speculate that they are responsible for mitigation of octanoic acid toxicity in the present approach. This is attributable not only to higher levels of oleic acid but also stearic acid. Increased stearic acid levels in *S. cerevisiae* have been observed in previous studies that

aimed to increase oleic acid levels to cope with membrane stress caused by with aliphatic alcohols (Yazawa et al., 2011; You et al., 2003), as well as exposure to 0.5 mM and 0.8 mM octanoic acid (Liu et al., 2013) and 35 µM of decanoic acid (Alexandre et al., 1996). However, it is important to note that this is a simplified analysis of lipid composition effects on the cell that does not consider the impact of lipids on membrane proteins, the presence of micro-domains on cell membrane organization and dynamics (Marguet et al., 2006; Rest et al., 1995), as well as other regulatory mechanisms involved in the cell response to stress (Fang et al., 2017; Legras et al., 2010; Nasutution et al., 2017).

3.5.5 Analysis of membrane integrity

In prior work, octanoic aid was shown to increase membrane permeability (Liu et al., 2013) due to its retention in the cell membrane (Borrull et al., 2015). Liu et al. (2013) used magnesium leakage as a measure of membrane permeability. Magnesium plays an essential role in many physiological cell functions such as cell growth, cell division, enzyme activity, repression of stress protein biosynthesis, and stabilization of the plasma membrane via interaction with phospholipids (Birch and Walker, 2000). It is thus a suitable model ion to evaluate membrane integrity.

To investigate whether the increased proportion of oleic acid resulting from $Acc1^{S1157A}$ expression reduces membrane permeability, we performed a magnesium leakage assay. Strains BY4741 and BY4741-ACC1m were cultivated in SDC-AU medium to OD_{600}=1, and then exposed to 1.5 mM octanoic acid for 25 minutes at 30°C. Extracellular magnesium was then measured via fluorescence by addition of a molecular probe. Reported values correspond to the difference in measured magnesium concentration between exposed and unexposed conditions, as previously reported (Liu et al., 2013; Prashar et al., 2003) and normalized by cell density prior to exposure. As seen in Figure 3.6, the strain expressing $Acc1^{S1157A}$ had an 11-fold decrease in extracellular magnesium concentration relative to baseline BY4741. This result supports that the observed

changes in fatty acid profile are linked to improved membrane integrity, and thus reduced C8 toxicity.

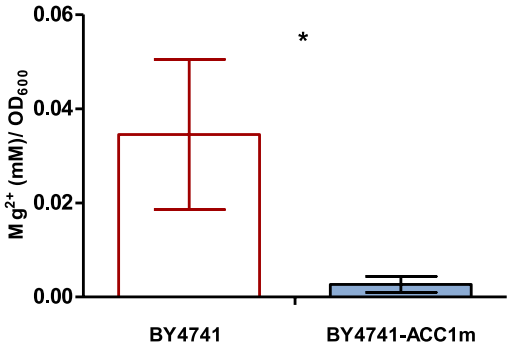

Figure 3.6. Concentration of extracellular magnesium (mM Mg^{2+} per OD_{600}) for BY4741 (n=6, open bar) and BY4741-ACC1m (n=6, filled bar) after exposure to 1.5 mM octanoic acid. Error bars represent SEM (*p<0.05, relative to baseline strain).

3.5.6 Resistance against other stressors

Increased synthesis of oleic acid has been associated with enhanced tolerance to short-chain alcohols such as ethanol, *n*-butanol and 2-propanol (Yazawa et al., 2011; You et al., 2003). This increase has also been observed as a response to exogenous addition of decanoic acid in complex media, where oleic acid levels shifted from 15.8% to 44.1% (Alexandre et al., 1996). Moreover, early studies have shown that exogenous addition of oleic acid partially alleviated toxicity of hexanoic acid (Nordström, 1964).

To determine whether the increase in oleic acid observed due to the $Acc1^{S1157A}$ mutant is capable of alleviating toxicity of these stressors, strains BY4741-ACC1m and BY4741 (control) were cultured in buffered SDC-A,U medium supplemented with either 8.75 mM hexanoic acid (C6), 0.3 mM decanoic acid (C10), 8% ethanol, 1.3% *n*-butanol, or 6% 2-propanol. Alcohol concentrations and time intervals were chosen based on values reported by Yazawa et al. (2011). Carboxylic acid concentrations were determined by screening and selecting the most inhibitory concentrations at 24 h and 48 h.

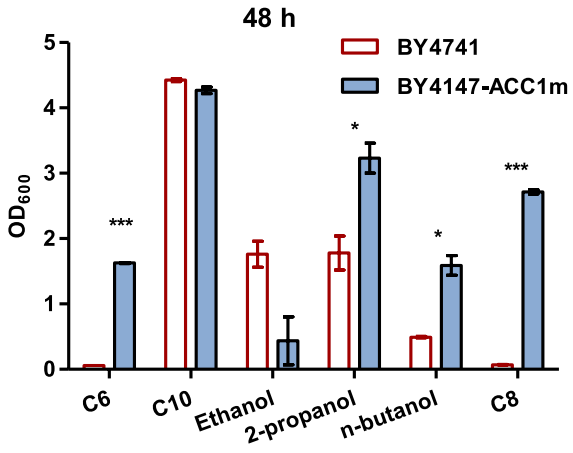

Figure 3.7. Cell density (OD_{600}) at 48 h for baseline strain (BY4741) and engineered strain (BY4741-ACC1m) upon exposure to 8.75 mM hexanoic acid (C6), 0.3 mM decanoic acid (C10), 8% ethanol, 6% 2-propanol and 1.3% *n*-butanol. The results for 1.25 mM octanoic acid (C8) have been included for comparison. Results show average and SEM of biological duplicates (*p<0.05, *** p<0.001, relative to baseline strain).

Following cultivation for 48 in the presence of the various stressors, cell density (OD) was measured and compared for BY4741-ACC1m and BY4741 (Figure 3.7). Expression of $Acc1^{S1157A}$ and the higher oleic acid content in the membrane increased resistance to hexanoic acid, 2-propanol, and n-butanol. This resulted in cell densities 29-, 1.8-, and 3.2-fold higher than the baseline strain, respectively. The results for octanoic acid at 1.25 mM (MIC) are shown for comparison. That no effect was observed for decanoic acid is likely a consequence of the different mechanisms that yeast employs to overcome octanoic and decanoic acids stress. While decanoic acid penetrates the cell and is esterified, octanoic acid remains in the membrane (Borrull et al., 2015; Legras et al., 2010). Interestingly, there was no improvement in ethanol resistance and significant drops in cell growth were observed at 24 h and 36 h; this contrasts with prior reports in the literature at lower oleic acid levels (Yazawa et al., 2011; You et al., 2003; Zheng et al., 2013). Even so, the improved resistance to hexanoic acid, octanoic acid, 2-propanol, and n-butanol demonstrates the general applicability of increasing oleic acid content via $Acc1^{S1157A}$ expression.

3.6 Conclusions

We have ameliorated the toxicity of octanoic acid on *Saccharomyces cerevisiae* by increasing the fraction of oleic acid through expression of the $Acc1^{S1157A}$ mutant of the native acetyl-CoA carboxylase. To our knowledge, this is the highest fraction of oleic acid (79% without C8 challenge, 64% with C8 challenge) reported to date. The engineered strain showed an optical density 19-fold higher upon exposure to 1.2 mM octanoic acid for 36 h and an increase in growth rate of 84% when cells were exposed to 0.7 mM C8. The minimal inhibitory concentration was 2.5 mM for the engineered strain and 1.25 mM for the baseline strain. We attribute this decrease in toxicity to changes in membrane composition, as we observed higher average lipid chain length and percentage of saturated fatty acids in the $Acc1^{S1157A}$ expressing cells exposed to 0.7 mM C8, indicators of increased membrane stability and lowered permeability. These changes resulted in enhanced membrane integrity, based on the 11-fold decrease in magnesium leakage observed. We have also shown that our approach can be applicable to other stressors and increases the tolerance to hexanoic acid, *n*-butanol and 2-propanol.

3.7 References

Alexandre H, Mathieu B, Charpentier C. 1996. Alteration in membrane fluidity and lipid composition, and modulation of H+-ATPase activity in Saccharomyces cerevisiae caused by decanoic acid. *Microbiology* **142**:469–475.

Arneborg N, Hoy CE, Jorgensen OB. 1995. The effect of ethanol and specific growth rate on the lipid content and composition of Saccharomyces cerevisiae grown anaerobically in a chemostat. *Yeast* **11**:953–959.

Augustyn OPH. 1989. Differentiation between Yeast Species, and Strains within a Species, by Cellular Fatty Acid Analysis. Saccharomyces cerevisiae. *South African J. Enol. Vitic.* **10**:8–17.

Birch RM, Walker GM. 2000. Influence of magnesium ions on heat shock and ethanol stress responses of Saccharomyces cerevisiae. *Enzyme Microb. Technol.* **26**:678–687.

Borrull A, López-Martínez G, Poblet M, Cordero-Otero R, Rozès N. 2015. New insights into the toxicity mechanism of octanoic and decanoic acids on Saccharomyces cerevisiae. *Yeast* **32**:451–460.

Brachmann CB, Davies A, Cost GJ, Caputo E. 1998. Designer Deletion Strains derived from Saccharomyces cerevisiae S288C : a Useful set of Strains and Plasmids for PCR-mediated Gene Disruption and Other Applications. *Yeast* **14**:115–132.

Bui LM, Lee JY, Geraldi A, Rahman Z, Lee JH, Kim SC. 2015. Improved n-butanol tolerance in Escherichia coli by controlling membrane related functions. *J. Biotechnol.* **204**:33–44.

Cabral MG, Viegas C a., Sá-Correia I. 2001. Mechanisms underlying the acquisition of resistance to octanoic-acid-induced-death following exposure of Saccharomyces cerevisiae to mild stress imposed by octanoic acid or ethanol. *Arch. Microbiol.* **175**:301–307.

Carlson WB. 2011. The Modeling of World Oil Production Using Sigmoidal Functions—Update 2010. *Energy Sources, Part B Econ. Planning, Policy* **6**:178–186.

Casal M, Paiva S, Queirós O, Soares-Silva I. 2008. Transport of carboxylic acids in yeasts. *FEMS Microbiol. Rev.* **32**:974–994.

Chen M, Smith PM, Wolcott MP. 2015. U . S . Biofuels Industry : A Critical Review of Opportunities and Challenges. *Bioprod. Bussinessiness* **2025**:42–57.

Choi JW, Da Silva NA. 2014. Improving polyketide and fatty acid synthesis by engineering of the yeast acetyl-CoA carboxylase. *J. Biotechnol.* **187**:56–59. http://dx.doi.org/10.1016/j.jbiotec.2014.07.430.

Demski C, Poortinga W, Pidgeon N. 2014. Exploring public perceptions of energy security risks in the UK. *Energy Policy* **66**:369–378. http://dx.doi.org/10.1016/j.enpol.2013.10.079.

Fang Z, Chen Z, Wang S, Shi P, Shen Y, Zhang Y, Xiao J, Huang Z. 2017. Overexpression of OLE1 enhances cytoplasmic membrane stability and confers resistance to cadmium in Saccharomyces cerevisiae. *Appl. Environ. Microbiol.* **83**:e02319-16.

Gunukula S, Keeling PL, Anex R. 2016. Risk advantages of platform technologies for biorenewable chemical production. *Chem. Eng. Res. Des.* **107**:24–33.

Hazel JR, Williams EE. 1990. The role of alteration in membrane lipid composition in enabling physiological adaptation of organisms to their physical environment. *Prog. Lipid Res.* **29**:167–227.

Hazel JR, Eugene Williams E. 1990. The role of alterations in membrane lipid composition in enabling physiological adaptation of organisms to their physical environment. *Prog. Lipid Res.* **29**:167–227.

Hori T, Nakamura N, Okuyama H. 1987. Possible involvement of acetyl coenzyme A carboxylase as well as fatty acid synthetase in the temperature-controlled synthesis of fatty acids in Saccharomyces cerevisiae. *J. Biochem.* **101**:949–956. http://www.ncbi.nlm.nih.gov/entrez/query.fcgi?cmd=Retrieve&db=PubMed&dopt=Citation&list_uids=2886496.

Jarboe LR, Royce L a, Liu P. 2013. Understanding biocatalyst inhibition by carboxylic acids. *Front. Microbiol.* **4**:272.

Leber C, Polson B, Fernandez-Moya R, Da Silva NA. 2015. Overproduction and secretion of free fatty acids through disrupted neutral lipid recycle in Saccharomyces cerevisiae. *Metab. Eng.* **28**:54–62.

Legras JL, Erny C, Le Jeune C, Lollier M, Adolphe Y, Demuyter C, Delobel P, Blondin B, Karst F. 2010. Activation of two different resistance mechanisms in Saccharomyces cerevisiae upon exposure to octanoic and decanoic acids. *Appl. Environ. Microbiol.* **76**:7526–35.

Liao JC, Mi L, Pontrelli S, Luo S. 2016. Fuelling the future: microbial engineering for the production of sustainable biofuels. *Nat. Rev. Microbiol.* **14**:288–304.

Liu P, Chernyshov A, Najdi T, Fu Y, Dickerson J, Sandmeyer S, Jarboe L. 2013. Membrane stress caused by octanoic acid in Saccharomyces cerevisiae. *Appl. Microbiol. Biotechnol.* **97**:3239–3251.

Lopes MSG. 2015. Engineering biological systems toward a sustainable bioeconomy. *J. Ind. Microbiol. Biotechnol.* **42**:813–38.

Marguet D, Lenne P-F, Rigneault H, He H-T. 2006. Dynamics in the plasma membrane: how to combine fluidity and order. *EMBO J.* **25**:3446–57.

Matsufuji Y, Fujimora S, Ito T, Nishizawa M, Miyaji T, Nakagawa J, Ohyama T, Tomizuka N, Nakagawa T. 2008. Acetaldehyde tolerance in Saccharomyces cerevisiae involves pentose phosphate pathway and oleic acid biosynthesis. *Yeast* **25**:825–833.

Mira NP, Teixeira MC, Sá-Correia I. 2010. Adaptive response and tolerance to weak acids in Saccharomyces cerevisiae: a genome-wide view. *OMICS* **14**:525–40.

Narendranath N V, Thomas KC, Ingledew WM. 2001. Effects of acetic acid and lactic acid on the growth of Saccharomyces cerevisiae in a minimal medium. *J. Ind. Microbiol. Biotechnol.* **26**:171–177.

Nasutution O, Lee YM, Kim E, Lee Y, Kim W, Choi W. 2017. Overexpression of OLE1 enhances stress tolerance and constituvely activates MAPK HOG pathway in Saccharomyces cerevisiae. *Biotechnol. Bioeng.* **114**:620–31.

Nordström K. 1964. Effect of higher fatty acids and toxicity of lower fatty acids. *J. Inst. Brew.* **70**:223–42. http://www.nature.com/nature/journal/v210/n5031/abs/210099a0.html.

Perlack RD, Wright LL, Turhollow AF, Graham RL, Strokes BJ, Erbach DC. 2005. Biomass as feedstock for a bioenergy and bioproducts industry: The technical feasibility of a billion-ton annual supply. Oak Ridge, Tenessee.

Piper P, Calderon CO, Hatzixanthis K, Mollapour M. 2001. Weak acid adaptation: The stress response that confers yeasts with resistance to organic acid food preservatives. *Microbiology* **147**:2635–2642.

Prashar A, Hili P, Veness RG, Evans CS. 2003. Antimicrobial action of palmarosa oil (Cymbopogon martinii) on Saccharomyces cerevisiae. *Phytochemistry* **63**:569–575.

Rest M, Kamminga AH, Nakano A, Anraku Y, Poolman B, Konings WILN. 1995. The Plasma Membrane of Saccharomyces cerevisiae: Structure, Function, and Biogenesis. *Microbiol. Rev.* **59**:304–322.

Rice WR. 1989. Analyzing Tables of Statistical. *Evolution (N. Y).* **43**:223–225.

Rodríguez-Vargas S, Sánchez-García A, Martínez-Rivas JM, Prieto JA, Randez-Gil F. 2007. Fluidization of membrane lipids enhances the tolerance of Saccharomyces cerevisiae to freezing and salt stress. *Appl. Environ. Microbiol.* **73**:110–116.

Sandoval NR, Papoutsakis ET. 2016. Engineering membrane and cell-wall programs for tolerance to toxic chemicals: Beyond solo genes. *Curr. Opin. Microbiol.* **33**:56–66.

Schwartz TJ, Shanks BH, Dumesic JA. 2016. Coupling chemical and biological catalysis: A flexible paradigm for producing biobased chemicals. *Curr. Opin. Biotechnol.* **38**:54–62.

Szmacinski H, Lakowicz JR. 1996. Fluorescence lifetime characterization of magnesium probes: Improvement of Mg(2+) dynamic range and sensitivity using phase-modulation fluorometry. *J. Fluoresc.* **6**:83–95.

Wojtczak L, Więckowski MR. 1999. The mechanisms of fatty acid-induced proton permeability of the inner mitochondrial membrane. *J. Bioenerg. Biomembr.* **31**:447–455.

Yazawa H, Kamisaka Y, Kimura K, Yamaoka M, Uemura H. 2011. Efficient accumulation of oleic acid in Saccharomyces cerevisiae caused by expression of rat elongase 2 gene (rELO2) and its contribution to tolerance to alcohols. *Appl. Microbiol. Biotechnol.* **91**:1593–1600.

You KM, Rosenfield C, Knipple DC. 2003. Ethanol tolerance in the yeast Saccharomyces cerevisiae is dependent on cellular oleic acid content. *Appl. Environ. Microbiol.* **69**:1499.

Zhang Y-M, Rock CO. 2008. Membrane lipid homeostasis in bacteria. *Nat. Rev. Microbiol.* **6**:222–233.

Zheng DQ, Liu TZ, Chen J, Zhang K, Li O, Zhu L, Zhao YH, Wu XC, Wang PM. 2013. Comparative functional genomics to reveal the molecular basis of phenotypic diversities and guide the genetic breeding of industrial yeast strains. *Appl. Microbiol. Biotechnol.* **97**:2067–2076.

Zhou YJ, Buijs NA, Zhu Z, Qin J, Siewers V, Nielsen J. 2016. Production of fatty acid-derived oleochemicals and biofuels by synthetic yeast cell factories. *Nat. Commun.* **7**:11709. http://www.nature.com/ncomms/2016/160525/ncomms11709/fig_tab/ncomms11709_F4.html.

Chapter 4

Increasing *Saccharomyces cerevisiae* tolerance to decanoic acid by overexpression of membrane transporters

4.1 Abstract

Alleviating the toxicity of decanoic acid (C10) is critical for synthesis of this biorenewable chemical precursors in yeast. Unlike octanoic acid, C10 does not accumulate in the membrane and the majority crosses into the cytoplasm, causing a myriad of negative effects, such as acidification, oxidative stress, dysregulation of internal ionic strength, and lipid peroxidation, among others. We thus decided to increase tolerance by exporting C10 via overexpression of efflux pumps. Seven candidate pumps were selected based on the literature. To determine their potential role in C10 transport, we screened strains with the transporter genes deleted for increased sensitivity to decanoic acid. This led to the selection of Tpo1, Pdr5, Snq2 and Pdr12 for further studies. Among these, the overexpression of Tpo1, Pdr5, or Pdr12 was found to be a promising strategy for improving C10 tolerance. We also found that expression levels need to be fine-tuned to have a balance between efficient C10 efflux and potential adverse effects associated with transporter protein overproduction. The optimal expression system for Tpo1 and Pdr5 was a low-copy centromeric plasmid, while Pdr12 provided more benefits against C10 when expressed from a 2µ-based plasmid. Efforts to further improve the function of Tpo1 by increasing the driving force of this H^+-antiporter through overexpression of *PMA1* led to an increase in cell density of up to 17-fold with respect to the control strain at 24 h.

4.2 Introduction

A highly regulated network of enzymes that functions on acyl-thioester intermediates mediates biological production of fatty acids in microorganisms. The network consists of an iterative set of reactions that can be divided into four main processes: chain initiation, elongation, termination and modification (Figure 4.1) (Pfleger et al., 2015). In yeast, the elongation cycle is repeated until palmitate and stearate are released, making 16 and 18 the primary chain lengths (Leibundgut et al., 2008). However, shorter hydrocarbon chains such as C8 and C10 are desired due to a wide range of applications, including as precursors to several industrial products such as flavoring components (Oguro et al.,2014), perfumes (Panda, 2010), alpha olefins (Ford et al., 2012), and cold flow agents (Aresta et al., 2012). This has made octanoic and decanoic acids the most expensive natural fatty acids (Aresta et al., 2012). Our lab has engineered *S. cerevisiae* to produce SCFAs by heterologous expression of human fatty acid synthase and a short chain thioesterase, obtaining titers of up to 111 mg/L of a C6, C8 and C10 mixture (Leber and Da Silva, 2013).

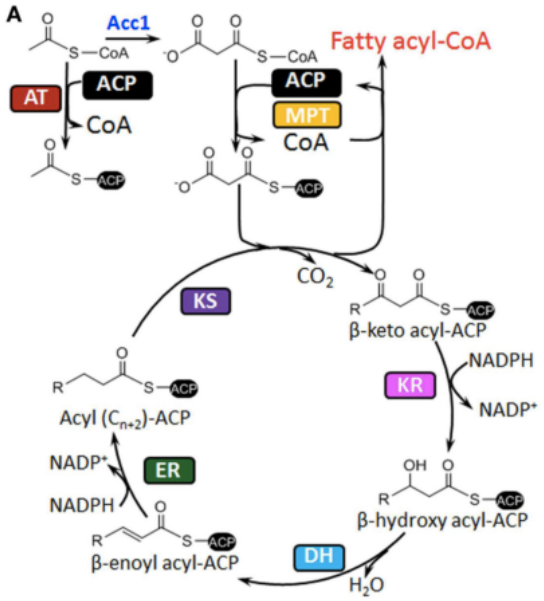

Figure 4.1.Fatty acid synthesis cyclic pathway in *S. cerevisiae* (Zhou et al., 2014).

Although *S. cerevisiae* does not naturally produce large quantities of fatty acids, it is considered a good candidate for their production due to its robustness, acid tolerance, and high availability of genetic information and molecular tools (Mira et al., 2010). However, carboxylic acids may have an antimicrobial effect depending on their chemical properties, mainly hydrophobicity and pKa, which are related to transport of these molecules into the cell (Jarboe et al., 2013). In Chapter 3, a strategy to improve tolerance to octanoic and hexanoic acid was discussed (Besada-Lombana et al., 2017). In this Chapter, the focus will be on the effects of decanoic acid, which has a different toxicity mechanism.

The properties of decanoic acid are shown in Table 4.1 (PubChem). According to the Henderson-Hesselbach equation, at a pH lower than 4.90, the lipid-soluble undissociated form of the acid is favored, enabling the weak acid to diffuse across the membrane (Casal et al., 2008; Jarboe et al., 2013). Diffusion can be either simple or facilitated by the aquaglyceroporin Fps1p (Mollapour and Piper, 2007). However, it is unlikely that facilitated diffusion is the mechanism responsible for decanoic import, given its high permeability coefficient, a consequence of its high partition coefficient (Kamp and Hamilton, 2006). In general, the diffusion process follows Overton's Rule, which states that the entry of the molecules into the cell is governed by its lipid solubility (Al-Awqati, 1999).

Table 4.1. Acid-base properties (pKa) and partition coefficient in octanol (logP) of decanoic acid.

	pKa (25ºC)	**logP**
Decanoic Acid	4.90	4.09

In contrast to octanoic acid, which accumulates in the membrane, affecting its integrity, the majority of decanoic acid crosses into the cytoplasm. It has been observed that upon 3 h of exposure to decanoic acid, 70% of the recovered acid comes from the intracellular fraction, while the remaining 30% is located in the cell wall (Borrull et al., 2015a). Once inside the cell, the near-

neutral pH of the cytosol leads to dissociation into protons and the carboxylate anion. The protons acidify the cytoplasm, altering several metabolic pathways, causing oxidative stress and disrupting the proton gradient maintained across the plasma membrane (Casal et al., 2008; Mira et al., 2010). Increasing intracellular concentration of counterions affects a wide range of cell functions, such as regulation of internal ionic strength, turgor pressure, lipid peroxidation, membrane trafficking, and plasma and vacuolar membrane organization (Teixeira et al., 2007).

In order to recover from the toxic effects of weak acids, cells trigger different mechanisms to cope with either cytosolic acidification or anion accumulation. To reduce proton concentration, plasma membrane H^+-ATPases, such as Pma1p, are activated. These enzymes couple the hydrolysis of ATP to proton extrusion (Viegas and Sá-Correia, 1991) and are also present in vacuolar membranes. Vacuolar H^+-ATPases are suggested to contribute to recovery of cytosolic pH by sequestration of protons into the lumen of the organelle (Mira et al., 2010). For recovery from carboxylate accumulation, decanoate esterification and transport to the outside of the cell via efflux pumps are the main mechanisms of defense (Borrull et al., 2015b; Legras et al., 2010). In this chapter, we will focus on the latter.

In yeast, the two most extensively studied families of transporters involved in efflux are the ATP-binding cassette transporters (ABC) and the major facilitator superfamily transporters (MFS) (Coleman and Mylonakis, 2009). Members of the ATP-binding cassette transporter superfamily utilize energy derived from ATP hydrolysis to export the substrate across the membrane (Coleman and Mylonakis, 2009). In *S. cerevisiae*, ABC transporters are involved in maintenance of diverse cellular functions such as maturation of cytosolic Fe/S proteins, pheromone transport, peroxisome biogenesis, stress response and lipid bilayer hemostasis (Ernst et al., 2005). This superfamily is subdivided into five families: ABCA, ABCB, ABCC, ABCD and ABCG. Among these families, only three are involved in efflux of toxic compounds and receive an

alternative nomenclature: ABCB or multi-drug-resistance (MDR); ABCC or multidrug resistance-associated proteins (MRP); and ABCG or pleiotropic drug resistance (PDR) (Coleman and Mylonakis, 2009). The ABCG family is capable of executing membrane translocation of a wide range of structurally and chemically unrelated substrates (Ernst et al., 2005; Mira et al., 2010) and will be a primary focus of this research. Despite the large substrate diversity, ABC transporters share a basic blueprint: two transmembrane domains (TMDs) that provide a passageway for the molecule being exported and two cytoplasmatic nucleotide-binding domains (NBDs), which bind and hydrolyze ATP (Figure 4.2A) (Hollenstein et al., 2007; Schmitt and Tampé, 2002). One of the proposed mechanisms of transport (Figure 4.2B) is based on the ATP-driven approach of NBDs chains, which appears to trigger a flipping of the TMDs from an inward-facing to an outward-facing conformation, allowing extrusion of the substrate. Once the ATP is hydrolyzed into ADP and inorganic phosphate, the transporter reverts back into the inward-facing conformation, and is able to recruit more substrate (Hollenstein et al., 2007).

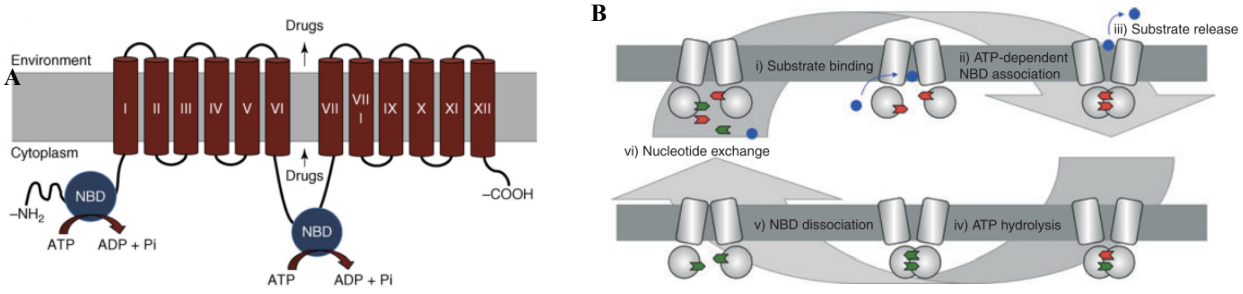

Figure 4.2. ABC transporter A) structure (Sá-Correia et al., 2009) B) proposed mechanism for substrate export (Ernst et al., 2010).

However, the phenomena of multi-drug resistance (MDR) (that is, increased tolerance to a wide range of structurally and functionally unrelated cytotoxic chemicals) does not only involve ABC transporters, but also the major facilitator superfamily (MFS) efflux pumps (Sá-Correia et al., 2009). MFS are secondary active transporters that translocate substrates at the expense of the free energy of the transmembrane electrochemical potential of protons generated by the primary

transporters (Forrest et al., 2011; Law et al., 2008). In yeast, the MFS-MDR transporters function by proton anti-port and are classified into two groups: the drug:H^+ antiporter-1 (DHA1), which consists of 12 proteins that have 12 transmembrane domains; and drug:H^+ antiporter-2 (DHA2), which includes 10 proteins that have 14 transmembrane domains (Figure 4.3) (Sá-Correia et al., 2009). One of the most recently proposed mechanisms for MFS antiporters is called the Rocker-Switch Model, in which global conformational changes of the protein drive solute extrusion by formation and breaking of salt bridges (Boyarskiy and Tullman-Ercek, 2015; Law et al., 2008). When a substrate binds effectively, the weak interactions that stabilize the initial conformation of the transporters are weakened. This allows formation of new interactions involved in domain rotation, bringing cytoplasmatic ends closer together while revealing the binding site to the periplasm. Upon outward facing conformational change and due to a change in pH, the interaction among substrate and binding site decreases, allowing it to be released.

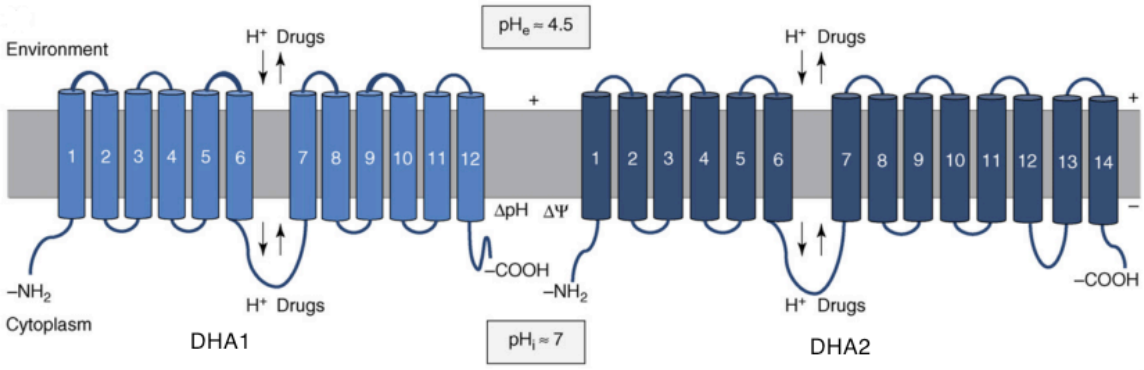

Figure 4.3. MSF transporters structure (Sá-Correia et al., 2009).

Based on this response, several attempts focused on increasing biofuel tolerance via membrane transporters have been published. Dunlop et al. (2011) overexpressed a series of efflux pumps in *E. coli* and performed a competitive assay to find those that confer resistance to several fuels, including limonene. They found that the native *E. coli* AcrAB pump and an unidentified transporter from *Alcanivorax borkumenis* consistently survived limonene competition. More

importantly, strains expressing the *A. borkumenis* pump produced significantly more limonene than those with no pump, providing poof-of-principle demonstration that efflux pumps which increase tolerance to exogenous biofuel are able to improve production yields. The following year, Teixeira et al. (2012) published a study in which an increased expression of the ABC transporter Pdr18p increased ethanol tolerance of *S.cerevisiae.* This resistance is thought to be a consequence of reduced ethanol-induced plasma membrane permeabilization due to the role of Pdr18 in ergosterol incorporation into the plasma membrane. Further studies on ethanol tolerance by means of transporter expression in yeast were reported by Yang et al. (2013). According to their results, overexpression of ABC efflux pump Adp1 allowed higher specific growth rate and, more interestingly, higher ethanol productivity than the wild type strain. Despite their promising role in overcoming toxicity and improving biofuel yields, overexpression of efflux pumps can be detrimental to growth due to overloading of membrane insertion machinery and changes in membrane composition; as a consequence, it is important to find a balance among pump toxicity and biofuel toxicity (Turner and Dunlop, 2014). In a recent approach, *E.coli* AcrAB and other target efflux pumps were overexpressed on high copy plasmids and no significant increase in titer of free fatty acids was achieved (Lennen et al., 2013). The authors speculate that this might be due to saturation of membrane protein insertion machinery.

4.2.1 Aims

The aim of this study was to determine the efflux pumps that contribute to detoxification of decanoic acid and find their optimal expression conditions. To establish the testing conditions, we first assessed C10 toxicity. Based on the literature, we then selected seven candidate transporters. To determine their potential role on C10 transport, we screened strains with those transporter genes deleted for increased sensitivity to decanoic acid. Once the candidates were selected, the genes were cloned into either a centromeric or a 2μ-based plasmid to elucidate the

optimal expression level that balances efficient C10 export with potential adverse effects associated with protein overproduction.

4.3 Materials and Methods

4.3.1 Construction of strains and expression vectors

Basic molecular biology protocols were based on (Sambrook and Green, 2012). Oligonucleotides were ordered from Integrated DNA Technologies (San Diego, CA) and are described on Table S4.1. T4 DNA ligase, NEBuilder® HiFi DNA Assembly Master Mix, OneTaq® Quickload® DNA polymerase, and deoxynucleotides were from New England Biolabs (Ipswhich, MA). Restriction enzymes were also purchased from New England Biolabs or from Thermo Fisher Scientific (Walthman, MA). KOD Hot Start DNA Polymerase was from Millipore Sigma (Burlington, MA). All PCR-amplified sequences were confirmed by Sanger sequencing analysis at Eaton Bioscience (San Diego, CA) or Genewiz (San Diego, CA). Transformation of plasmids were performed using Frozen-EZ Yeast Transformation II Kit from Zymo Research (Irvine, CA). The resulting plasmids and strains are summarized on Table 4.2.

To create pCA, the ubi-tagged *URA3* marker of the vector pUb (Leber et al., 2015) was swapped by a non-tagged *URA3* marker (with its native promoter and terminator) via cloning, using restriction sites *PacI* and *NheI* and the amplification product of primers FW_URA3 and RV_URA3 using pJC742 as a template (Choi and Da Silva, 2014). The centromeric origin of replication was then added from the PCR product of FW_CEN/ARS and RV_CEN/ARS using pJC742 as template via Gibson-assembly (Gibson et al., 2009) to the ~6.7 kb fragment of the *EcoRI*-digested plasmid.

To create pUb-Snq2, pCA-Snq2, pUb-Pdr5 and pCA-Pdr5, via Gibson Assembly, two partially overlapping parts were used: i) amplification product of genomic sequence using primer pairs FW_SNQ2+RV_SNQ2 or FW_PDR5+RV_PDR5, and ii) linearized pUb or pCA with RsrII (for Snq2) or NotI (for Pdr5).

Pdr12 and Pma1 gene sequences were isolated via PCR from the BY4741 genome using the primer pairs FW_PDR12+RV_PDR12 and FW_PMA1+FW_PMA1. Amplicons, pUB, and pCA were digested with *SpeI*-HF and *RsrII* in Cutsmart Buffer and sticky-end ligation was performed using T4 DNA ligase (3:1 insert vector molar ratio). This enabled the creation of plasmids pUb-Pdr12, pCA-Pdr12 and pCA-Pma1. To generate plasmids pUb-Tpo1 and pCA-Tpo1, the ORF of *TPO1* was cloned using a similar procedure by amplifying with FW_TPO1+RV_TPO1 and digesting with *SacII* and *NotI*-HF. Finally, the vector pCA-Pma1-Tpo1 was created by inserting Pma1 into pCA-Tpo1.

Table 4.2. List of strains and plasmids

Strain/Plasmid	**Relevant Genotype**	**Reference**
Strains		
BY4741	MATa *his*3Δ1 *leu*2Δ0 *met*15Δ0 *ura*3Δ0	Open Biosystems
BYΔ*tpo1*	BY4741 *tpo1*::KanMx	Open Biosystems
BYΔ*pdr12*	BY4741 *pdr12*::KanMx	Open Biosystems
BYΔ*aqr1*	BY4741 *aqr1*::KanMx	Open Biosystems
BYΔ*yor1*	BY4741 *yor1*::KanMx	Open Biosystems
BYΔ*snq2*	BY4741 *snq2*::KanMx	Open Biosystems
BYΔ*pdr5*	BY4741 *pdr5*::KanMx	Open Biosystems
Plasmids		
pUb	Yeast 2μ plasmid, two *TEF1* promoters, two *CYC1* terminators, ubi-tagged *URA3* selectable maker	Based on pXP842U-Bi (Leber et al., 2016)
pCA	C/A plasmid, two *TEF1* promoters, two *CYC1* terminators and *URA3* maker	This study
pUb-Snq2	pUb expressing the ABC plasma membrane transporter Snq2 in Multicloning site I (SpeI/RsrII/XhoI/PmeI)	This study
pUb-Pdr5	pUb expressing the ABC plasma membrane transporter Pdr5 in Multicloning site II (SacII/BglII/NotI/PmlI)	This study
pUb-Pdr12	pUb expressing the ABC plasma membrane transporter Pdr12 in Multicloning site I (SpeI/RsrII/XhoI/PmeI)	This study
pUb-Tpo1	pUb expressing the MFS H^+-antiporter Tpo1 in Multicloning site II (SacII/BglII/NotI/PmlI)	This study
pCA-Snq2	pCA expressing the ABC plasma membrane transporter Snq2 in Multicloning site I (SpeI/RsrII/XhoI/PmeI)	This study

pCA-Pdr5	pCA expressing the ABC plasma membrane transporter Pdr5 in Multicloning site II (SacII/BglII/NotI/PmlI)	This study
pCA-Pdr12	pCA expressing the ABC plasma membrane transporter Pdr12 in Multicloning site I (SpeI/RsrII/XhoI/PmeI)	This study
pCA-Tpo1	pCA expressing MFS H^+-antiporter Tpo1 in Multicloning site II in Multicloning site II (SacII/BglII/NotI/PmlI)	This study
pCA-Pma1	pCA expressing the proton ABC plasma membrane transporter Pma1 in Multicloning site I (SpeI/RsrII/XhoI/PmeI)	This study
pCA-Pma1+Tpo1	pCA expressing the proton ABC plasma membrane transporter Pma1 in Multicloning site I (SpeI/RsrII/XhoI/PmeI) and the MFS H^+-antiporter Tpo1 in Multicloning site II (SacII/BglII/NotI/PmlI)	This study

4.3.2 Media and cultivation

Plasmid-containing *Escherichia coli* (XL-Blue) were selected cultivation in Luria Bertani (LB) medium containing either 100 mg/ml of Ampicillin.

Saccharomyces cerevisiae strains were inoculated from fresh SDC-A plates (20 g/L dextrose, 5 g/L casamino acids, 5g/L ammonium sulfate, 1.7 g/L yeast nitrogen base without amino acids, 50 mg/L adenine, 20% agar) into 5 ml of liquid SDC-A and grown overnight. Cells were then transferred (initial OD_{600}=0.05) to fresh 5 ml of SDC-A and cultivated 18-20 h. This culture was used as the inoculum for the subsequent tube and flask cultures (initial OD_{600}=0.05) in SDC-A,U supplemented with either decanoic acid (from a 100 mM stock in 70% ethanol, as previously described (Liu et al., 2013)) or an equivalent amount of 70% ethanol for the control cultures. Maximum concentration of ethanol did not exceed 1% (v/v), a concentration at which there is no detectable effect on yeast growth (Cabral et al., 2001). For all conditions studied, media was buffered using 100 mM MES (2-(4-Morpholino) ethane Sulfonic Acid) and pH was adjusted to 5.5 before inoculation to prevent the effects of pH variation due to addition of decanoic acid. All cells were cultivated at 30°C at 250rpm in an agitated shaker, and growth was monitored by optical density measurements at 600 nm in a Shimadzu UV-2450 spectrophotometer (Columbia, MD).

4.3.3 Statistical analysis

Statistical analysis was performed by one-way or two-way ANOVA using Post Hoc Tukey's test to account for multiple comparisons (the variance is estimated from the whole set of data).

4.4 Results and Discussion

4.4.1 Determination of decanoic acid toxicity in baseline strain

Assessment of decanoic acid toxicity is an important step to determine the optimal testing conditions for screening candidate efflux pumps. Strain BY4741 was cultured in buffered SDC-A,U medium supplemented with increasing concentrations of decanoic acid, and cell optical density (OD) was measured at 24 h (Figure 4.4). At 24 h, cell density decreased by approximately half at the lowest concentration tested (0.15 mM). Optical density continued to decrease progressively as concentration increased, resulting in no cellular growth (i.e., OD600 equal to that at inoculation) at 0.35 mM of decanoic acid.

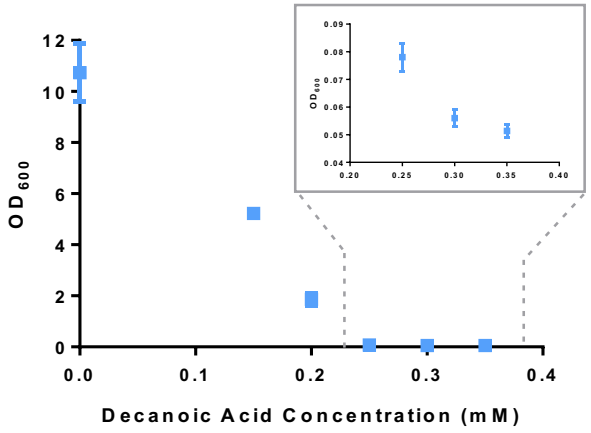

Figure 4.4. Dose-response curves showing the toxic effects of decanoic acid at pH=5.50. The graphs show optical density measurements at different concentrations of the fatty acid 24 h after inoculation. Initial OD (600 nm) was 0.05. The insert shows a zoom of the effect on cell density of the highest concentrations tested: 0.25 mM, 0.30 mM and 0.35 mM.

4.4.2 Identification of transporters involved in decanoic acid tolerance

The most abundant PDR pumps in *S.cerevisiae* are Pdr5p, Snq2p and Yor1p. Identified substrates of Pdr5p and Snq2p include mutagens, steroids, anticancer drugs and fungal azoles, among others (Ernst et al., 2005). A recent study showed promising results in the utilization of Pdr5p and Snq2 ABC transporters in the biofuel field. Transcriptional analysis by Ling et al. (2013)

showed that, upon exposure to 2%(v/v) of either decane or undecane, *S. cerevisiae* presented a significantly induced expression of *PDR5* and *SNQ2* . Transporters *PDR15* and *YOR1* also showed increased expression, but to a lesser extent. Based on these results, they overexpressed either *SNQ2* or *PDR5* on high copy plasmids and observed a decrease of intracellular alkane of approximately 25% and 33%, respectively, when cells were exposed to decane. For undecane, the reduction was 87.4% when *SNQ2* was overexpressed, and 94.4% for *PDR5*. This considerable reduction of intracellular alkanes resulted in enhanced tolerance levels against decane and undecane. These results, along with the ability of Pdr5 and Snq2 to transport diverse substrates (Zhou et al., 2014), suggest that overexpression of Snq2 and Pdr5 could potentially alleviate toxicity of structurally similar substrates such as medium-chain fatty acids.

To identify other transporters that have affinity for substrates with similar chemical properties to decanoic acid, an additional search in the literature and the *Saccharomyces Genome Database* (SGD) was performed. These candidates and their SGD description are listed in Table 4.3. Although Tpo1 it is reported to be a polyamine MSF transporter in SGD, a transcriptional analysis of the wine yeast strain U13 upon exposure for 20 min to 50 μM of decanoic acid showed an up regulation of this gene (Legras et al., 2010). This was also the case for Pdr12, an ABC transporter whose gene transcription levels significantly increased, although to a lesser extent. Similar results for Pdr12 were obtained in an earlier 2003 study, where a strong induction by moderately lipophilic carboxylic acids (C6-C8) was observed via a LacZ reporter fusion (Hatzixanthis et al., 2003).

Table 4.3. Candidate decanoic acid transporters found in Saccharomyces Genome Database and literature (Legras et al., 2010; Ling et al., 2013).

Transporter	SGD Description	Source
TPO1	Polyamine transporter of the major facilitator superfamily.	(Legras et al., 2010)
PDR12	Plasma membrane ATP-binding cassette (ABC) transporter; weak-acid-inducible multidrug transporter required for weak organic acid resistance.	(Legras et al., 2010), SGD
AQR1	Plasma membrane transporter of the major facilitator superfamily; member of the 12-spanner drug: H(+) antiporter DHA1 family; confers resistance to short-chain monocarboxylic acids and quinidine.	SGD
YOR1	Plasma membrane ATP-binding cassette (ABC) transporter; multidrug transporter mediates export of many different organic anions including oligomycin.	SGD
SNQ2	Plasma membrane ATP-binding cassette (ABC) transporter; multidrug transporter involved in multidrug resistance and resistance to singlet oxygen species	(Ling et al., 2013)
PDR5	Plasma membrane ATP-binding cassette (ABC) transporter; multidrug transporter actively regulated by Pdr1p; also involved in steroid transport, cation resistance, and cellular detoxification during exponential growth.	(Ling et al., 2013)

To assess which of these are good candidates to alleviate decanoic acid toxicity, strains with these transporter genes deleted were grown in the presence and absence of decanoic acid (C10). Those knock-out strains that show reduced growth in the presence of C10 indicate transporters with a role in C10 detoxification. The six knock-out strains (Table 4.3) were grown in buffered SDC-A,U at pH=5.50 either in presence or absence of 0.2 mM decanoic acid (a very inhibitory level – Figure 4.4), and optical density was monitored over 32 h (Figure 4.5).

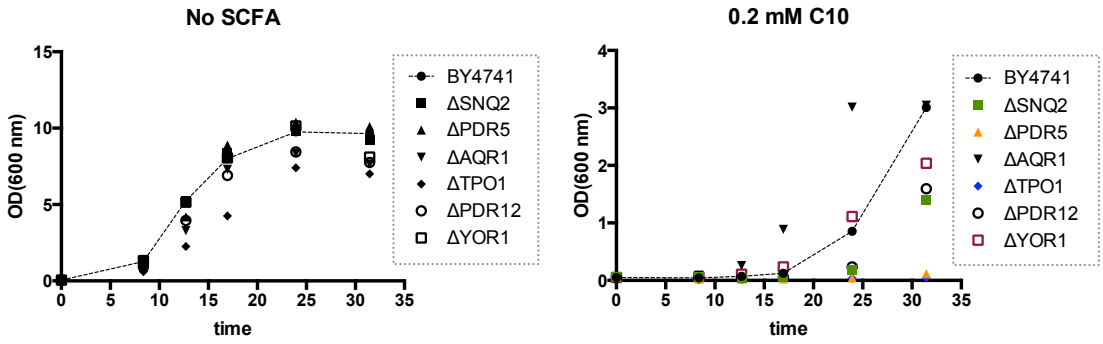

Figure 4.5. Growth of strains that have different transporter genes deleted grown in SDC-A,U medium A) without supplementation of decanoic acid B) with 0.2 mM of decanoic acid. Transporters that show decreased growth in the presence of C10 are colored and the growth of the baseline strain is shown with a dotted line.

The deletion of *TPO1*, *PDR12* and *AQR1* had a slight negative effect on cell growth in the absence of C10 (Figure 4.5A), with final cell densities approximately 20% to 30% lower than the baseline strain. However, the negative effects on growth were significantly greater when the *TPO1* and *PDR12* knock-out strains were exposed to decanoic acid (Figure 4.5B), with decreases in final cell density of 98% and 48%, respectively. These results indicate that Tpo1 and Pdr12 aid in cell detoxification in the presence of decanoic acid. The deletion of *PDR5* and *SNQ2* also reduced growth in the presence of C10 by up to 77.8% for Snq2 and 96.0% for Pdr5. In the presence of C10, the *YOR1* knock-out strain had a 32% lower optical density at 32 h with respect to the control; however, growth at earlier stages was similar to that of the control. Interestingly, the *AQR1* knock-out strain showed higher cell densities throughout the time evaluated, but the final OD_{600} was the same as for the baseline strain. Based on these results Tpo1, Pdr5, Snq2 and Pdr12 likely aid in C10 transport and were chosen for overexpression studies.

4.4.3 Overexpression of candidate efflux pumps: Tpo1, Pdr5, Snq2 and Pdr12.

It is known that overexpression of efflux pumps can be detrimental for growth due to competition for transcription and translation factors, overloading of membrane insertion machinery and changes in membrane composition (Deparis et al., 2017; Turner and Dunlop, 2014).

Therefore, it is important to fine tune protein expression and find a balance between yielding the highest export of the substrate and a lowered burden derived from pump production. For this study, the candidate transporters were cloned into two different plasmids: i) a high-copy plasmid pUb harboring a 2μ origin of replication and a ubiquitin/N-degron auxotrophic marker (Chen et al., 2012) that ensures only cells with high numbers of the plasmid survive and ii) a low-copy plasmid pCA that has a centromeric origin of replication with the auxotrophic marker under the control of the native promoter without a degron. For an initial screen, the strains were grown in buffered selective SDC-A medium with or without 0.22 mM of decanoic acid at pH=5.50 (Figure 4.6).

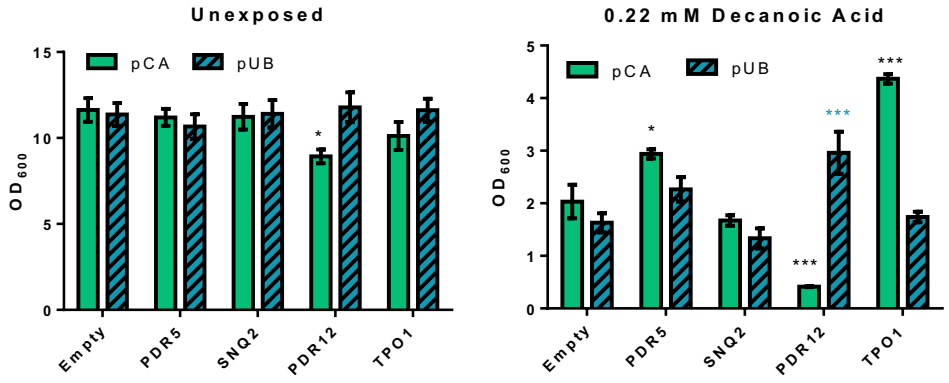

Figure 4.6. Growth at 24 h of engineered strains overexpressing selected transporters either in a low-copy plasmid (pCA, green solid bars) or high-copy plasmid (pUb blue slashed bars). The 'empty' represents strains transformed with pCA or pUb plasmids and serves as a control. A) Non-exposed cells B) cells exposed to 0.22 mM decanoic acid. Black asterisks represent *p*-value with respect to control for low-copy plasmid and blue asterisks *p*-value for high-copy plasmids (*p<0.05, ***p<0.001).

Overexpression of the membrane transporters did not significantly affect cell density for unexposed cells at 24 h, except for the strain with plasmid pCA-Pdr12, where a 23% reduction was observed (Figure 4.6A). Since all proteins are under the control of the strong *TEF1*p constitutive promoter, this indicates there is no significant metabolic burden associated with the transporter expression with either vector. The effects of 0.22 mM of decanoic acid on cell density after 24 h of growth are shown in Figure 4.6B. Transporter overexpression from a multi-copy

plasmid resulted in poorer cell growth, with the exception of Pdr12. This indicates that higher efflux pumps levels do not necessarily result in more detoxification, and other factors such as overwhelming the insertion machinery and changes in membrane protein composition may negatively affect the resistance of cells against decanoic acid. Other phenomena such as mis-sorting of the proteins toward the vacuole could also be taking place, as observed when *TPO1* was expressed on the multi-copy vector YEp351 (Uemura et al., 2005). In contrast, overexpression of Pdr12 in pUb showed higher cell density than the control with the empty vector. Expression of each transporter should be thus fine-tuned on a case-by-case basis. Interestingly, when Pdr12 is expressed on a low-copy plasmid (pCA-Pdr12), there is a decrease in cell density both in presence and absence of decanoic acid. We have not found a reasonable explanation for this observation and it could be a topic of further investigation. Of all plasmids screened, pCA-Pdr5 and pCA-Tpo1 showed the most promising results, with increases of 1.4-fold and 2.1-fold, respectively. The strains that had deletions of *PDR5* or *TPO1* were the ones that presented a major decrease in growth when exposed to decanoic acid (Figure 4.5), further confirming the importance of these transporters in reducing decanoic acid toxicity.

4.4.4 Increasing Tpo1 driving force

The best-performing transporter Tpo1 belongs to the MFS DAH1 drug: H^+ antiporter family (SGD), which means that its activity depends on the proton motive force. When undissociated molecules of decanoic acid penetrate the cell and dissociate into the decanoate anion and a proton there is an acidification of the cytosol and consequent decrease of the proton motive force. To maintain function of Tpo1, we overexpressed it on pCA along with the plasma membrane H^+-ATPase Pma1. Pma1 is a plasma membrane protein that couples ATP hydrolysis to proton excretion out of the cell, playing a key role in regulation of cytosolic pH and plasma membrane potential (Rest et al., 1995; Viegas et al., 1998). The decision to overexpress Pma1 is supported

by the transcriptional upregulation of Hrk1 (a kinase associated with activation of Pma1) upon exposure to decanoic acid (Legras et al., 2010). We then compared growth of the cells containing the plasmid pCA, pCA-Tpo1, pCA-Pma1 and pCA-Pma1+Tpo1 in buffered SDC-A with and without 0.2 mM decanoic acid for 24 h, at pH=5.50 (Figure 4.9).

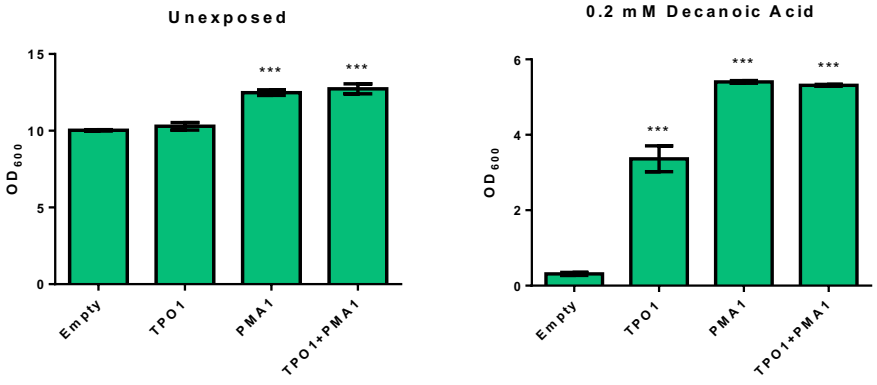

Figure 4.7. 24 h optical density at 600 nm (y-axis) of engineered strains overexpressing TPO1, PMA1 or a combination of both in a centromeric plasmid. A) Non-exposed cells B) cells exposed to 0.2 mM decanoic acid. Asterisks represent p-value with respect to control plasmid (**p<0.01, ***p<0.001).

Overexpression of *PMA1* (both in the absence and presence of *TPO1*) resulted in 24% higher cell density when no C10 was added (Figure 4.7A). A much greater increase relative to the control was observed in the presence of decanoic acid (Figure 4.7B). It is worth noting that the cell density of the control strain in Figure 4.7B is lower than that observed in Figure 4.6B. This could be due to small variations in pH during media preparation, which result in changes of undissociated decanoic acid concentration, thus greatly altering its toxicity (Liu et al., 2013). Under the experimental conditions of this screen, it was observed that overexpression of Tpo1 increased cell density by 10.8-fold, while overexpression of Pma1 (both with and without Tpo1 expression) showed a 17-fold improvement. This could indicate that one of the main inhibitory effects of decanoic acid toxicity is acidulation of the cytosol and consequent reduction of the proton electrochemical gradient. The importance of electrochemical gradient was illustrated in a 2014 study, where maintenance of appropriate K^+ and H^+ gradients across the yeast membrane led to

significant improvements in ethanol tolerance and production (Lam et al., 2014). Further support for Pma1 is provided by a recent study that demonstrated overexpression of *PMA1* improves resistance to stresses induced by ethanol, acetic acid, benzoic acid, and propionic acid (Lee et al, 2017).

4.5 Conclusions and Future Work

Biorenewable decanoic acid has the potential to functionally replace petroleum-derived precursors of α-olefins (Leber and Da Silva, 2013) and other chemical compounds. However, biological production in *S. cerevisiae* at industrially relevant quantities is hindered by its toxic effects on the cell. In this study, we observed that overexpression of efflux pumps Tpo1, Pdr5 and Pdr12 are a promising strategy for improving cell robustness. It has also been shown that expression levels have to be fine-tuned in order to have a balance between efficient efflux of toxic compounds and potential adverse effects associated with protein overproduction. In our work, the most promising plasmids constructed were pCA-TPO1, pCA-PDR5 and pUb-PDR12. Efforts to further improve the function of Tpo1 by increasing the diving force of this H^+-antiporter through overexpression of Pma1 led to an increase in cell density of up to 17-fold with respect to the control strain at 24 h. Overexpression of Pma1 alone leads to comparable growth improvements, indicating that H^+ export is key for increasing tolerance. These results are preliminary and have to be confirmed with complete growth studies and dose-response curves for all strains.

To optimize this strategy, it is important to consider obstacles to overexpression of efflux pumps. First, they are all ATP-dependent, either directly (for Pma1, Pdr12 and Pdr5) or indirectly (for Tpo1). This can be a disadvantage when using a Carbtree-positive platform organism such as *S. cerevisiae* (Pfeiffer and Morley, 2014), which ferments in the presence of oxygen, resulting in a lower ATP yield than respiration alone. Substrate promiscuity coupled with constitutive overexpression of these transporters may lead to depletion of ATP pools, required for anabolic processes such as ribosome biogenesis and protein synthesis. Transporter expression under the control of a medium chain fatty acid sensor such as the *PDR12* promoter (Baumann et al., 2018) can potentially address this issue, as the overexpression of efflux pump will be triggered by C10.

Other potential issues are related to transporter activation control and trafficking. The catalytic unit of Pma1 is autoinhibited by interaction with the C-terminal tail. In the presence of glucose, this interaction is alleviated via phosphorylation (Rest et al., 1995; Sychrová, 2016). This post-translational mode of repression can be by-passed either by deletion of the 11 C-terminal residues or by mimicking the negative charge from phosphorylation in residue S899 creating $Pma1^{S899D}$ (Sychrová, 2016). Phosphorylation also plays a key role in activity and localization of Tpo1, and expression of Tpo1 in a multi-copy vector led to localization of the transporter to the vacuolar membrane (Uemura et al., 2005). This trafficking defect was due to the activity of cAMP-dependent protein kinases 1 and 2 at Ser^{342}. The mutation of this residue to the negatively charged amino acid glutamate led to proper protein sorting. Other serine mutations to glutamate (S19E and T52E) led to higher activity with respect to the wild type (Uemura et al., 2005). By using Tpo1 variants harboring these mutations, it may be possible to overexpress this transporter at higher rates or display it in more active form, resulting in increased decanoic acid tolerance. Finally, it will be interesting to test some of the interventions explored in the Chapter 1. Deletion of *PAH1* has demonstrated improvements in membrane protein overexpression for *Y. lipolytica* (Guerfal et al., 2013). It is possible that these benefits can be translated to *S. cerevisiae*, based on the increased protein secretion (Chapter 1) and display of GPI-anchored proteins (Chapter 2) observed with BYΔ*pah1*. Furthermore, protein insertion into the secretory pathway can be improved by changing the *CYC1*t to either *PMP1*t or the efflux pump native terminator. Finally, membrane protein exit from the endoplasmic reticulum can be improved by overexpressing the Erv14 COPII-vesicle adaptor, which mimics the function of Erv29 for transmembrane proteins (Pagant et al., 2015).

4.6 References

Al-Awqati Q. 1999. One hundred years of membrane permeability: does Overton still rule? *Nat. Cell Biol.* **1**:E201–E202.

Aresta M, Dibenedetto A, Dumeignil F eds. 2012. Biorefinery: From Biomass to Chemicals and Fuels. Berlin, Boston: DE GRUYTER 27 p. https://www.degruyter.com/view/books/9783110260281/9783110260281/9783110260281.xml.

Baumann L, Rajkumar AS, Morrissey JP, Boles E, Oreb M. 2018. A Yeast-Based Biosensor for Screening of Short- and Medium-Chain Fatty Acid Production. *ACS Synth. Biol.*:acssynbio.8b00309. http://dx.doi.org/10.1021/acssynbio.8b00309.

Besada-Lombana PB, Fernandez-Moya R, Fenster J, Da Silva NA. 2017. Engineering Saccharomyces cerevisiae fatty acid composition for increased tolerance to octanoic acid. *Biotechnol. Bioeng.* **114**:1531–1538.

Borrull A, López-Martínez G, Poblet M, Cordero-Otero R, Rozès N. 2015a. New insights into the toxicity mechanism of octanoic and decanoic acids on Saccharomyces cerevisiae. *Yeast* **32**:451–460.

Borrull A, López-Martínez G, Poblet M, Cordero-Otero R, Rozès N. 2015b. New insights into the toxicity mechanism of octanoic and decanoic acids on Saccharomyces cerevisiae. *Yeast* **32**:451–460. http://doi.wiley.com/10.1002/yea.3071.

Boyarskiy S, Tullman-Ercek D. 2015. Getting pumped: membrane efflux transporters for enhanced biomolecule production. *Curr. Opin. Chem. Biol.* **28**:15–19. http://linkinghub.elsevier.com/retrieve/pii/S1367593115000526.

Cabral MG, Viegas C a., Sá-Correia I. 2001. Mechanisms underlying the acquisition of resistance to octanoic-acid-induced-death following exposure of Saccharomyces cerevisiae to mild stress imposed by octanoic acid or ethanol. *Arch. Microbiol.* **175**:301–307.

Casal M, Paiva S, Queirós O, Soares-Silva I. 2008. Transport of carboxylic acids in yeasts. *FEMS Microbiol. Rev.* **32**:974–994.

Chen Y, Partow S, Scalcinati G, Siewers V, Nielsen J. 2012. Enhancing the copy number of episomal plasmids in Saccharomyces cerevisiae for improved protein production. *FEMS Yeast Res.* **12**:598–607.

Choi JW, Da Silva NA. 2014. Improving polyketide and fatty acid synthesis by engineering of the yeast acetyl-CoA carboxylase. *J. Biotechnol.* **187**:56–59. http://dx.doi.org/10.1016/j.jbiotec.2014.07.430.

Coleman JJ, Mylonakis E. 2009. Efflux in fungi: la pièce de résistance. *PLoS Pathog.* **5**:e1000486. http://www.pubmedcentral.nih.gov/articlerender.fcgi?artid=2695561&tool=pmcentrez&rendertype=abstract.

Deparis Q, Claes A, Foulquié-Moreno MR, Thevelein JM. 2017. Engineering tolerance to industrially relevant stress factors in yeast cell factories. *FEMS Yeast Res.* **17**:1–17.

Dunlop MJ, Dossani ZY, Szmidt HL, Chu HC, Lee TS, Keasling JD, Hadi MZ, Mukhopadhyay A. 2011. Engineering microbial biofuel tolerance and export using efflux pumps. *Mol. Syst. Biol.* **7**:487. http://www.pubmedcentral.nih.gov/articlerender.fcgi?artid=3130554&tool=pmcentrez&rendertype=abstract.

Ernst R, Klemm R, Schmitt L, Kuchler K. 2005. Yeast ATP-binding cassette transporters: cellular cleaning pumps. In: . *Methods Enzymol.*, Vol. 400, pp. 460–84. http://www.ncbi.nlm.nih.gov/pubmed/16399365.

Ernst R, Kueppers P, Stindt J, Kuchler K, Schmitt L. 2010. Multidrug efflux pumps: substrate selection in ATP-binding cassette multidrug efflux pumps--first come, first served? *FEBS J.* **277**:540–9. http://www.ncbi.nlm.nih.gov/pubmed/19961541.

Ford JP, Immer JG, Lamb HH. 2012. Palladium Catalysts for Fatty Acid Deoxygenation: Influence of the Support and Fatty Acid Chain Length on Decarboxylation Kinetics. *Top. Catal.* **55**:175–184. http://link.springer.com/10.1007/s11244-012-9786-2.

Forrest LR, Krämer R, Ziegler C. 2011. The structural basis of secondary active transport mechanisms. *Biochim. Biophys. Acta* **1807**:167–188. http://dx.doi.org/10.1016/j.bbabio.2010.10.014.

Gibson DG, Young L, Chuang RY, Venter JC, Hutchison CA, Smith HO. 2009. Enzymatic assembly of DNA molecules up to several hundred kilobases. *Nat. Methods* **6**:343–345.

Hatzixanthis K, Mollapour M, Seymour I, Bauer BE, Krapf G, Schüller C, Kuchler K, Piper PW. 2003. Moderately lipophilic carboxylate compounds are the selective inducers of the Saccharomyces cerevisiae Pdr12p ATP-binding cassette transporter. *Yeast* **20**:575–85. http://www.ncbi.nlm.nih.gov/pubmed/12734796.

Hollenstein K, Dawson RJP, Locher KP. 2007. Structure and mechanism of ABC transporter proteins. *Curr. Opin. Struct. Biol.* **17**:412–8. http://www.ncbi.nlm.nih.gov/pubmed/17723295.

Jarboe LR, Royce L a, Liu P. 2013. Understanding biocatalyst inhibition by carboxylic acids. *Front. Microbiol.* **4**:272.

Kamp F, Hamilton J a. 2006. How fatty acids of different chain length enter and leave cells by free diffusion. *Prostaglandins Leukot. Essent. Fat. Acids* **75**:149–159.

Lam FH, Ghaderi A, Fink GR, Stephanopoulos G. 2014. Engineering alcohol tolerance in yeast. *Science (80-.).* **346**:71–76.

Law CJ, Maloney PC, Wang D-N. 2008. Ins and outs of major facilitator superfamily antiporters. *Annu. Rev. Microbiol.* **62**:289–305.

Leber C, Choi JW, Polson B, Silva NA Da. 2016. Disrupted Short Chain Specific b - Oxidation and Improved Synthase Expression Increase Synthesis of Short Chain Fatty Acids in Saccharomyces cerevisiae **113**:895–900.

Leber C, Polson B, Fernandez-Moya R, Da Silva NA. 2015. Overproduction and secretion of free fatty acids through disrupted neutral lipid recycle in Saccharomyces cerevisiae. *Metab. Eng.* **28**:54–62.

Leber C, Da Silva NA. 2013. Engineering of Saccharomyces cerevisiae for the synthesis of short chain fatty acids. *Biotechnol. Bioeng.* **111**:347–358. http://www.ncbi.nlm.nih.gov/pubmed/23928901.

Legras JL, Erny C, Le Jeune C, Lollier M, Adolphe Y, Demuyter C, Delobel P, Blondin B, Karst F. 2010. Activation of two different resistance mechanisms in Saccharomyces cerevisiae upon exposure to octanoic and decanoic acids. *Appl. Environ. Microbiol.* **76**:7526–35.

Leibundgut M, Maier T, Jenni S, Ban N. 2008. The multienzyme architecture of eukaryotic fatty acid synthases. *Curr. Opin. Struct. Biol.* **18**:714–725.

Lennen RM, Politz MG, Kruziki M a, Pfleger BF. 2013. Identification of transport proteins involved in free fatty acid efflux in Escherichia coli. *J. Bacteriol.* **195**:135–44. http://www.pubmedcentral.nih.gov/articlerender.fcgi?artid=3536169&tool=pmcentrez&rendertype=abstract.

Ling H, Chen B, Kang A, Lee J-M, Chang MW. 2013. Transcriptome response to alkane biofuels in Saccharomyces cerevisiae: identification of efflux pumps involved in alkane tolerance. *Biotechnol. Biofuels* **6**:95. http://www.pubmedcentral.nih.gov/articlerender.fcgi?artid=3717029&tool=pmcentrez&rendertype=abstract.

Liu P, Chernyshov A, Najdi T, Fu Y, Dickerson J, Sandmeyer S, Jarboe L. 2013. Membrane stress caused by octanoic acid in Saccharomyces cerevisiae. *Appl. Microbiol. Biotechnol.* **97**:3239–3251.

Mira NP, Teixeira MC, Sá-Correia I. 2010. Adaptive response and tolerance to weak acids in Saccharomyces cerevisiae: a genome-wide view. *OMICS* **14**:525–40.

Mollapour M, Piper PW. 2007. Hog1 mitogen-activated protein kinase phosphorylation targets the yeast Fps1 aquaglyceroporin for endocytosis, thereby rendering cells resistant to acetic acid. *Mol. Cell. Biol.* **27**:6446–6456.

Oguro D, Haraguchi K, Takaku H. 2014. US9775371B2.

Pagant S, Wu A, Edwards S, Diehl F, Miller EA. 2015. Sec24 Is a Coincidence Detector that Simultaneously Binds Two Signals to Drive ER Export. *Curr. Biol.* **25**:403–412. http://linkinghub.elsevier.com/retrieve/pii/S0960982214015711.

Panda H. 2010. Perfumes and Flavours Technology Handbook. Asia Pacific Business Press Inc.

Pfeiffer T, Morley A. 2014. An evolutionary perspective on the Crabtree effect. *Front. Mol. Biosci.* **1**:3–8. http://journal.frontiersin.org/article/10.3389/fmolb.2014.00017/abstract.

Pfleger BF, Gossing M, Nielsen J. 2015. Metabolic engineering strategies for microbial synthesis of oleochemicals. *Metab. Eng.* **29**:1–11. http://linkinghub.elsevier.com/retrieve/pii/S1096717615000117.

Rest M, Kamminga AH, Nakano A, Anraku Y, Poolman B, Konings WILN. 1995. The Plasma Membrane of Saccharomyces cerevisiae: Structure, Function, and Biogenesis. *Microbiol. Rev.* **59**:304–322.

Sá-Correia I, dos Santos SC, Teixeira MC, Cabrito TR, Mira NP. 2009. Drug:H+ antiporters in chemical stress response in yeast. *Trends Microbiol.* **17**:22–31.

Sambrook J, Green MR. 2012. Molecular Cloning: A Laboratory Manual. Ed. Micahel R Green, J Sambrook 4th Erditi. Cold Spring Harbor. Vol. 1 1-2028 p.

Schmitt L, Tampé R. 2002. Structure and mechanism of ABC transporters. *Proteins*:754–760.

Sychrová H. 2016. Yeast Membrane Transport. Ed. José Ramos, Hana Sychrová, Maik Kschischo. Cham: Springer International Publishing. Vol. 892. Advances in Experimental Medicine and Biology. http://link.springer.com/10.1007/978-3-319-25304-6.

Teixeira MC, Godinho CP, Cabrito TR, Mira NP, Sá-Correia I. 2012. Increased expression of the yeast multidrug resistance ABC transporter Pdr18 leads to increased ethanol tolerance and ethanol production in high gravity alcoholic fermentation. *Microb. Cell Fact.* **11**:98.

Teixeira MC, Duque P, Sá-Correia I. 2007. Environmental genomics: mechanistic insights into toxicity of and resistance to the herbicide 2,4-D. *Trends Biotechnol.* **25**:363–370.

Turner WJ, Dunlop MJ. 2014. Trade-Offs in Improving Biofuel Tolerance Using Combinations of Efflux Pumps. *ACS Synth. Biol.*

Uemura T, Tachihara K, Tomitori H, Kashiwagi K, Igarashi K. 2005. Characteristics of the polyamine transporter TPO1 and regulation of its activity and cellular localization by phosphorylation. *J. Biol. Chem.* **280**:9646–9652.

Viegas C a, Sá-Correia I. 1991. Activation of plasma membrane ATPase of Saccharomyces cerevisiae by octanoic acid. *J. Gen. Microbiol.* **137**:645–651.

Viegas CA, Almeida PF, Cavaco M, Sá-Correia I. 1998. The H+-ATPase in the plasma membrane of Saccharomyces cerevisiae is activated during growth latency in octanoic acid-supplemented medium accompanying the decrease in intracellular pH and cell viability. *Appl. Environ. Microbiol.* **64**:779–783.

Yang K-M, Woo J-M, Lee S-M, Park J-B. 2013. Improving ethanol tolerance of Saccharomyces cerevisiae by overexpressing an ATP-binding cassette efflux pump. *Chem. Eng. Sci.* **103**:74–78. http://linkinghub.elsevier.com/retrieve/pii/S0009250912005829.

Zhou YJ, Buijs N a., Siewers V, Nielsen J. 2014. Fatty Acid-Derived Biofuels and Chemicals Production in Saccharomyces cerevisiae. *Front. Bioeng. Biotechnol.* **2**:1–61. http://www.frontiersin.org/Synthetic_Biology/10.3389/fbioe.2014.00032/abstract.

Appendix 1. Supplementary information from Chapter 1

Table S1.1. List of primers and gBlocks used in this study.

Primer /gBLOCK	Sequence	Ref.
FW_URA3	TTTTGCTAGCTCGACTCTAGAGGATCCCCGGGATAAC	This study
RV_URA3	GCCGTTAATTAA GAATTCGAGCTCGGTACCCGGGATAAC	This study
FW_CEN/ARS	GCGGTCCTAGGGGGTACCGAGCTCGAATTCATCACGTGCTATAAAAATAA	This study
RV_CEN/ARS	CAGCTATGACCATGATTACGAATTCGTAACTTACACGCGCCTCGTATCTT	This study
FW_CelAt	GGGGTTTCCGGGGTTTAAACAAAACAATGAGATTTCCTTCAATTTTTACTGCAG	This study
RV_CelAt	AATAAATTTTATCGGACCGTCTAGTGGTGGTGGTGGTGGTGATAAGGTAGGTGGGGT	This study
FW_Ost1pro	CTAGTTGATATACGTAAAATCGTTTAAACAAAACAATGAGGCAGGTTTGGTTCTCTTGGA	This study
RV_Ost1pro	AGGCACACCTGCATCGATAAGCTTTGGTTCGCCTTCCTCTCTTTTATCCAAAGATAC	This study
FW_proMFa-BGlDf	GAGGAAGGCGAACCAAAGCTTATCGATAAGGATGACTTGGCCTACTCGCCGCCTTTCTA	This study
RV_proMFa-BGlDf	AATGTAAGCGTGACATAACTAATCTCGAGCGGTCCGCGTCAATGATGATGATGATGATG	This study
FW_proMFa-4420	GAAGGCGAACCAAAGCTTATCGATGACGTCGTTATGACTCAAACAC	This study
RV_4420	AGGCCCCGGGACCGCCAC	This study
FW_mRFP	ACGCGTGGTGGCGGTCCCGGGGCCTCCTCCGAGGACGTCATCAAG	This study
RV_mRFP	AATGTAAGCGTGACATAACTAATCTCGAGCGGTCCGCGTCAGGCGCCGGTGGAGTGG	This study
FW_3UTR_tPMP1	CGGACCGCTCGAGAAAGGGCGGAGCGAGCCATTTTATT	This study
RV_3UTR_tPMP1	CGAGCTAGCGAGAAAAAGTAGATCATAACTATAAGTTGTGCATACT	This study
FW_3UTR_tPMP2	GACCGCTCGAGGCGATCACTAGCAAGCCAAACGAGCTTGATGTT	This study
RV_3UTR_tPMP2	GAGCTAGCAGCACTAGAGTAAGGAGATAGTAGGCGACACTTCGAAAATCTA	This study
FW_3UTR_tPGK1	CGGACCGCTCGAGGAATTGAATTGAAATCGATAGATCAATTTTTTTC	This study
RV_3UTR_tPGK1	CGAGCTAGTTTTGTTGCAAGTGGGATGAGCT	This study
FW_ERV29	AAGTTTTAATTACAAACACGTGGCGGCCGCAAAACAATGTCTTACAGAGGACCTATTG	This study
RV_ERV29	GTGAATGTAAGCGTGACATAACTAATCCGCGGCTAGTAAATCTTCTTCTTTTCATCAAC	This study
FW_gRNA_PHA1KO	GACTTTGATTGAGGGGGGCTTGATG	(Arendt et al., 2017)
RV_gRNA_PAH1KO	AAACCATCAAGCCCCCCTCAATC	(Arendt et al., 2017)
FW_Donor_PAH1KO_fullORF	TTTACCTTCTAAGAAACATACAGGGAAGAAATTACTGAAGATAGACACATCGGTCGATT	This study
RV_Donor_PAH1KO_fullORF	AGTATGGATCGTTATAAATAATATTCGGCTACAAGAATCAATCGACCGATGTGTCTATC	This study
FW_gRNA_XI-3	GACTTTCCCAACCGGCTGCTTTCATG	This study
RV_gRNA_XI-3	AAACCATGAAAGCAGCCGGTTGGG	This study
FW_XI-3_Up_CYC1t	GAAGCATCGGTTCAGATCGAGCAAACTGTAGGGAGAAAGGCAAATTAAAGCCTTCGAGC	This study
RV_XI-3_Down_TEF1	GGAGCAGAGACTTCTTTTCTTAGAAGAGGTTTTGTTACCGACCGCGAATCCTTACATCA	This study
Ost1proMFa gBLOCK	AAACAAAACAATGAGGCAGGTTTGGTTCTCTTGGATTGTGGGATTGTTCCTATGT TTTTTCAACGTGTCTTCTGCTGCTCCAGTCAACACTACAACAGAAGATGAAACCG CACAAATTCCGGCTGAAGCTGTCATCGGTTACTTGGATTTAGAAGGGGATTTCG ATGTTGCTGTTTTGCCATTTTCCAACAGCACAAATAACGGGTTATTGTTTATAAA TACTACTATTGCCAGCATTGCTGCTAAAGAAGAAGGGGTATCTTTGGATAAAAG AGAGGAAGGCGAACCA	This study
Ost1proMFaREST gBLOCK	AAACAAAACAATGAGGCAGGTTTGGTTCTCTTGGATTGTGGGATTGTTC CTATGTTTTTCAACGTGTCTTCTGCTGCTCCAGTCAACACTACAACAGAAGA TGAAACCGCACAAATTCCGGCTGAAGCGGTAATAGGTTATCTTGATTTAGA AGGCGATTTCGATGTTGCTGTTTTGCCATTTTCCAACAGCACAAATAACGG GTTATTGTTTATAAATACTACTATTGCCAGCATTGCTGCTAAAGAAGAAGGG GTATCTTTGGATAAAAGAGAGGAAGGCGAACCA	This study

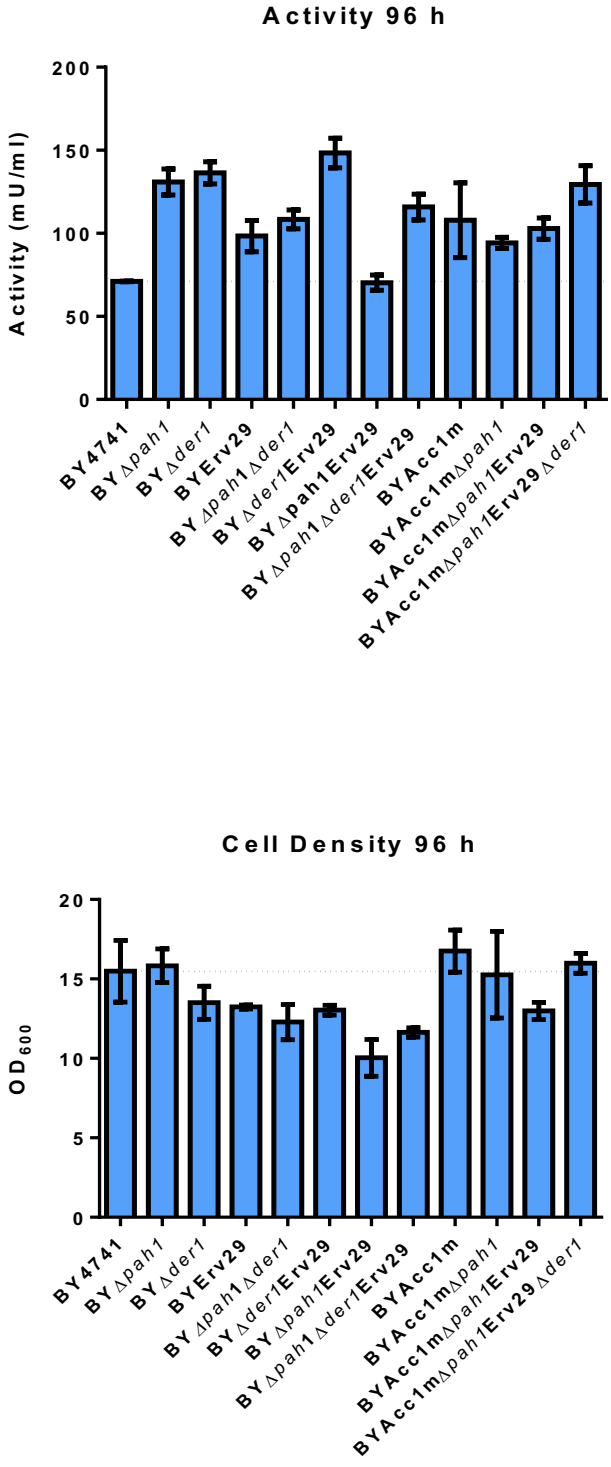

Figure S1.1. Activity and cell density at 96 h of different engineered strains transformed with pUbOMα-CelAt.

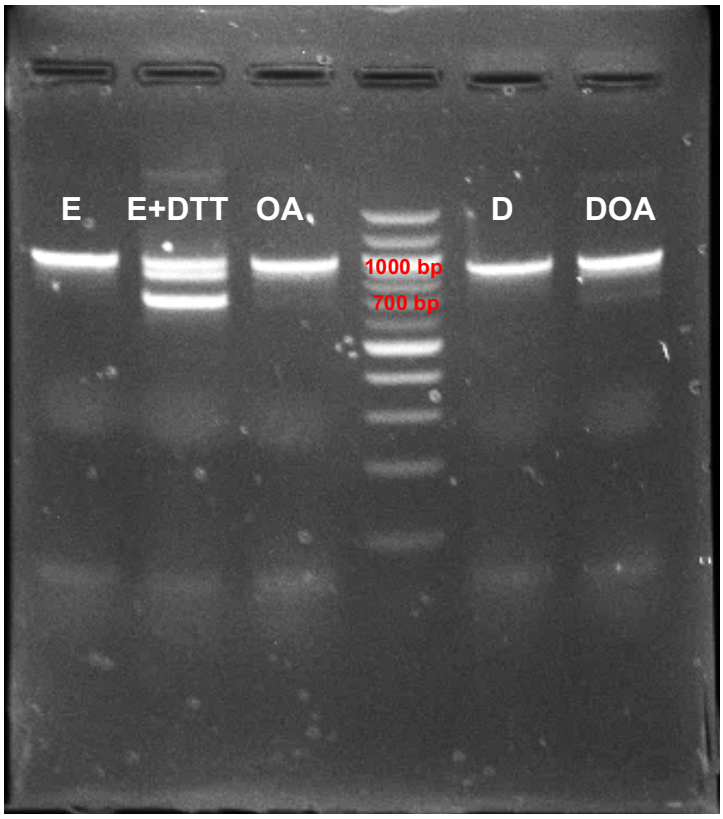

Figure S1.2. UPR activation in different strains. Protocol based on (Tang et al., 2015) To determine levels of Hac1 splicing, cells were inoculated from plates, grown overnight in 5 ml tubes and re-inoculated at OD=0.05 in 50 ml of SDC(A). Cells were grown for 4 h until OD~0.3-0.5. At that point, DTT was added to the positive control strain and incubated for 2 h. Cells were then spun down, and RNA was extracted using Quick-RNA Miniprep Kit (Zymo Research). cDNA (from 1 µg of RNA extracted) was generated by reverse transcription using random primers and PrimeScript Reverse Transcriptase (Takara). Hac1-specific primers were used to determine splicing using 10µl of the cDNA mixture in 50 µl Taq DNA Polymerase (without Magnesium Chloride). Bands expected: 969 bp for non-spliced and 717 bp for spliced. E: BY4741 transformed with empty plasmid, E+DTT: BY4741 transformed with empty plasmid and used as a positive control (DTT induces ER stress by disrupting formation of disulfide bonds), OA: BY4741 transformed with pUbOMα-CelAt, D: BYΔder1 transformed with empty plasmid, DOA: BYΔder1 transformed with pUbOMα-CelAt.

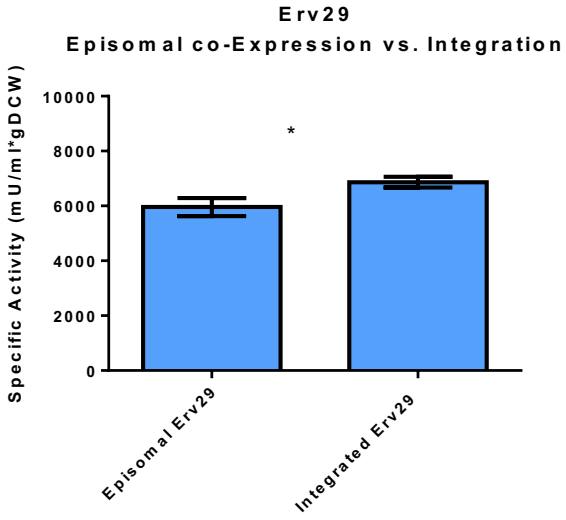

Figure S1.3. Extracellular endoglucanase specific activity of endoglucanase when Erv29 was co-overexpressed on the bigenic vector vs. when integrated in site XI-3. Both use *TEF1*p and *CYC1*t.

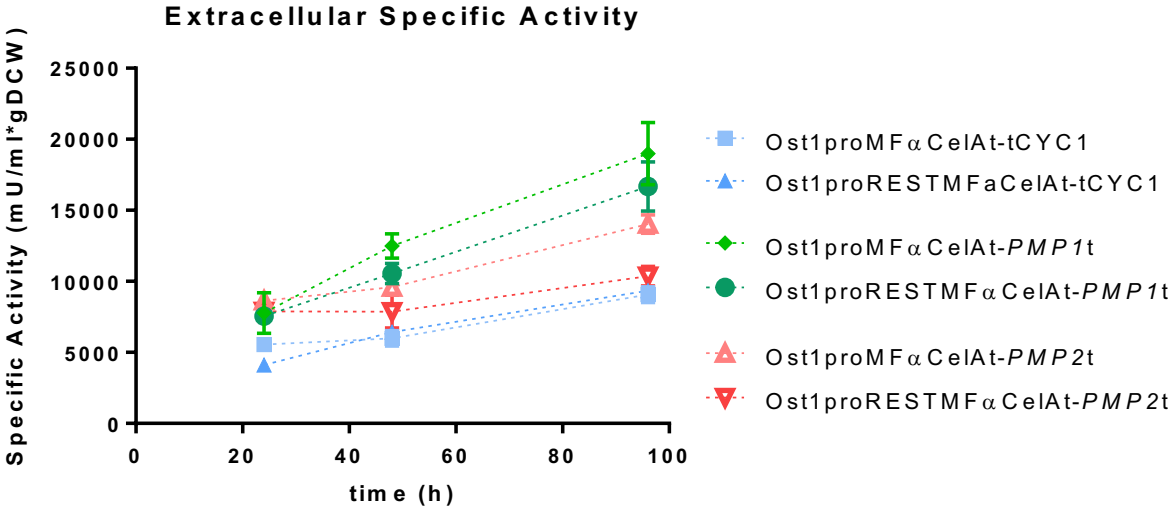

Figure S1.4. Extracellular endoglucanase specific activity for BY4741 transformed with pUbOMα-CelAt, pUbOrestMα-CelAt pUbOMα-CelAt-*PMP1*t, pUbOrestMα-CelAt-*PMP1*t, pUbOMα-CelAt-*PMP2*t, and pUbOrestMα-CelAt-*PMP2*t. Cells were inoculated in SDC(A) 2% (OD600=0.05) and grown for 96 h. Samples were taken at 24 h, 48 h and 96 h, cell density at 600 nm was measured, and activity of the supernatant was measured using CELLG5 kit (Megazyme).

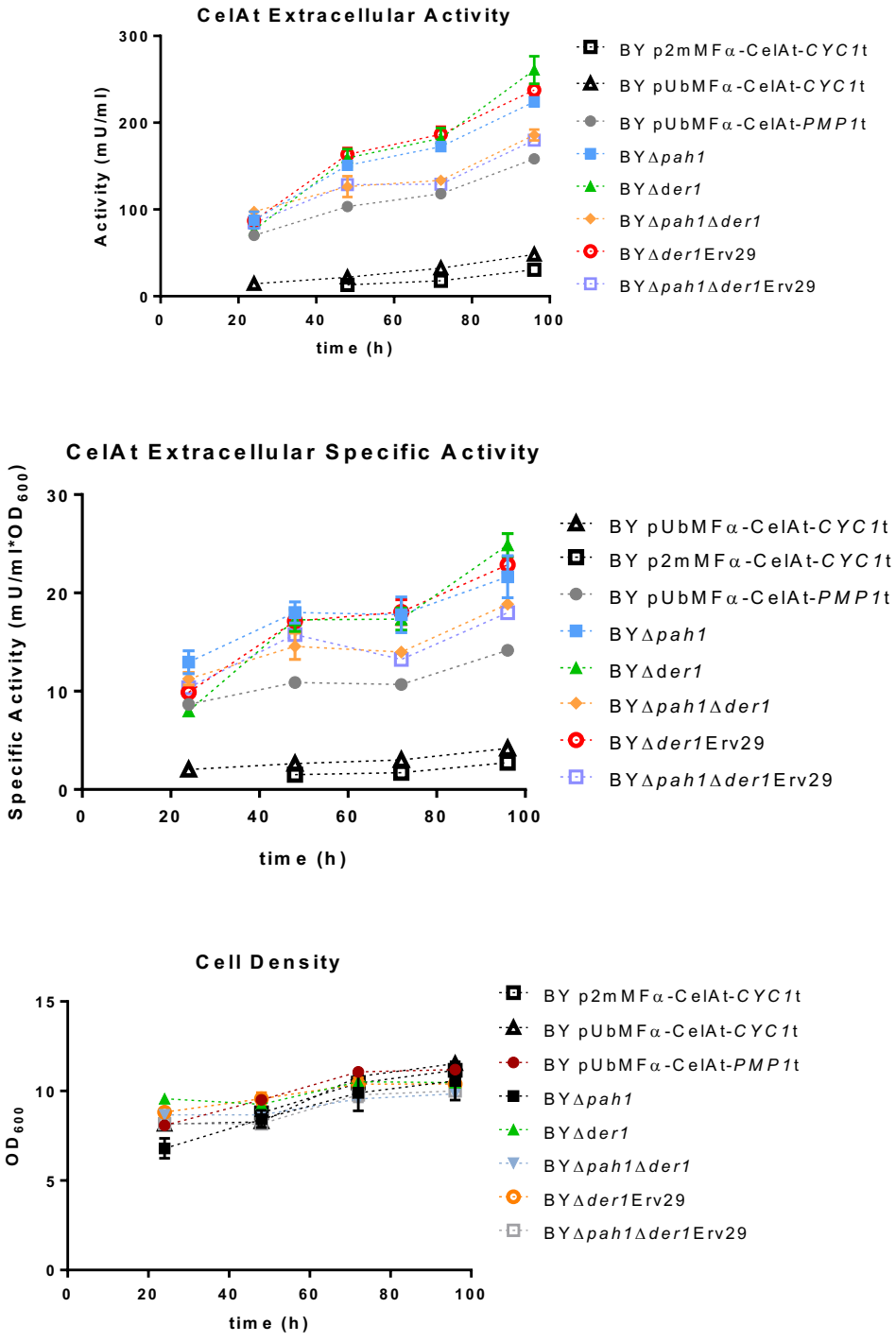

Figure S1.5. Extracellular endoglucanase specific activity, and cell density for different engineered strains transformed with pUbOMα-CelAt-*PMP1*t (colored lines) at 24 h, 48 h, 72 h and 96 h. Control strains (black) are BY4741 transformed with p2mMFα-CelAt and pUbMFα-CelAt.

Appendix 2. Supplementary information from Chapter 2

Table S2.1. List of primers

Primer	Sequence	Reference
FW_HXT1	TTTAAATTTAAAGCGG CCGCACTTGCGCATGCGCTCGGATTATCTTCATTT	This study
RV_HXT1	GGGCCCCCCGTTTAA ACGATTTTACGTATA TCAACTAGTTGACGATT	This study
FW_MFalpha	GGGGTTTCCGGGGTTTAAACAAAACAATGAGATTTCCTTC AATTTTTACTGC	This study
RV_CelA	AATAAATTTTATCGGACCGCTAGTGGTGGTGGTGGTGGTG ATAAGGTAGGTGGGGT	This study
RV_Bglf	AATAAAGGGGATCGGACCGTCAATGATGATGATGATGAT GTTGAGGAAGTG	This study
FW_HXT1THD3core	ATCATTTGAATTAGTATATTGAAATTATATAAAGACGGTA GGTATTGATTGTAATTCTG	This study
RV_HXT1THD3core	TCAACTAGTTGACGATTATGATATCTTGGTGTTTTAAAACT AAAAAAAAGACTAACTA	This study
FW_HXT1Core1	AATCATTTGAATTAGTATATTGAAATTATAAAAGAGCACT GTTGGGCGTGAGTGGAGGC	This study
RV_HXT1Core1	TCAACTAGTTGACGATTATGATATCTTGGTGTTTTCCGGCG CCTCCACTCACGCCCAACA	This study
FW_HXT1engBackbone	AGATATCATAATCGTCAACTAGTTGA	This study
RV_HXT1engBackbone	ATTTCAATATACTAATTCAAATGATTAAAAACGT	This study
FW_pHXT1_YTK2	GCATCGTCTCATCGGTCTCAAACGTTGCGCATGCGCTCGGA TTATCTTCATTTTT	This study
RV_pHXT1_YTK2	ATGCCGTCTCAGGTCTCACATAGATTTTACGTATATCAACT AGTTGACGATTATGATATC	This study
FW_Aga1_YTK3	GCATCGTCTCATCGGTCTCATATGACATTATCTTTCGCTCAT TTTACCTACCTG	This study
RV_Aga1_YTK3	ATGCCGTCTCAGGTCTCAGGATCCACTGAAAATTACATTG CAAGCAACTGCCAT	This study
FW_Aga2_YTK3a	GCATCGTCTCATCGGTCTCATATGCAGTTACTTCGCTGTTTT TCAATATTTTCTG	This study
RV_Aga2_YTK3a	ATGCCGTCTCAGGTCTCAAGAACCAAAAACATACTGTGTG TTTATGGG	This study
FW_prepoMFa_YTK3a	GCATCGTCTCATCGGTCTCATATGAGATTTCCTTCAATTTTT ACTGCAG	This study
RV_prepoMFa_YTK3a	ATGCCGTCTCAGGTCTCAAGAACCATCGATAAGCTTTGGT TCGCCTTC	This study
FW_Bgl1 _YTK3b	GCATCGTCTCATCGGTCTCATTCTAAGGATGACTTGGCCTAC TCGCCGCCTTTC	This study
RV_Bgl1_NoDockerin_YTK3b	ATGCCGTCTCAGGTCTCAGGATCCGTAAGGGGGAAGCGGT GCCTGCAGGTGCAG	This study
FW_BglDfSDM_Piece1	GGCGGAGGCCTACCGCAGGGCTGTCGACTTCGTTTCGCAG CTGAC	This study
RV_ BglDfSDM_Piece1	CGCCATAAGCACACCGGTCAGGACGGGGTCAGGAGAGAA ACCCTC	This study
FW_ BglDfSDM_Piece2	GACCCCGTCCTGACCGGTGTGCTTATGGCGGAAACGATCA AGGGT	This study
RV_ BglDfSDM_Piece2	CCTGTTCCATCTGGTCCAGGGCACCATTGTCGGTGACAGC ACTCA	This study

FW_ BglDfSDM_Piece3	ACAATGGTGCCCTGGACCAGATGGAACAGGTTGCGTCCCA GGCCA	This study
RV_ BglDfSDM_Piece3	GTACTTGTCGAACCTTCTGTAGTCGATGAAGACGCCCTCG GTGAAGTC G	This study
FW_ BglDfSDM_Piece4	TTCATCGACTACAGAAGGTTCGACAAGTACAACGAAACGC CCATCTATGAGTTCGG	This study
RV_ BglDfSDM _Piece4	AAGTCGACAGCCCTGCGGTAGGCCTCCGCCCACTCTCCG	This study
FW_AgaAlpha_4a	GCATCGTCTCATCGGTCTCAATCCAGCGCCAAAAGCTCTTTT ATCTCAACCAC	This study
RV_AgaAlpha_4a	ATGCCGTCTCAGGTCTCAGCCATTAGAATAGCAGGTACGA CAAAAGCAGAA	This study

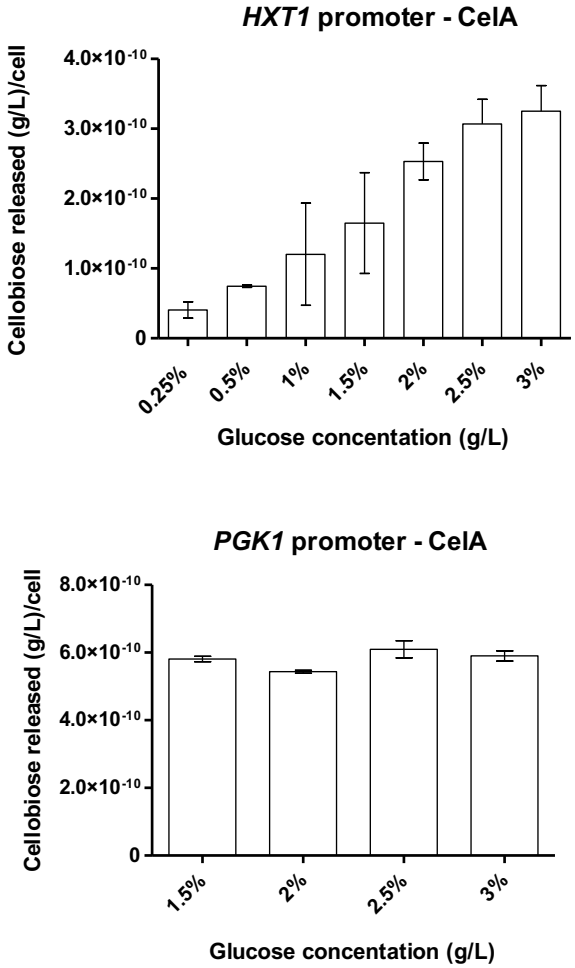

Figure S2.1. Comparison of extracellular levels of endoglucanase per cell as a function of glucose concentration when transcription is controlled by the *HXT1* promoter or the *PGK1* promoter. BY4741 was transformed with pJC842-HXT1p-CelAt or pAt (Tsai et al. 2010). Cells were grown overnight in SGC(A) 2% and inoculated in SDC(A) with increasing glucose concentrations (OD_{600}=0.05). After 20 h, cell density was measured and the supernatant was incubated with 0.1% PASC. Endoglucanse levels are determined via HPLC based on cellobiose released. An empty plasmid was used as a control and subtracted.

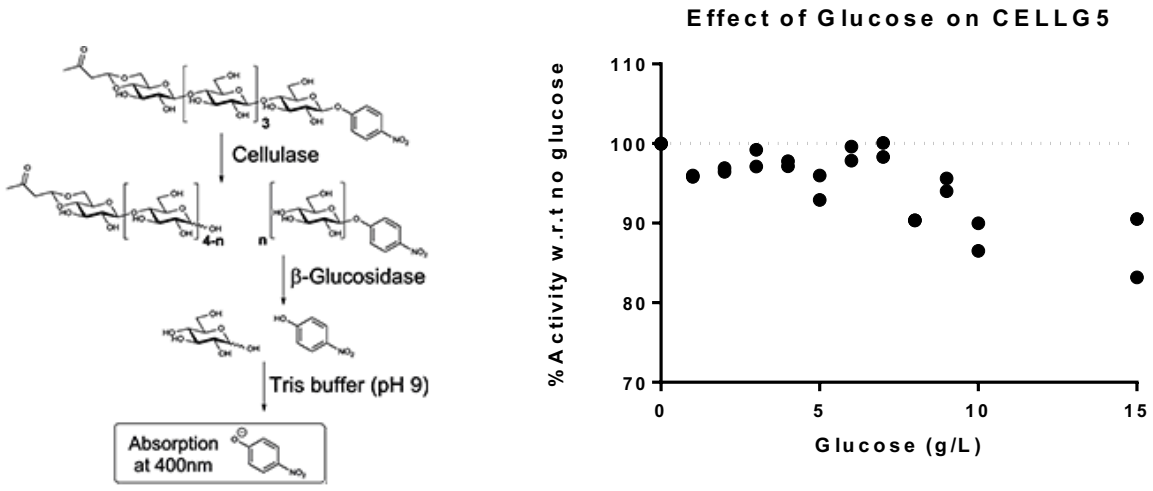

Figure S2.2. Effect of presence of glucose in CelAt CELLG5 activity assay: activity reduced by up to ~15% at glucose concentrations of 15 g/L. Glucose inhibition is due to the involvement of β-glucosidase in the assay.

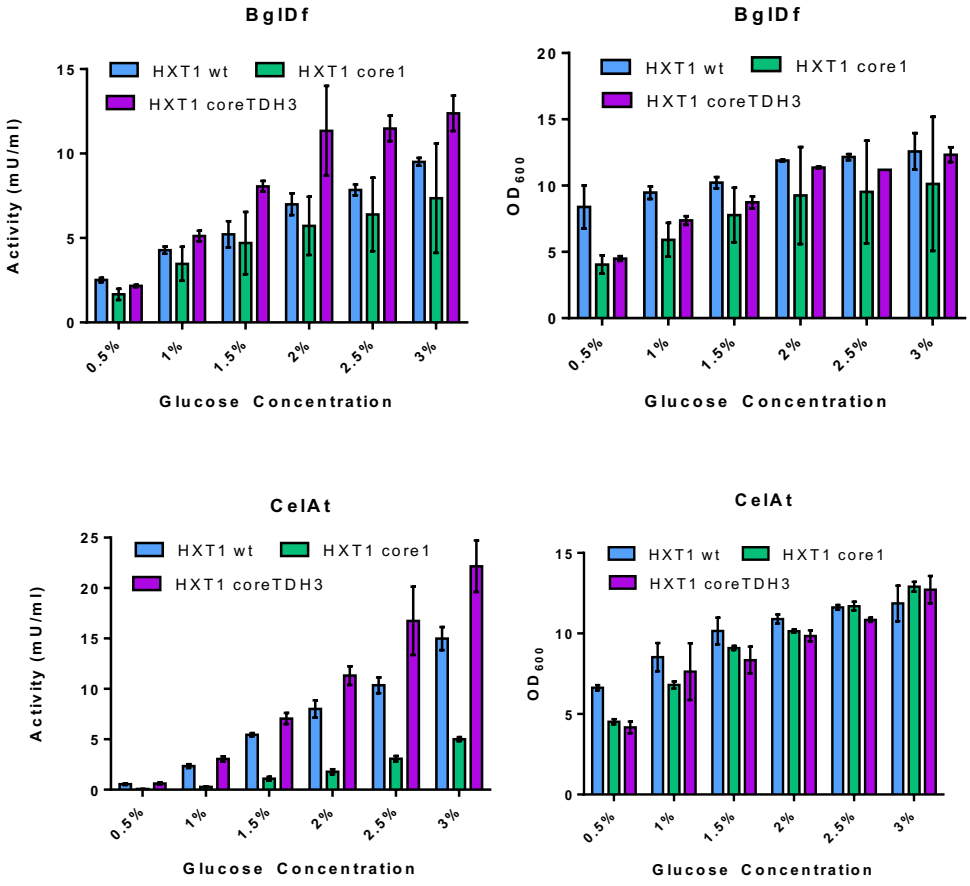

Figure S2.3. Extracellular specific activity of β-glucosidase (BglDf) and endoglucanase (CelAt). Raw data for Figure 2.8.

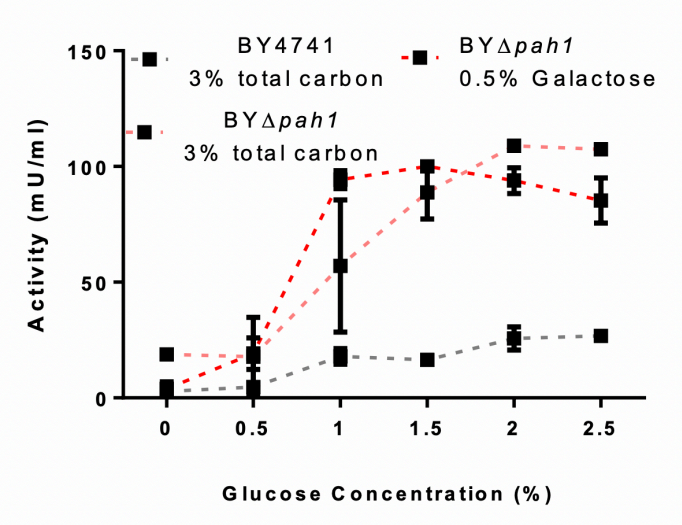

Figure S2.4. Activity of surface displayed β-glucosidase as a function of glucose concentrations. BY4741 (gray line) or BYΔ*pah1* (pink and red lines) were transformed with the plasmid Bgl1-mTurquoise2. Cells were grown overnight in selective media containing galactose as a sole carbon source, then re-inoculated (OD_{600}=0.05) in two types of media: 0.5% SGC(A) with increasing glucose concentrations (0.5% galactose, red lines) or keeping total carbon concentration at 3% across glucose concentration (3% total carbon, pink lines); e.g., 0.5% glucose, 2.5% galactose. Activity was measured at 24 h. The only discrepancy between the two methods (3% total carbon and 0.5% galactose) was observed at 1% glucose (*p<0.05). This is also the concentration that shows higher signal variability; therefore, it will be interesting to perform these experiments to evaluate this divergence.

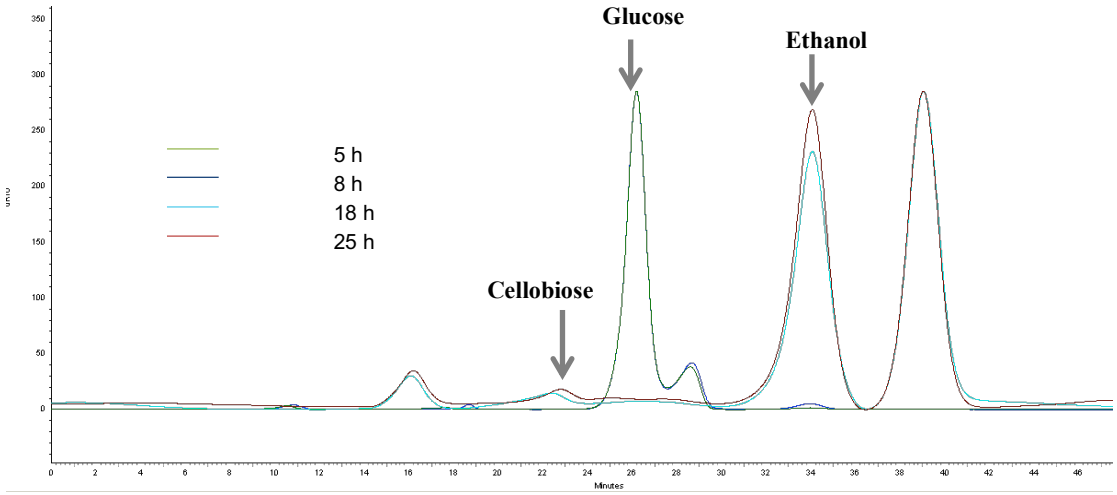

Figure S2.5. Overlay of chromatograms derived from hydrolysis products of PASC after exposure to supernatant of BY4741-pJC842-At at different stages of growth: 5 h, 8 h, 18 h and 25 h after inoculation at OD_{600}=0.05.

Appendix 3. Supplementary information from Chapter 4

Table S4.1. List of primers

Primer	Sequence	Reference
FW_URA3	TTTTGCTAGCTCGACTCTAGAGGATCCCCGGGATAAC	This study
RV_URA3	GCCGTTAATTAA GAATTCGAGCTCGGTACCCGGGATAAC	This study
FW_CEN/ARS	GCGGTCCTAGGGGGTACCGAGCTCGAATTCATCACGTGCTATAAAAATAA	This study
RV_CEN/ARS	CAGCTATGACCATGATTACGAATTCGTAACTTACACGCGCCTCGTATCTT	This study
FW_SNQ2	AATCTAATCTAAGTTTTAATTACAAAACTAGTAAAACAATGAGCAATATCAAAAGCACGC	This study
RV_ SNQ2	TCTTGCTCATTAGAAAGAAAGCATAGCAATCTAAGTTTTAATTACAAAACTAGT	This study
FW_PDR5	TAATCTAAGTTTTAATTACAAACACGTGGCGGCCGCAAAACAATGCCCGAGGCCAAGCTT	This study
RV_PDR5	TCTAAGTTTTAATTACAAACACGTGGCGGCCGCATGCCCGAGGCCAAGCTTAACAATA	This study
FW_PDR12	ATTACAAAACTAGTAAAACAATGTCTTCGACTGACGAACATATTG	This study
RV_PDR12	CTAATCTCGAGCGGTCCGTTATTTCTTCGTGATTTTATTTTCG	This study
FW_TPO1	GTGACATAACTAATCCGCGGTTAAGCGGCGTAAGCATACTTGGAT	This study
RV_TPO1	AAACACGTGGCGGCCGCAAAACAATGTCGGATCATTCTCCCAT	This study
PMA1_FW	CGCGCACTAGTAAAACAATGACTGATACATCATCCTCTTCATCATCC	This study
PMA1_RV	GGATGCGGTCCGTTAGGTTTCCTTTTCGTGTTGAGTAGAGAC	This study